Université du Québec
à Rimouski

CARACTÉRISATION DE LA CHIMIE DES CARBONATES ET COMPOSITION DE LA MATIÈRE ORGANIQUE DISSOUTE DES EAUX SUPRAPERGÉLISOL DANS LE CONTINUUM TERRE-À-OCÉAN CÔTIER ARCTIQUE (CAMBRIDGE BAY, NU)

Mémoire présenté

dans le cadre du programme de maîtrise en océanographie

en vue de l'obtention du grade de maître ès sciences

PAR

© CAROLE-ANNE GUAY

Juin 2025

Composition du jury :

André Pellerin, président du jury, Université du Québec à Rimouski

Gwénaëlle Chaillou, directrice de recherche, Université du Québec à Rimouski

Stephanie Kusch, codirectrice de recherche, Université du Québec à Rimouski

Alfonso Mucci, codirecteur de recherche, Université McGill

Huy Dang, examinateur externe, Université Trent

Dépôt initial le 20 avril 2025 Dépôt final le 30 juin 2025

Dans le doute, gaz au bout. Sauf dans l’eau, c’est mollo.

REMERCIEMENTS

À Rimouski, merci pour ton chaleureux accueil et de m'avoir ouvert les yeux sur l'ampleur de nos richesses à protéger. Tu auras à tout jamais une place dans mon cœur, mais surtout, tu resteras l'endroit où j'ai découvert un monde qui m'était inconnu : l'océanographie.

À Gwen, je te remercie de m'avoir accueillie dans ton laboratoire, avec bienveillance, malgré le fait que je n'avais AUCUNE expérience. Je me souviens du moment exact où tu m'as dit « *Tout le monde doit commencer quelque part* ». Eh bien, mon été de stage passé dans ton laboratoire fut révélateur : j'adore la bouette et l'eau ! Ton influence ne s'est pas arrêtée là. Tu as su parsemer mon parcours à la maitrise avec de folles opportunités qui m'ont autant forgée professionnellement que personnellement. Je suis reconnaissante d'avoir pu t'accompagner à deux reprises en Arctique et d'avoir été ta chauffeuse désignée de quad. Bref, je te remercie de ta confiance, initialement aveugle, et de ton encouragement constant même dans mes moments de doute. Bon bon bon je pourrais en dire long, mais ça suffit ! Par contre, sache que si je me sens aussi accomplie aujourd'hui, c'est en partie grâce à toi. Je nous souhaite encore plein de beaux projets.

À mes codirecteurs, Stephanie et Alfonso, merci pour votre accompagnement exemplaire tout au long de mon parcours. Vous étiez toujours, mais vraiment toujours, disponible pour répondre à mes questions, et ce, sans jugement. Vous avez fait de moi une fervente partisane des carbonates et de la matière organique ! Alfonso, ce fut un plaisir de vous côtoyer lors de mon premier terrain. Je n'aurais pu rêver d'un meilleur accompagnement. Stephanie, merci de m'avoir fait confiance malgré mon manque de connaissances sur la DOM et de m'avoir permis de m'y initier en Allemagne. Cette expérience, je ne l'oublierai jamais.

À mes partenaires de terrain, Sam, Bay, Steph et David, j'espère un jour être aussi cool que vous. Je n'ai sincèrement rien d'autre à dire que faire du terrain avec vous est un réel plaisir. On se refait ça n'importe quand.

À Gwendo et Ludo, merci de m'avoir accompagnée dans mon parcours autant pour me fournir des cafés (même si ce n'était pas gratuit), des conseils ou même une place dans votre bureau. Nos parties de badminton et de spikeball me manquent, mais j'ai déjà hâte à ma prochaine visite. P.S. Je suis désolée de vous avoir abandonnés.

À Jeanne, Alexie, Charlotte, Raphaël, Alicia, Éléonore et Alyson, vous êtes mes découvertes. Je garde en tête nos apéros sur la plage, nos travaux d'équipe (parfois chiant), nos soupers et nos soirées film. Sans vous, mon passage à Rimouski n'aurait pas été aussi plaisant. Je m'ennuie, mais on se voit bientôt sur un bateau près de chez vous.

À mes parents, merci pour votre soutien inconditionnel et de me fournir d'aussi beaux exemples de passion et d'acharnement. Vous n'avez jamais douté de mes choix et m'avez toujours poussée à être la meilleure version de moi-même. Ce n'est pas tout le monde qui a ce privilège et j'en suis éternellement reconnaissante.

À Jonathan, je crois sincèrement que je n'aurais pas été capable de terminer cette maitrise sans ton support. Ton positivisme et ta confiance en moi m'ont permis de repousser mes limites. Je souhaite à tout le monde d'avoir un cheerleader comme toi dans la vie.

Allez, maintenant je pars jouer dans l'eau !

RÉSUMÉ

Le pergélisol côtier arctique, représentant 34 % du littoral mondial, est de plus en plus affecté par des processus induits des changements climatiques, tels que la modification des régimes hydrologiques, l'épaississement de la couche active, l'érosion côtière accélérée et l'élévation du niveau de la mer. Par l'intermédiaire des eaux souterraines suprapergélisol, qui circulent dans la couche active dégelée, d'importantes quantités de carbone réactif, incluant du carbone organique dissous (DOC) labile, de la matière organique dissoute (DOM), de la matière organique particulaire (POM) et des nutriments, peuvent être mobilisées et exportées vers l'océan côtier à travers les sédiments perméables des plages. Au sein de l'estuaire souterrain (STE), où les eaux douces continentales interagissent avec les eaux marines, ces composés subissent des transformations biogéochimiques et un mélange physique. Ces processus peuvent modifier la composition moléculaire de la DOM, favoriser le dégazage du CO_2 et influencer les paramètres du système des carbonates tels que le pH, l'alcalinité totale (TA) et le carbone inorganique dissous (DIC). La contribution des eaux souterraines suprapergélisol aux flux de carbone et à la dynamique acido-basique des eaux côtières arctiques demeure toutefois peu documentée. Comprendre ces transformations est donc essentiel afin de quantifier la capacité tampon des zones côtières face à l'acidification des océans.

Cette étude caractérise le rôle des eaux souterraines suprapergélisol dans la modulation de la chimie des carbonates et de la composition de la matière organique dissoute (DOM) le long d'un continuum terre-à-océan côtier, près d'Iqaluktuuttiaq (Cambridge Bay, Nunavut, Canada). En combinant des traceurs isotopiques stables, des mesures du système des carbonates et une caractérisation moléculaire de la DOM par spectrométrie de masse à ultra-haute résolution (FT-ICR-MS), nous présentons un aperçu détaillé des gradients géochimiques entre les eaux douces continentales et l'eau de mer de surface. Nos résultats révèlent une forte diminution de la pCO_2 le long du gradient de salinité, passant de 5155 µatm à 306 µatm, suggérant un important dégazage de CO_2 lors du déversement dans le STE et une exportation limitée du DIC, issu du pergélisol, vers les eaux côtières. Les concentrations en DOC diminuent significativement entre les eaux douces et les eaux marines (de 1918 µmol kg^{-1} à 62 µmol kg^{-1}), accompagnées de modifications de la composition moléculaire de la DOM vers des structures moins aromatiques et plus aliphatiques, suggérant une minéralisation hétérotrophe dans les sédiments de plage. Malgré une forte variabilité moléculaire, la composition de la DOM semble avoir une influence plus limitée sur les paramètres du système des carbonates que la concentration en DOC. Ces résultats mettent en évidence le rôle des plages arctiques comme filtres biogéochimiques actifs, régulant les flux de carbone inorganique et organique lors du déversement des eaux souterraines, et renforçant la résilience des eaux côtières face à l'acidification des océans.

Mots-clés : Eau souterraine suprapergélisol, carbone inorganique, carbone organique, matière organique dissoute, pergélisol côtier, plage, FT-ICR-MS

ABSTRACT

Arctic coastal permafrost, which accounts for 34% of the world's coastline, is increasingly affected by climate-driven processes such as altered hydrological regimes, thickening of the active layer, accelerated coastal erosion and rising sea levels. Through suprapermafrost groundwater flowing within the seasonally thawed active layer, large quantities of reactive carbon, including labile dissolved organic carbon (DOC), dissolved organic matter (DOM), particulate organic matter (POM), and nutrients, can be mobilized and discharged into the coastal ocean via permeable beach sediments. Within the subterranean estuary (STE), where continental freshwater interacts with marine waters, these compounds are subject to biogeochemical transformations and physical mixing. These processes can alter the molecular composition of DOM, enhance CO_2 degassing, and influence carbonate system parameters such as pH, total alkalinity (TA), and dissolved inorganic carbon (DIC). The contribution of suprapermafrost groundwater to carbon fluxes and acid–base dynamics in Arctic coastal waters, however, remains poorly documented. Understanding these transformations is therefore essential for quantifying the coastal buffering capacity against ocean acidification.

This study characterizes the role of suprapermafrost groundwater in modulating carbonate chemistry and DOM composition along a land-to-coastal ocean continuum near Iqaluktuuttiaq (Cambridge Bay, Nunavut, Canada). By combining stable isotope tracers, carbonate system measurements, and DOM molecular characterization through ultrahigh-resolution mass spectrometry (FT-ICR-MS), we provide a detailed overview of geochemical gradients from inland freshwater to surface seawater. Our results show a sharp decrease in pCO_2 along the salinity gradient, from 5155 µatm to 306 µatm, suggesting substantial CO_2 degassing upon discharge into the STE and limited export of permafrost-derived DIC to coastal waters. DOC concentrations decline significantly from freshwater to marine waters (from 1918 µmol kg^{-1} to 62 µmol kg^{-1}), accompanied by shifts in DOM molecular composition toward less aromatic, more aliphatic structures, indicative of heterotrophic mineralization within beach sediments. Despite high molecular variability, DOM composition appears to have a limited influence on carbonate parameters compared to DOC concentration. These findings underscore the function of Arctic beaches as active biogeochemical filters, regulating both inorganic and organic carbon fluxes during groundwater discharge and enhancing the resilience of coastal waters to acidification.

Keywords: Suprapermafrost groundwater, inorganic carbon, organic carbon, dissolved organic matter, coastal permafrost, beach, FT-ICR-MS

TABLE DES MATIÈRES

LISTE DES TABLEAUX

LISTE DES FIGURES

LISTE DES ABRÉVIATIONS, DES SIGLES ET DES ACRONYMES

AO Acidification des océans

A_c Alcalinité carbonique (ou *carbonate Alkalinity*)

AI_{mod} Index d'aromaticité modifié (AI_{mod} pour *modified Aromaticity Index*)

ALG Eau souterraine de la couche active (ALG pour *Active Layer Groundwater*)

aCDOM Absorbance de la matière organique dissoute colorée (aCDOM pour *absorbance of Chromophoric Dissolved Organic Matter*)

BG Eau souterraine de la plage (BG pour *Beach Groundwater*)

Ca Calcium

CDOM Matière organique dissoute colorée (CDOM pour *Chromophoric Dissolved Organic Matter*)

DIC Carbone inorganique dissous (DIC pour *Dissolved Inorganic Carbon*)

DOC Carbone organique dissous (DOC pour *Dissolved Organic Carbon*)

DOM Matière organique dissoute (DOM pour *Dissolved Organic Matter*)

DOMt Matière organique dissoute terrigène (DOMt pour *terrestrial Dissolved Organic Matter*)

DON Azote organique dissous (DON pour *Dissolved Organic Nitrogen)*

DOP Phosphore organique dissous (DOP pour *Dissolved Organic Phosphorus)*

***f*CO_2** Fugacité du CO_2 (ou *fugacity of* CO_2)

GMWL Ligne météorique globale des eaux (GMWL pour *Global Meteoric Water Line*)

LMWL Ligne météorique locale des eaux (LMWL pour *Local Meteoric Water Line*)

NCA Alcalinité non carbonique (NCA pour *Non-Carbonate Alkalinity*)

N-CBIs Bases inorganiques non carboniques (N-CBIs pour *Non-Carbonate Inorganic Bases*)

MO Matière organique (OM pour *Organic Matter*)

Org-Alk Alkalinité organique (Org-Alk pour *Organic Alkalinity*)

Org-Alk$_m$ Alkalinité organique mesurée (Org-Alk$_m$ pour *measured Organic Alkalinity*)

***p*CO$_2$** Pression partielle de CO_2 (ou *partial pressure of* CO_2)

POM Matière organique particulaire (POM pour *Particulate Organic Matter*)

SNW Eau surnageante (SNW pour *Supernatent Water*)

Sp Salinité pratique (ou *practical Salinity*)

SPE Extraction en phase solide (SPE pour *Solid Phase Extraction*)

SSW Eau de mer de surface (SSW pour *Surface Seawater*)

STE Estuaire souterrain (STE pour *Subterranean Estuary*)

TA Alcalinité totale (TA pour *Total Alkalinity*)

TDN Azote dissoute totale (TDN pour *Total Dissolved Nitrogen*)

INTRODUCTION GÉNÉRALE

Le contexte actuel de réchauffement climatique global impose une compréhension approfondie des processus influençant le bilan de carbone afin de développer des modèles climatiques mondiaux (MCM) fiables à long terme. De prime abord, ces modèles reconnaissent le rôle fondamental de l'océan dans l'atténuation du réchauffement planétaire par l'absorption de ~25% des émissions de dioxyde de carbone (CO_2) anthropiques au cours des 40 dernières années et le stockage de 90% de la chaleur excédentaire (Friedlingstein et al., 2022; Gruber et al., 2023; Riser et al., 2016; Roemmich et al., 2019; Sabine et al., 2004). Ce n'est toutefois pas sans conséquence puisque celui-ci connait, globalement, une diminution moyenne de 0,1 unité de pH depuis le siècle dernier et une augmentation moyenne de température de 0,11°C chaque décennie depuis 50 ans (Caldeira & Wickett, 2005; Rhein et al., 2013). Ces changements ont causé une augmentation de 30% de l'acidité de l'eau de mer, provoquant le phénomène dommageable d'acidification des océans (AO) (Caldeira & Wickett, 2005; Doney et al., 2009; Pachauri & Reisinger, 2007; Riser et al., 2016; Roemmich et al., 2019). Selon le scénario SSP2-4.5 du GIEC, qui représente une trajectoire moyenne d'émissions de GES anthropiques futures, la diminution du pH pourrait s'accentuer de 0,20 unité d'ici 2100, exacerbant l'AO et son impact sur les écosystèmes marins (Lee et al., 2021; Orr et al., 2018).

Ces scénarios ne prennent toutefois pas en considération certains environnements clés, dont la contribution potentielle au cycle du carbone est sous-étudiée, tels que le pergélisol côtier. Ce dernier, couvrant 11% de la surface continentale mondiale, est un sol unique qui caractérise la région arctique et qui emmagasine deux fois plus de carbone que l'atmosphère, soit 60% du carbone organique mondial (Obu et al., 2019; Tarnocai et al., 2009; Zimov et al., 2006). L'Arctique subit un réchauffement 4 fois plus rapide que la moyenne globale, exposant ainsi le pergélisol terrestre et côtier à une combinaison de

pressions thermiques et mécaniques sans précédent : modification du régime hydrologique, épaississement de la couche active, augmentation du taux d'érosion côtière, élévation du niveau marin, hausse des températures de l'eau de mer, évènements de tempêtes plus violents et diminution de la glace de mer (Günther et al., 2015; Jones et al., 2009; Rawlins & Karmalkar, 2023; Schuur et al., 2015). L'omission des processus liés à la fonte du pergélisol continental dans les MCM sous-estime les projections climatiques, notamment en raison de son potentiel d'émission de CO_2 et de méthane (Burke et al., 2012; Koven et al., 2011). Le pergélisol côtier, quant à lui, n'est pas considéré dans ces modèles. Pourtant, il représente 34% des côtes mondiales et subit un taux d'érosion moyen de 0,5 m an^{-1}, qui pourrait s'amplifier d'un facteur 2 à 3 d'ici 2100 (Lantuit et al., 2012, 2013; Nielsen et al., 2022; Philipp et al., 2023). Dans certains secteurs de l'Arctique, comme dans la région de la mer de Beaufort, les taux de recul atteignent jusqu'à 1,1 m an^{-1} (Philipp et al., 2023). **Sachant que le pergélisol stocke ~1600 pétagrammes de carbone organique présumé labile, cela soulève des inquiétudes quant aux impacts de la remobilisation de ce « nouveau » carbone, à l'océan côtier, et la rétroaction sur le cycle global du carbone** (Hugelius et al., 2014; Schuur et al., 2015).

LE PERGÉLISOL : PILIER CLIMATIQUE ET ENVIRONNEMENTAL

Au Canada, la région de l'Arctique représente jusqu'à 46% du territoire (Brown et al., 1997 ; Obu et al., 2019) et est marquée par un climat polaire et la présence de pergélisol pouvant atteindre une épaisseur de plus de 700 mètres dans l'Extrême-Arctique (Heginbottom et al., 1995b). Le pergélisol est défini comme « un sol (ou roche) qui demeure à une température de 0°C ou moins pendant au moins deux années consécutives » (Permafrost Subcommittee, 1988). Les sols de l'Arctique canadien se divisent en quatre types de pergélisol, chacun ayant un pourcentage de recouvrement spécifique soit le pergélisol continu (plus de 90%), discontinu (entre 50 et 90%), sporadique (entre 10 et 50%) et isolé (moins de 10%) (Figure 1; Obu et al., 2019). Chaque type est associé à des structures physiques et des fonctions qui lui sont propres et qui dictent le régime hydrologique local en

réponse à la végétation, la topographie et la conductivité thermique des matériaux du sol (Goodrich, 1982; Judge, 1973).

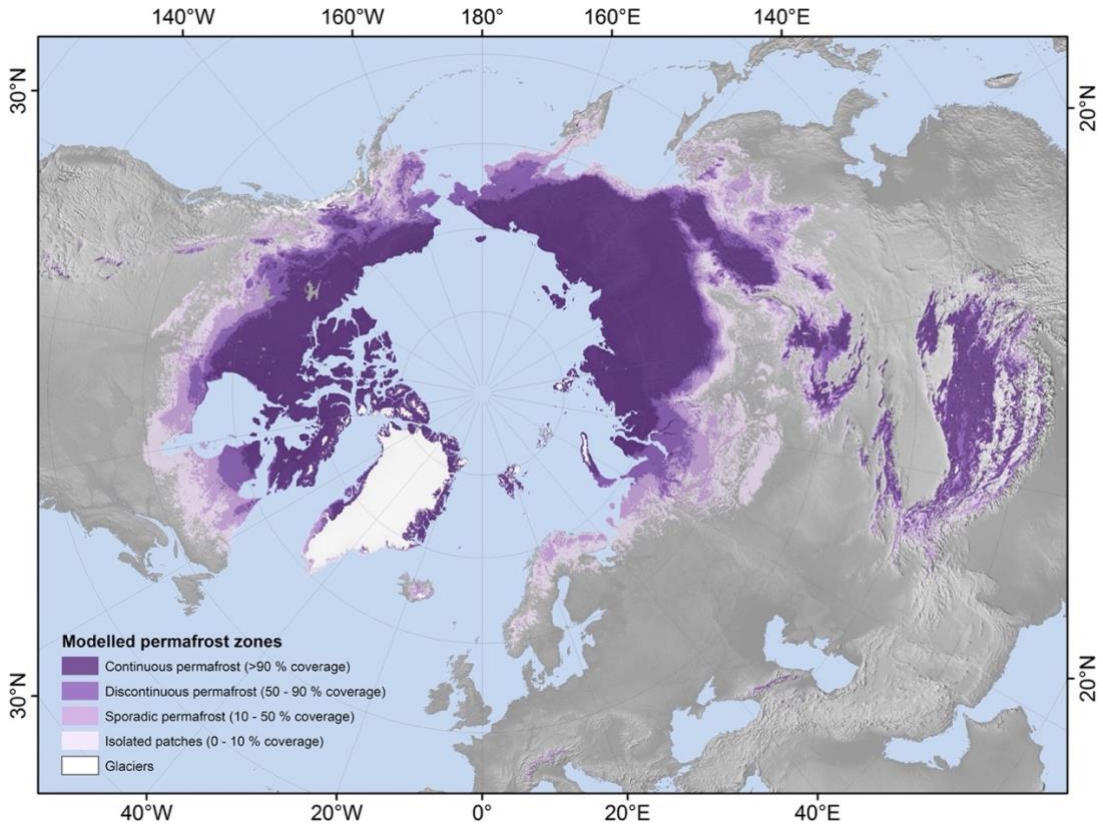

Figure 1. Distribution des types de pergélisol dans l'hémisphère nord (figure de Obu et al., 2019).

Le pergélisol est accompagné d'une strate superficielle, appelée la couche active, qui subit des cycles de gel et de dégel en fonction des fluctuations saisonnières de température (Figure 2; Burn, 1998). Cette couche, dont l'épaisseur varie de 0,5 à 2,0 mètres au Canada, est directement influencée par la profondeur du manteau neigeux, la présence de matière organique (MO), l'humidité du sol, la végétation et la topographie (Heginbottom et al., 1995a; Luo et al., 2016). Bien que la couche active soit distincte du pergélisol, elle représente un milieu important pour divers processus biogéochimiques, écologiques, hydrologiques et géologiques (Dobiński, 2020; Hinzman et al., 1991).

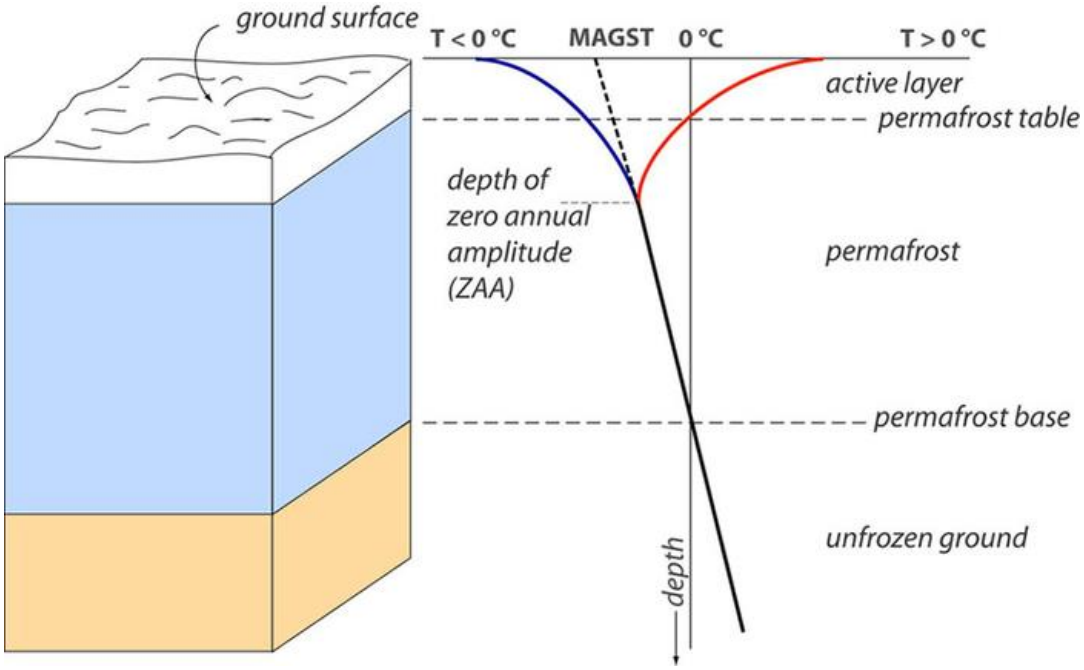

Figure 2. Schématisation d'une coupe dans un environnement de pergélisol (à gauche) et son profil transversal de température (à droite). Ce profil illustre que les variations saisonnières de température (courbe bleue en hiver et courbe rouge en été) se produisent au-dessus de la zone d'amplitude annuelle nulle (ZAA). On observe des températures positives en été et des températures négatives en hiver (figure de Noetzli et al., 2009).

Le pergélisol est constitué d'un amalgame de sédiments, de composés inorganiques, de glace, de matière organique particulaire (POM) et dissoute (DOM) ainsi que d'autres substances (Zimov et al., 2006). La connectivité superficielle de la couche active avec le pergélisol confère à celle-ci des conditions froides et humides, ralentissant certains processus biogéochimiques tels que la dégradation de la MO (Ping et al., 2015). Par conséquent, il stocke une quantité significative de carbone organique préservé depuis des milliers d'années, dont 1035 ± 150 PgC se trouvent exclusivement dans les trois premiers mètres (Gorham, 1991; Hugelius et al., 2014; Mishra et al., 2021; Schuur et al., 2015; Zimov et al., 2006).

En réponse à la hausse des températures ambiantes, la couche active du pergélisol s'épaissit et, selon le scénario SSP2-4.5 du GIEC considéré comme modéré, elle pourrait s'épaissir en moyenne de ~43 cm d'ici 2100 (Li et al., 2022). Ces changements ont des conséquences affectant l'intégrité des écosystèmes arctiques (e.g. modification du patron de

végétation, modification du régime hydrologique, perte d'habitat, etc.), la stabilité des infrastructures (e.g. subsidence et affaissement des sols, routes et bâtiments endommagés, etc.) et le cycle du carbone (Belshe et al., 2012; Rodenhizer et al., 2020; Schuur & Abbott, 2011; Schuur & Mack, 2018; Shaver et al., 2000). L'épaississement de la couche active libère du carbone organique dissous (DOC) labile pour les microorganismes, dont l'activité métabolique, stimulée par l'augmentation des températures ambiantes, a le potentiel d'émettre du CO_2 et du CH_4 vers l'atmosphère (Dutta et al., 2006; Knoblauch et al., 2018; Schädel et al., 2016; Schuur et al., 2015; Zimov et al., 2006).

LE PERGÉLISOL CÔTIER : AUX PREMIÈRES LOGES DU RÉCHAUFFEMENT PLANÉTAIRE

Alors que le pergélisol continental est au cœur des préoccupations des scientifiques du climat depuis plusieurs décennies, le pergélisol côtier, localisé dans la zone supralittorale, demeure peu étudié en raison des défis d'échantillonnage qui lui sont associés : inaccessibilité par les navires de recherche, manque d'infrastructures côtières et coûts importants (Fritz et al., 2017). Pourtant, il représente 70% du littoral canadien et 34% des côtes mondiales (Lantuit et al., 2012; Way, 2024). En soi, les milieux côtiers sont des zones de flux d'énergie, de transferts biogéochimiques, physiques et thermiques (Wright et al., 2019). Par conséquent, les côtes arctiques sont particulièrement vulnérables aux impacts des changements climatiques, notamment à la diminution de la glace de mer, la hausse du niveau marin, la hausse des températures des eaux de surface et l'augmentation des évènements de tempêtes et de submersions (Günther et al., 2015; Schuur et al., 2015). Ces pressions ont pour conséquences d'accentuer l'altération des côtes, déjà fragilisées par l'épaississement de la couche active. Ces changements intensifient alors la remobilisation verticale de carbone vers l'atmosphère (dégazage) et la remobilisation latérale (transport), par l'érosion côtière ou par les écoulements suprapergélisol, de DOM, de POM, de carbone et de nutriments vers les eaux côtières (Figure 3; Romanovsky & Osterkamp, 2000; Walvoord & Striegl, 2007; Fritz et al., 2017; Lizotte et al., 2022). Au cours de l'écoulement, les composés remobilisés subissent de nombreux processus biotiques (e.g. reminéralisation, oxydoréduction, décomposition, etc.)

et abiotiques (e.g. adsorption et coprécipitation sur des phases minérales, dégazage) qui contrôlent les flux exportés à l'océan (Sawyer et al., 2016). Wegner et al. (2015) estiment un relargage d'environ 14 Tg de carbone organique annuellement dans les zones côtières, exclusivement lié à l'érosion côtière alors que Connolly et al. (2020), et plus récemment Kipp et al. (en révision), illustre l'importance des écoulements suprapergélisol le long de la côte de la mer de Beaufort. En effet, ceux-ci estiment qu'entre 400 à 2100 m^3 d'eau douce sont déversés quotidiennement dans l'océan côtier de juin à octobre, lorsque la couche active atteint sa profondeur maximale (Connolly et al., 2020).

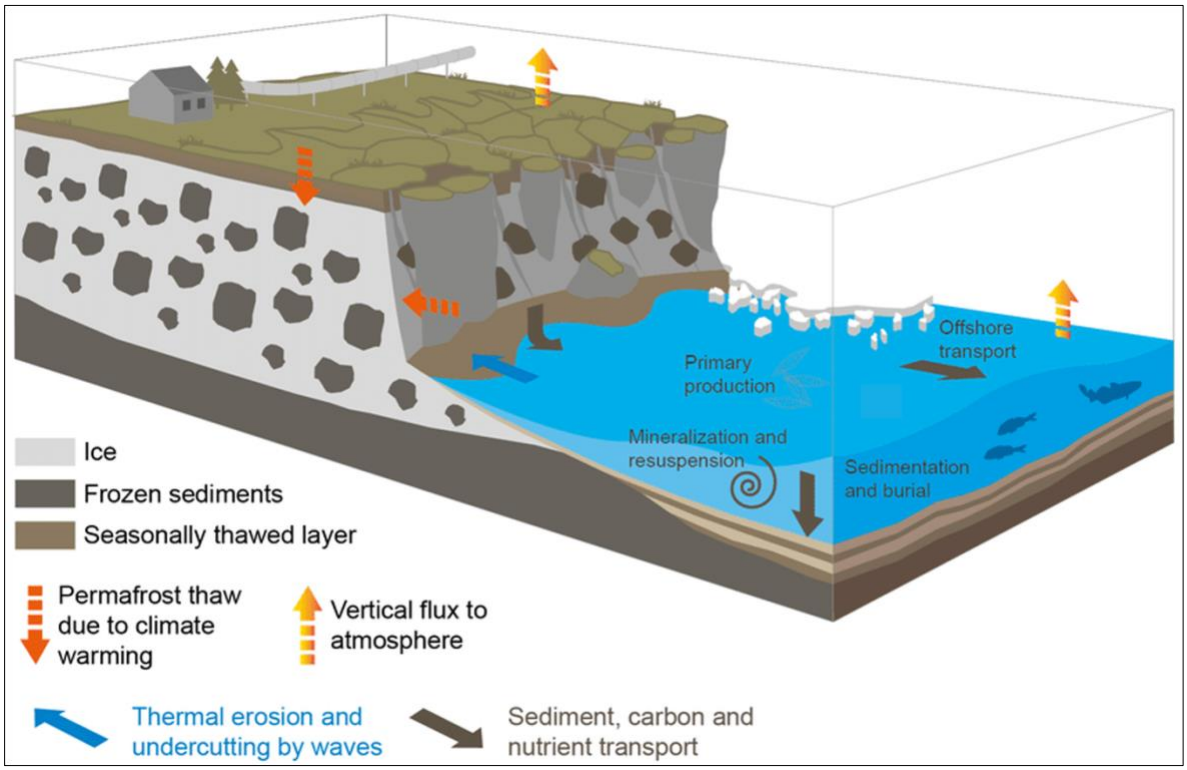

Figure 3. Schématisation d'un environnement de pergélisol qui subit des pressions associées aux changements climatiques (pressions thermiques (flèches rouges) et mécaniques (flèche bleue)) ainsi que les conséquences de ces pressions telles que les flux verticaux de carbone (flèches jaunes) , le transport latéral et l'enfouissement de composés (flèches noires) (modifié de Fritz et al., 2017).

En suivant le gradient hydraulique, les eaux souterraines suprapergélisol, chargées en divers composés réactifs (e.g. azote, phosphore, métaux traces, carbone organique et inorganique), se déchargent à l'océan côtier à travers les sédiments perméables des plages

(Connolly et al., 2020; Lecher, 2017; Kipp et al., (en révision); Flamand et al., (en révision)). Dans le continuum terre-mer, les plages sont des zones de mélange entre les eaux souterraines continentales et les eaux marines qui composent un estuaire souterrain dynamique (STE; Moore, 1999; Santos et al., 2009). Les plages ont longtemps été considérées comme des « déserts » géochimiques en raison de leur faible concentration de POM (Huettel et al., 1996; Boudreau et al., 2001). Cependant, bien que pauvre en POM, les plages de sable sont dominées par le transport advectif qui favorise la décomposition rapide de la DOM, et ce, en fonction de la perméabilité des sédiments (Anschutz et al., 2009; Riedl & Machan, 1972). Dans les STE, les apports de DOC et DOM d'origine marine, par les marées et les vagues, contrôlent la biogéochimie des plages et les processus de minéralisation (Anschutz et al., 2009; Charbonnier et al., 2022; Kim et al., 2012; McLachlan & Brown, 2006; Robinson et al., 2018). Cependant, des études récentes démontrent également que les eaux souterraines contribuent significativement aux apports de MO terrigène (Beck et al., 2007; Chaillou et al., 2016; Couturier et al., 2016; Linkhorst et al., 2017; Seidel et al., 2014; Sirois et al., 2018). Ces apports seraient minéralisés (Chaillou et al., 2024; Liu et al., 2017) et/ou séquestrés (Linkhorst et al., 2017; Sirois et al., 2018). Ces transformations sont une source majeure de nutriments et de carbone pour les eaux côtières (Anschutz et al., 2009; Moore, 1999, 2010; Robinson et al., 2018) et peuvent être un facteur négligé de l'eutrophisation et de l'acidification (Chaillou et al., 2024; Kwon et al., 2017; Liu et al., 2017; Maher et al., 2013; Santos et al., 2011). Sur les côtes de la mer de Beaufort, Flamand et al. (en révision) ont montré que la DOM transportée par les eaux souterraines suprapergélisol perdait rapidement sa signature terrigène, les composantes terrigènes étant probablement piégées sélectivement ou minéralisées dans la zone de décharge de la plage avant même d'atteindre l'océan. **Dans le continuum terre-à-océan côtier arctique, le rôle des plages et des décharges d'eaux souterraines sur la chimie des eaux côtières est encore peu documenté**.

LE SYSTÈME DES CARBONATES

L'équilibre thermodynamique du système des carbonates régule la capacité de l'eau à absorber ou émettre du CO_2 sous forme gazeuse. Plus particulièrement, ce système est typiquement caractérisé par quatre paramètres analytiques, soit le carbone inorganique dissous (DIC), l'alcalinité totale (TA), le pH ainsi que la fugacité [fCO_2] ou la pression partielle du CO_2 (pCO_2) (Dickson et al., 2007; Zeebe et al., 2001). Il s'exerce un échange gazeux à l'interface eau-air qui est régi par la loi de Henry (solubilité du CO_2 dans l'eau) et dont la direction et l'intensité dépendent du gradient de pCO_2 à l'interface. Si la pCO_2 atmosphérique excède celle des eaux de surface, il y a une absorption nette du CO_2 atmosphérique par la phase liquide. Le CO_2 absorbé est alors dissous (Eq. 1) puis réagit avec l'eau pour former de l'acide carbonique (H_2CO_3) (Eq. 2). En tant qu'acide faible, une partie de H_2CO_3 se dissocie rapidement en ions bicarbonate (HCO_3^-) et hydrogène (H^+) (Eq. 3). Selon le pH de l'eau, les ions HCO_3^- peuvent être subséquemment dissociés en ions carbonates (CO_3^{2-}) et H^+ (Eq. 4) (Figure 4; Dickson et al., 2007). Cependant, au pH de l'eau de mer, une partie des protons issus de la dissociation de l'acide carbonique réagissent avec les ions carbonates pour produire des ions bicarbonates (Eq. 4 inversée).

$$CO_2\,(g) \rightleftharpoons CO_2\,(aq) \qquad \text{(Eq. 1)}$$
$$CO_2\,(aq) + H_2O\,(l) \rightleftharpoons H_2CO_3\,(aq) \qquad \text{(Eq. 2)}$$
$$H_2CO_3\,(aq) \rightleftharpoons H^+\,(aq) + HCO_3^-\,(aq) \qquad \text{(Eq. 3)}$$
$$HCO_3^-\,(aq) \rightleftharpoons H^+\,(aq) + CO_3^{2-}\,(aq) \qquad \text{(Eq. 4)}$$

Le carbone inorganique dissous et l'alcalinité totale et carbonatée

Le DIC, tel que présenté dans l'équation 5, est équivalent à la somme des ions carbonate, bicarbonate et [CO_2^*], qui inclut toutes les formes moléculaires de CO_2, soit le CO_2 et l'acide carbonique (Dickson et al., 2007). L'abondance relative des espèces de DIC dans l'eau est fonction du pH (Figure 4; Raven et al., 2005).

$$DIC = [CO_2^*] + [HCO_3^-] + [CO_3^{2-}] \qquad \text{(Eq. 5)}$$

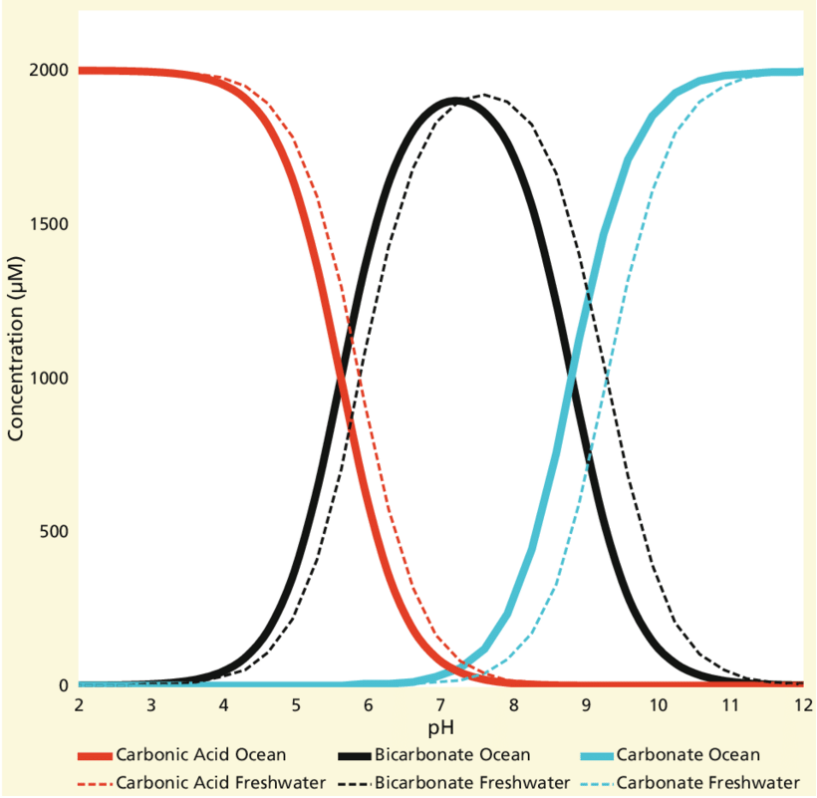

Figure 4. Abondance relative de CO_2^* (rouge), d'ions bicarbonates (noir) et d'ions carbonates (bleu) en fonction du pH dans un environnement océanique (ligne pleine) ou d'eau douce (ligne pointillée) (figure de Middelburg, 2019).

L'alcalinité totale correspond à la capacité de l'eau à neutraliser un acide avant de subir une modification significative du pH (Egleston et al., 2010). Plus pratiquement, elle est égale à la quantité d'acide fort nécessaire pour neutraliser les bases dissoutes dans l'eau jusqu'à une condition qui correspond à la conversion des ions bicarbonates en acide carbonique, soit :

$$TA = [HCO_3^-] + 2\,[CO_3^{2-}] + [OH^-] + [B(OH)_4^-] + [H_3SiO_4^-] + [HS^-] + [HPO_4^{2-}] + 2[PO_4^{3-}] + [NH_3] - [H^+] + [\text{Org-Alk}] \quad \text{(Eq. 6)}$$

Contrairement aux autres paramètres du système carbonaté, la TA est une propriété conservative, en système ouvert ou fermé, par rapport à la température et à la salinité, et elle est indépendante de l'ajout ou du retrait de CO_2 (Butler, 1982). Par conséquent, sa facilité d'échantillonnage et d'entreposage ainsi que la précision des mesures font d'elle l'un des

paramètres les plus utilisés dans les calculs des autres paramètres du système carbonaté (Wolf-Gladrow et al., 2007). Jusqu'à récemment, la définition standard de TA ne tenait compte que de l'alcalinité inorganique, qui inclut l'alcalinité carbonique (A_c, Eq. 7), ainsi que l'alcalinité des borates, phosphates et silicates dissous, telle que décrite dans l'équation 9 (Boyd, 2015; Dyrssen & Sillén, 1967).

$$A_c = [HCO_3^-] + 2[CO_3^{2-}] + [OH^-] - [H^+] \quad \text{(Eq. 7)}$$

Cette définition de la TA inorganique, bien qu'adéquate en océan ouvert, n'est toutefois pas adéquate dans les milieux côtiers où l'on retrouve une source importante de matière organique dissoute terrigène (DOMt ou DOM allochtone), un mélange constitué d'acides humiques et de substances organiques qui peuvent aussi agir comme des accepteurs ou donneurs de protons (Kuliński et al., 2014; Martell-Bonet & Byrne, 2023). Tandis que les concentrations de DOMt dans les eaux côtières sont modulées par différents processus tels que l'activité microbienne, la photodégradation et l'enfouissement dans les sédiments (Hansell et al., 2014 ; Lalonde et al., 2014), une fraction de la DOMt demeure présente dans l'eau avec le potentiel de contribuer positivement (Song et al., 2020) ou négativement (Delaigue et al., 2020) à la TA (Egleston et al., 2010; Kerr et al., 2023; Kuliński et al., 2014). **Cette alcalinité organique (Org-Alk) peut donc biaiser l'interprétation de la capacité tampon d'une masse d'eau ainsi que l'évaluation des autres paramètres du système des carbonates** (Abril et al., 2015; Kerr et al., 2021; Kim & Lee, 2009; Yang et al., 2015).

En pratique, il est possible de calculer l'alcalinité organique ($Org\text{-}Alk_c$, Eq. 8) en soustrayant A_c ainsi que les bases inorganiques non carboniques (N-CBIs, Eq. 9) de la TA (Dickson, 1981; Wolf-Gladrow et al., 2007). Il est également possible de déterminer Org-Alk directement ($Org\text{-}Alk_m$, Eq. 10) par titrage en retour de l'alcalinité non carbonique (NCA).

$$TA = A_c + \text{N-CBIs} + Org\text{-}Alk_c \quad \text{(Eq. 8)}$$

$$\text{N-CBIs} = [HPO_4^{2-}] + 2\,[PO_4^{3-}] + [NH_3] + [HS^-] + [B(OH)_4^-] + [HSO_4^-] - [H_3PO_4] \quad \text{(Eq. 9)}$$

$$Org\text{-}Alk_m = \text{NCA} - \text{N-CBIs} \quad \text{(Eq. 10)}$$

Pression partielle de CO_2

Le gradient de pCO_2 à l'interface air-mer détermine la direction et l'intensité des flux de CO_2, permettant ainsi d'évaluer le rôle de source ou de puits de l'océan, et ce, en fonction de l'activité biologique, la température, la circulation océanique, et la force des vents près de la surface (DeGrandpre et al., 1996; Joos et al., 1991; Peng & Broecker, 1991). Bien qu'il soit possible de mesurer la pCO_2, elle est plus souvent calculée à l'aide de deux paramètres analytiques. Cela est dû notamment à ses importantes variations spatiales et temporelles et aux coûts des instruments de mesure, comme les systèmes de détection directe infrarouge (Abril et al., 2015). Abril et al. (2015) ont démontré que l'utilisation du couple pH-TA pour calculer la pCO_2 dans les eaux riches en matière organique, et par conséquent avec une Org-Alk significative, résultait en une surestimation de la pCO_2 variant jusqu'à 300% comparativement à la pCO_2 mesurée in situ. Par conséquent, il est recommandé d'utiliser le couple le plus robuste, soit DIC-pH, dans le calcul de la pCO_2 (Hunt et al., 2011).

État de saturation en carbonate de calcium

Le phénomène d'acidification des océans fait référence à un déplacement de l'équilibre du système des carbonates. En effet, l'ajout de CO_2 dissous dans l'eau de mer, suite à l'augmentation des apports anthropiques à l'atmosphère, provoque la formation de H_2CO_3, un acide faible qui, lors de sa dissociation partielle, libère des ions H^+ en solution. Bien qu'une partie de ces ions H^+ réagissent avec le CO_3^{2-} de l'eau de mer pour former des ions HCO_3^-, il provoque quand même une diminution du pH (Doney et al., 2009; Duarte et al., 2013; Gattuso et al., 2011). Cela entraine également une diminution des concentrations relatives des ions CO_3^{2-} par rapport aux ions HCO_3^- et une diminution de l'état de saturation (Ω) de l'eau par rapport aux minéraux de carbonate de calcium ($CaCO_3$), dont la calcite (Ω_{cal}) et l'aragonite (Ω_{ara}) sont les polymorphes dominants dans le milieu marin (Duarte et al., 2013; Millero et al., 2002). L'état de saturation de ces minéraux, constitués de carbone inorganique, se calcule en fonction de l'équation 11 où [i] sont les concentrations totales de calcium et

d'ions carbonate et K^*_{SP} est la constante de solubilité stœchiométrique (définie en termes du produit des concentrations totales à l'équilibre) de ces minéraux (Mucci, 1983).

$$\Omega_{c,\,a} = [Ca^{2+}]\,[CO_3^{2-}] / K^*_{SP} \qquad \text{(Eq. 11)}$$

Une valeur $\Omega > 1$ indique une sursaturation des eaux en $CaCO_3$, ce qui crée des conditions favorables à la précipitation de ce minéral ainsi qu'un puits potentiel de DIC. À l'inverse, une valeur $\Omega < 1$ indique une sous-saturation des eaux en $CaCO_3$, une condition propice à sa dissolution ainsi qu'une source potentielle de DIC. Le $CaCO_3$ est un composé essentiel à la formation de squelettes et de coquilles de plusieurs organismes marins (coccolithophores, foraminifères, ptéropodes, bivalves, échinodermes, coraux, etc.) (Doney et al., 2009; Kroeker et al., 2013). Ainsi, une diminution du degré de saturation peut ralentir ou complètement inhiber la calcification et influencer les taux de croissance et de survie de ces organismes calcifiants menaçant alors l'intégrité des écosystèmes marins (Orr et al., 2005; Raven et al., 2005; Doney et al., 2009; Caldeira & Wickett, 2003; Leung et al., 2022).

LA MATIÈRE ORGANIQUE

La MO est constituée d'un mélange hétérogène de substances organiques d'origine eucaryotique (animale ou végétale) ou procaryotique (bactérienne ou archéenne) (Bianchi & Bauer, 2011; Stevenson & Cole, 1999). Dans les environnements aquatiques, la MO peut être issue de sources naturelles autochtones (e.g. végétation benthique, production microbienne, phytoplancton, etc.), allochtones (e.g. MO du sol et des plantes vasculaires, exsudats de racines, litière, métabolites de microorganismes) ou de sources anthropiques (e.g. fertilisants, pesticides, eaux usées urbaines ou industrielles, etc.) (Aitkenhead-Peterson et al., 2003; Baines & Pace, 1991; Münster, 1993). Elle s'y trouve sous diverses formes communément distinguée selon la fraction qui est retenue ou non par un filtre de porosité prédéterminée, soit sous forme dissoute (< 0,45 µm), particulaire (> 0,45 µm) ou colloïdale (entre 1 nm et 1 µm) (Aitkenhead-Peterson et al., 2003; Benner, 2003; He et al., 2016; Repeta & Aluwihare, 2024). Bien qu'il n'y ait pas de consensus quant à la taille des pores du filtre qui distingue le dissous du particulaire, celle de 0,45 µm est arbitraire, mais la plus couramment adoptée.

En milieu aquatique, une grande partie de la matière organique se trouve sous forme dissoute, où elle agit en tant que moteur d'énergie pour les microorganismes hétérotrophes. Elle régule la disponibilité et l'abondance des nutriments et des métaux dissous, modifie les propriétés optiques de l'eau et influence le pH (Azam, 1987; Carlson et al., 2007; Kuliński et al., 2014; Oliver et al., 1983; Pomeroy, 1974; Rodenhizer et al., 2020; Wetzel, 1992). Cette DOM est composée majoritairement d'atomes de carbone, accompagnés d'atomes d'hydrogène, d'oxygène, d'azote, de phosphore et de soufre, formant des fragments de différents poids moléculaires (< 100 000 Da) (Carlson & Hansell, 2015; Dittmar & Stubbins, 2014). Le réservoir océanique de carbone organique dissous (DOC) est d'amplitude similaire à la quantité de CO_2 emmagasinée dans l'atmosphère (Dittmar & Stubbins, 2014; Sharp, 2002). De ce fait, les processus biogéochimiques régissant le cycle de la DOM dans les milieux aquatiques influencent les flux globaux de carbone (Azam, 1987; Carlson et al., 2007; Kuliński et al., 2014; Rodenhizer et al., 2020; Sharp, 2002; Stubbins & Dittmar, 2014). Bien que la composition de la DOM soit diversifiée et que sa complexité chimique diffère selon son origine, elle comprend essentiellement une combinaison de substances humiques dissoutes, incluant des acides humiques et fulviques, ainsi que des composés simples tels que des monomères (e.g. carbohydrates, acides aminés, acides carboxyliques, etc.) (Catalán et al., 2021; Kaplan & Newbold, 2003).

La matière brute composant la DOM peut être quantifiée notamment par l'analyse de trois sous-éléments soit le DOC, l'azote organique dissous (DON) et le phosphore organique dissous (DOP) (Sharp, 2002). En complémentarité, la DOM peut être quantifiée optiquement grâce à sa fraction colorée (CDOM) qui absorbe dans le spectre de longueurs d'onde ultraviolet (UV) et visible (Coble et al., 2015; Sharp, 2002). En plus de représenter 20 à 70% du réservoir de DOC, la CDOM agit sur les propriétés optiques de l'eau, notamment par sa coloration jaune et brunâtre, influençant la profondeur de la zone euphotique (pénétration de la lumière solaire) et les processus biogéochimiques et photochimiques qui s'y produisent (Laane & Koole, 1982; Urtizberea et al., 2013). Cette analyse permet de déterminer des coefficients d'absorption à différentes longueurs d'onde, des indicateurs optiques, qui

informent alors sur l'origine, le poids moléculaire et le degré de dégradation photochimique de la CDOM (Hayase & Shinozuka, 1995; Helms et al., 2008; Stubbins et al., 2012).

Il existe différents outils spectroscopiques (e.g. spectroscopie de résonance magnétique nucléaire (NMR), spectrométrie de masse à trappe orbitale (Orbitrap), spectrométrie de masse à résonance cyclonique ionique (FT-ICR-MS), etc.) qui permettent sa caractérisation au niveau moléculaire. Le FT-ICR-MS se démarque par sa haute résolution inégalée qui permet d'identifier la masse exacte de molécules individuelles avec une précision de 0,1 mDa et ce, pour les dizaines de milliers de molécules qui composent la DOM (Dittmar & Stubbins, 2014). Suite à l'acquisition de ces données, il est possible de calculer les formules élémentaires des molécules en plus d'obtenir des informations sur leur saturation en carbone, azote ou oxygène ainsi que la densité des doubles liaisons de C=C dans les molécules (Dittmar & Stubbins, 2014; Koch & Dittmar, 2006; Stenson et al., 2003; Stubbins et al., 2010). Cette technique est utilisée pour caractériser la DOM dans les eaux continentales de surface (Zhao et al., 2023), les eaux souterraines (Linkhorst et al., 2017; McDonough et al., 2020; Seidel et al., 2015; Waska et al., 2021) et l'eau de mer (Lechtenfeld et al., 2024; Seidel et al., 2022). Elle apparait donc comme une technique de pointe, complémentaire à la quantification permise par les approches optiques.

Les environnements côtiers sont fortement influencés par les apports continentaux de matière particulaire et dissoute, qui modifient la salinité, la turbidité, la production primaire et les taux de respiration (Connelly et al., 2015). La transformation et la dégradation de la DOM altèrent la balance ionique des eaux, ce qui régule le pH des écosystèmes aquatiques et contrôle la capacité tampon de l'eau face aux apports de CO_2 (Kuliński et al., 2014). **Il est donc essentiel d'examiner l'influence de la DOM sur l'équilibre acide-base et la capacité des milieux côtiers arctiques à amortir les fluctuations de CO_2. Cela est d'autant plus vrai pour les environnements des hautes latitudes où la forte solubilité du CO_2 dans les eaux froides rend ces écosystèmes particulièrement sensibles aux changements de la chimie des carbonates** (Borges & Abril, 2011; Shen et al., 2019).

OBJECTIFS

Malgré son potentiel de contribution au cycle global du carbone, le pergélisol côtier arctique fait face à un manque flagrant de connaissances en regard au pergélisol continental. Cet environnement complexe et dynamique, au cœur des changements climatiques, requiert une compréhension de son rôle en tant que puits ou source de carbone à l'océan côtier arctique et à l'atmosphère. De plus, sachant que la DOMt, issue de la cryosphère et remobilisée à travers le continuum terre-à-océan côtier, est fortement biodégradable et disponible pour l'activité microbienne (Fritz et al., 2015; Spencer et al., 2015; Vonk & Gustafsson, 2013), une approche exploratoire se doit d'être réalisée afin de comprendre si elle influence les paramètres du système des carbonates et la capacité tampon des eaux côtières.

L'objectif principal de cette étude est de **caractériser le rôle des eaux suprapergélisol dans la modulation de la chimie des carbonates et de la composition de la DOM le long du continuum terre-à-océan côtier arctique près d'Iqaluktuuttiaq (Cambridge Bay, Nunavut, Canada)**. Plus particulièrement, elle vise à comprendre la dynamique du système des carbonates et de la composition moléculaire de la DOM, depuis les eaux douces terrestres jusqu'aux eaux côtières marines. Pour ce faire, ce mémoire est structuré en un chapitre s'articulant autour des trois sous-objectifs suivants :

1. **Caractériser les variations spatiales des paramètres du système des carbonates le long du continuum;**
2. **Évaluer la capacité tampon des eaux souterraines suprapergélisol et identifier les sources et les processus potentiels affectant cette capacité;**
3. **Caractériser la composition de la DOM le long du continuum et explorer son influence potentielle sur la chimie des carbonates.**

Cette étude s'insère dans la section « biogéochimie » d'un vaste projet de recherche qui vise à combler le manque de données face à l'érosion côtière en Arctique, et ce, en

collaboration avec Savoir Polaire et la Station canadienne de recherche sur l'Extrême-Arctique (*SCREA*) de Cambridge Bay (Nunavut). Ce projet est dirigé par une équipe multidisciplinaire (Stéphanie Coulombe (*Savoir Polaire*), David Didier (*UQAR*) et Gwénaëlle Chaillou (*UQAR-ISMER*)) qui cherche à développer un modèle d'érosion du pergélisol côtier par la prise de données in situ en lien avec les processus thermiques, mécaniques et biogéochimiques sur le territoire d'Iqaluktuuttiaq. Les deux principaux sites à l'étude (Augustus Hill et Longpoint) ont été désignés par le Ekaluktutiak Hunters & Trappers Organization (*HTO*) comme étant des lieux fortement utilisés par ses membres. Ceux-ci ont d'ailleurs partagé leurs inquiétudes quant à la transgression rapide et drastique du trait de côte.

CONTRIBUTION DE L'AUTEURE ET PUBLICATIONS

Ce mémoire est présenté sous la forme d'un article scientifique rédigé en anglais et intitulé « Suprapermafrost Groundwater Carbonate Chemistry and Dissolved Organic Matter Composition along An Arctic Land-to-Coastal Ocean Continuum (Cambridge Bay, NU) ». Cet article sera soumis au cours de l'automne 2025.

Les données présentées dans ce mémoire ont été recueillies lors d'une campagne d'échantillonnage à Cambridge Bay (NU, Canada) du 25 juillet au 31 août 2023. J'ai organisé et participé activement à cette campagne grâce à une bourse du Programme de Formation Scientifique dans le Nord (PFSN), et ce, accompagnée de ma directrice de recherche (Gwénaëlle Chaillou) et de mon codirecteur (Alfonso Mucci). Nous avons échantillonné, à chacune des 28 stations désignées, les paramètres inorganiques caractérisant la chimie des carbonates (pH sur l'échelle totale, TA et DIC), les paramètres organiques (DOC, TDN, CDOM, DOMt) ainsi que d'autres paramètres connexes (isotopes stables de l'eau, $\delta^{18}O$ et $\delta^{2}H$, nutriments, métaux traces). Nous avons également récolté des échantillons de radon et de radium et des traceurs des écoulements souterrains en milieu côtier, pour Laisa Ramos Peixoto, candidate au doctorat à l'ISMER-UQAR. Lors de mon séjour, en plus d'assister l'équipe sur le terrain à l'installation et l'entretien d'instruments (e.g. RBR, piézomètres, ADCP, station météorologique, etc.), j'ai eu la chance de présenter mes travaux de recherche au Young Leaders' Summit on Northern Climate Change 2023 qui se tenait à Cambridge Bay.

J'ai effectué les analyses de TA, par titrage acido-basique, et de pH, par potentiométrie, dans le laboratoire de la SCREA directement à Cambridge Bay. Les autres échantillons ont été transportés à l'UQAR afin d'être analysés au cours de l'automne 2023 et de l'hiver 2024. J'ai analysé les échantillons de DIC, de calcium dissous et de NCA dans le laboratoire de chimie de l'UQAR à l'aide respectivement d'un analyseur de DIC, d'un spectromètre d'émission atomique par plasma micro-ondes (MP-AES) et d'un titrateur automatique accompagné d'un dosimètre. J'ai également analysé les échantillons de CDOM

par spectrométrie UV-vis dans le Laboratoire d'optique aquatique et de télédétection (AquaTel) de Simon Bélanger de l'UQAR. Les nutriments (phosphate, silicate, nitrite, nitrate) ont été analysés par Pascal Rioux à l'UQAR-ISMER. Les isotopes stables de l'eau ($\delta^{18}O$, $\delta^{2}H$) ont été analysés par Jean-François Hélie au Laboratoire de géochimie des isotopes stables légers (GEOTOP-UQAM, Montréal, QC, Canada).

Au cours de ma maitrise, j'ai eu l'opportunité de participer à deux missions en mer. Tout d'abord, la mission PLAINE du Réseau Québec Maritime (RQM) s'est déroulée du 5 au 12 juillet 2023 à bord du Coriolis II où j'ai assisté à la collecte et à l'analyse d'échantillons biogéochimiques (DIC, N_2/Ar, pH, oxygène dissous, nutriments, etc.). Le but de celle-ci était d'acquérir et de mettre à jour les données quant aux impacts de la navigation commerciale sur les écosystèmes du fleuve Saint-Laurent (Qc, Canada). J'ai également eu la chance de participer à la mission du programme de recherche Transformer l'Action pour le Climat (TCA) qui s'est tenue du 3 au 20 octobre 2024 à bord du brise-glace de la garde côtière canadienne NGCC Amundsen. Cette mission visait à récolter des échantillons d'eau de mer pour l'analyse de N_2/Ar et de N_2O afin de comprendre le cycle de l'azote dans différentes masses d'eau de la Baie de Baffin, en collaboration avec le professeur Jean-Éric Tremblay de l'Université Laval. J'ai également eu le privilège d'approfondir mes compétences et mes connaissances sur la caractérisation moléculaire de la DOM lors d'un séjour de recherche appliquée à l'Université d'Oldenburg (Allemagne) afin d'analyser mes échantillons à l'aide d'un FT-ICR-MS. Ce séjour s'est effectué du 25 mars au 12 avril 2024 en collaboration avec Dr. Michael Seidel de l'Institute for Chemistry and Biology of the Marine Environment. De plus, j'ai eu la possibilité de retourner à Cambridge Bay, du 27 juin au 11 juillet 2024, afin de récolter des échantillons, majoritairement de radon et de radium, pour une candidate au doctorat qui débutera à l'hiver 2025 et dont la recherche portera sur les décharges souterraines dans les environnements côtiers arctiques. J'ai rédigé ce mémoire avec le soutien de ma directrice, Gwénaëlle Chaillou, de mon codirecteur, Alfonso Mucci, et de ma codirectrice, Stephanie Kusch et avec la collaboration de la chercheuse Stéphanie Coulombe.

CHAPITRE 1
CARACTERISATION DE LA CHIMIE DES CARBONATES ET COMPOSITION DE LA MATIERE ORGANIQUE DISSOUTE DES EAUX SUPRAPERGÉLISOL DANS LE CONTINUUM TERRE-À-OCÉAN CÔTIER ARCTIQUE (CAMBRIDGE BAY, NU)

1.1. RÉSUMÉ EN FRANÇAIS DU PREMIER ARTICLE

Le pergélisol côtier arctique, représentant 34 % du littoral mondial, est de plus en plus affecté par des processus induits des changements climatiques, tels que la modification des régimes hydrologiques, l'épaississement de la couche active, l'érosion côtière accélérée et l'élévation du niveau de la mer. Par l'intermédiaire des eaux souterraines suprapergélisol, qui circulent dans la couche active dégelée, d'importantes quantités de carbone réactif, incluant du carbone organique dissous (DOC) labile, de la matière organique dissoute (DOM), de la matière organique particulaire (POM) et des nutriments, peuvent être mobilisées et exportées vers l'océan côtier à travers les sédiments perméables des plages. Au sein de l'estuaire souterrain (STE), où les eaux douces continentales interagissent avec les eaux marines, ces composés subissent des transformations biogéochimiques et un mélange physique. Ces processus peuvent modifier la composition moléculaire de la DOM, favoriser le dégazage du CO_2 et influencer les paramètres du système des carbonates tels que le pH, l'alcalinité totale (TA) et le carbone inorganique dissous (DIC). La contribution des eaux souterraines suprapergélisol aux flux de carbone et à la dynamique acido-basique des eaux côtières arctiques demeure toutefois peu documentée. Comprendre ces transformations est donc essentiel afin de quantifier la capacité tampon des zones côtières face à l'acidification des océans.

Cette étude caractérise le rôle des eaux souterraines suprapergélisol dans la modulation de la chimie des carbonates et de la composition de la matière organique dissoute (DOM) le long d'un continuum terre-à-océan côtier, près d'Iqaluktuuttiaq (Cambridge Bay, Nunavut, Canada). En combinant des traceurs isotopiques stables, des mesures du système des carbonates et une caractérisation moléculaire de la DOM par spectrométrie de masse à ultra-haute résolution (FT-ICR-MS), nous présentons un aperçu détaillé des gradients géochimiques entre les eaux douces continentales et l'eau de mer de surface. Nos résultats révèlent une forte diminution de la pCO_2 le long du gradient de salinité, passant de 5155 µatm à 306 µatm, suggérant un important dégazage de CO_2 lors du déversement dans le STE et une exportation limitée du DIC, issu du pergélisol, vers les eaux côtières. Les concentrations en DOC diminuent significativement entre les eaux douces et les eaux marines (de 1918 µmol kg^{-1} à 62 µmol kg^{-1}), accompagnées de modifications de la composition moléculaire de la DOM vers des structures moins aromatiques et plus aliphatiques, suggérant une minéralisation hétérotrophe dans les sédiments de plage. Malgré une forte variabilité moléculaire, la composition de la DOM semble exercer une influence plus limitée sur les paramètres du système des carbonates que la concentration en DOC. Ces résultats mettent en évidence le rôle des plages arctiques comme filtres biogéochimiques actifs, régulant les flux de carbone inorganique et organique lors du déversement des eaux souterraines, et renforçant la résilience des eaux côtières face à l'acidification des océans.

Cet article, intitulé « Suprapermafrost Groundwater Carbonate Chemistry and Dissolved Organic Matter Composition along An Arctic Land-to-Coastal Ocean Continuum (Cambridge Bay, NU) » a été rédigé par moi-même et révisé par les professeures Gwénaëlle Chaillou et Stephanie Kusch ainsi que le professeur émérite Alfonso Mucci. Les données issues de ce projet ont été présentées sous forme d'affiche scientifique lors d'un congrès national et d'un congrès international :

C-A. Guay, G. Chaillou, S. Kusch, A. Mucci, S. Coulombe : *Influence de l'alcalinité organique sur la capacité tampon des eaux côtières arctiques de la région de Kitikmeot au Nunavut*. Réunion Scientifique Annuelle Québec-Océan, Rivière-du-Loup, Canada.

C-A. Guay, G. Chaillou, S. Kusch, M. Seidel, A. Mucci : *Characterization of Terrestrial Dissolved Organic Matter within the Permafrost-Coastal Ocean Continuum.* ArcticNet's Arctic Change 2024, Ottawa, Canada.

1.2. SUPRAPERMAFROST GROUNDWATER CARBONATE CHEMISTRY AND DISSOLVED ORGANIC MATTER COMPOSITION ALONG AN ARCTIC LAND-TO-COASTAL CONTINUUM (CAMBRIDGE BAY, NU)

Carole-Anne Guay[1], Gwénaëlle Chaillou[1], Alfonso Mucci[2], Stephanie Kusch[1], Stéphanie Coulombe[3-4], David Didier[4], Michael Seidel[5]

[1] Québec-Océan, Institut des Sciences de la Mer, Université du Québec à Rimouski, 310 Allée des Ursulines, Rimouski, Québec, G5L 3AL, Canada.
[2] Department of Earth and Planetary Science and Geotop Research Centre, McGill University, 3450 University Street, Montréal, QC, H3A 0E8, Canada.
[3] Polar Knowledge Canada, Government of Canada, 1 Uvajuq Place, Cambridge Bay, Nunavut, X0B 0C0, Canada.
[4] Département de Biologie, Chimie et Géographie, Université du Québec à Rimouski, 300, allée des Ursulines, Rimouski, G5L 3A1, Canada.
[5] Research Group for Marine Geochemistry, Institute for Chemistry and Biology of the Marine Environment (ICBM), University of Oldenburg, 26129 Oldenburg, German

1.2.1. Abstract

Arctic coastal permafrost, which accounts for 34% of the world's coastline, is increasingly affected by climate-driven processes such as altered hydrological regimes, thickening of the active layer, accelerated coastal erosion and rising sea levels. Through suprapermafrost groundwater flowing within the seasonally thawed active layer, large quantities of reactive carbon, including labile dissolved organic carbon (DOC), dissolved organic matter (DOM), particulate organic matter (POM), and nutrients, can be mobilized and discharged into the coastal ocean via permeable beach sediments. Within the subterranean estuary (STE), where continental freshwater interacts with marine waters, these compounds are subject to biogeochemical transformations and physical mixing. These processes can alter the molecular composition of DOM, enhance CO_2 degassing, and influence carbonate system parameters such as pH, total alkalinity (TA), and dissolved inorganic carbon (DIC). The contribution of suprapermafrost groundwater to carbon fluxes and acid–base dynamics in Arctic coastal waters, however, remains poorly documented.

Understanding these transformations is therefore essential for quantifying the coastal buffering capacity against ocean acidification.

This study characterizes the role of suprapermafrost groundwater in modulating carbonate chemistry and DOM composition along a land-to-coastal ocean continuum near Iqaluktuuttiaq (Cambridge Bay, Nunavut, Canada). By combining stable isotope tracers, carbonate system measurements, and DOM molecular characterization through ultrahigh-resolution mass spectrometry (FT-ICR-MS), we provide a detailed overview of geochemical gradients from inland freshwater to surface seawater. Our results show a sharp decrease in pCO_2 along the salinity gradient, from 5155 µatm to 306 µatm, suggesting substantial CO_2 degassing upon discharge into the STE and limited export of permafrost-derived DIC to coastal waters. DOC concentrations decline significantly from freshwater to marine waters (from 1918 µmol kg^{-1} to 62 µmol kg^{-1}), accompanied by shifts in DOM molecular composition toward less aromatic, more aliphatic structures, indicative of heterotrophic mineralization within beach sediments. Despite high molecular variability, DOM composition appears to have a limited influence on carbonate parameters compared to DOC concentration. These findings underscore the function of Arctic beaches as active biogeochemical filters, regulating both inorganic and organic carbon fluxes during groundwater discharge and enhancing the resilience of coastal waters to acidification.

1.3. INTRODUCTION

The Arctic is warming four times faster than the global average, subjecting terrestrial and coastal permafrost to an increasing combination of thermal and mechanical stresses. These include altered hydrological regimes, thickening of the active layer, accelerated coastal erosion, rising sea levels, warmer ground and seawater temperatures, more intense storm events and reduced sea-ice extent (Günther et al., 2015; Jones et al., 2009; Rawlins & Karmalkar, 2023; Schuur et al., 2015). Permafrost, defined as ground that remains at a temperature of 0°C or less for at least two consecutive years (Permafrost Subcommittee, 1988), is widespread in the Arctic and boreal regions of the Northern Hemisphere. It consists of a variety of materials, including mineral and organic soil and rock, and often contains significant amounts of ground ice. It has accumulated vast stocks of inorganic compounds, both particulate and dissolved organic matter (POM and DOM), as well as other substances (French, 2017). Permafrost is estimated to store twice as much carbon as the atmosphere and about 60% of the world's organic carbon reservoir (Obu et al., 2019; Tarnocai et al., 2009; Zimov et al., 2006). This ancient organic carbon pool, which accumulated during the Pleistocene, is globally estimated at 1,000 ± 200 PgC within the top three meters of permafrost (Gorham, 1991; Hugelius et al., 2014; Mishra et al., 2021; Schuur et al., 2015; Zimov et al., 2006).

The omission of terrestrial permafrost in global climate models (GCMs) has been shown to underestimate climate projections, particularly due to its potential to emit carbon dioxide (CO_2) and methane (CH_4) (Burke et al., 2012; Koven et al., 2011). As climate-driven changes, such as warming temperatures, increased snow cover and precipitation, and altered soil moisture, deepen the active layer, permafrost releases labile dissolved organic carbon (DOC) that can fuel microbial respiration and greenhouse gas production (GHGs), a process further stimulated by rising ambient temperatures (Dutta et al., 2006; Knoblauch et al., 2018; Schädel et al., 2016; Schuur et al., 2015; Zimov et al., 2006). Whereas many climate models include this so-called “permafrost-carbon feedback” (e.g., Lee et al., 2023), most climate projections overlook the fate of coastal permafrost, as it remains understudied due to the

inherent sampling challenges, including its inaccessibility by research vessels, the lack of coastal infrastructure, and the high associated costs (Fritz et al., 2017). Coastal permafrost accounts for 34% of the world's coastline and experiences an average global erosion rate of 0.5 m yr^{-1}, a rate that could increase by a factor of 2–3 by 2100 (Lantuit et al., 2012, 2013; Nielsen et al., 2022; Philipp et al., 2023). In certain regions of the Arctic, erosion rates are higher, reaching 1.1 m yr^{-1} in the Beaufort Sea area (Philipp et al., 2023) and between 5.3–28.4 m yr^{-1} at Nutepel'men in Eastern Siberia (Wang et al., 2022).

As coastal degradation and erosion intensify, the release of metabolic carbon dioxide to the atmosphere (degassing) and the lateral remobilization (transport) of carbon, DOM, POM, and nutrients to coastal waters via coastal erosion and/or suprapermafrost groundwater flow also increase (Romanovsky & Osterkamp, 2000; Walvoord & Striegl, 2007; Fritz et al., 2017; Lizotte et al., 2022; Lecher, 2017). Suprapermafrost groundwater refers to water that flows through the seasonally thawed active layer and unfrozen coastal sediments and undergoes annual freeze-thaw cycles (Permafrost Subcommittee, 1988). As groundwater flows toward coastal waters, guided by hydraulic gradients, remobilized compounds undergo various biotic (e.g., redox transformations) and abiotic (e.g., adsorption and co-precipitation on solid surfaces, degassing) processes that control export fluxes to the ocean (Sawyer et al., 2016). Globally, Wegner et al. (2015) estimated that ~14 Tg of organic carbon is released annually into coastal waters through coastal erosion. More recently, Connolly et al. (2020) and Kipp et al. (in revision) estimated that daily groundwater discharge to the Beaufort Sea ranges from 400 to 2,100 m^3 of freshwater from June to October, when the active layer reaches its maximum depth.

Suprapermafrost groundwater carries various biologically reactive compounds (e.g., nitrogen, phosphorus, trace metals, organic and inorganic carbon) and discharges them into the coastal ocean through permeable beach sediments (Connolly et al., 2020; Demir et al., 2024; Flamand et al. (in revision); Kipp et al. (in revision); Lecher, 2017). Yet, biogeochemical processes in beach sediments remain poorly understood, particularly in the Arctic (Connolly et al., 2020; Lecher, 2017). Along the land-to-coastal ocean continuum,

beaches act as mixing zones where continental groundwater and marine surface water interact, forming a subterranean estuary (STE) (Moore, 1999; Santos et al., 2009). Whereas beaches have long been considered geochemically poor environments (Boudreau et al., 2001; Huettel et al., 1996), recent studies suggest that sandy beaches, although poor in POM, are a locus of advective transport and rapid organic matter (OM) decomposition (Anschutz et al., 2009; Chaillou et al., 2024; Charbonnier et al., 2022; Jickells & Rae, 2005; Riedl & Machan, 1972). Through advection of fluids driven by pressure gradients generated by tides and waves, marine DOM inputs control beach biogeochemistry and mineralization processes within the STE (Anschutz et al., 2009; Charbonnier et al., 2022; Kim et al., 2012; McLachlan & Brown, 2006; Robinson et al., 2018). Recent studies, however, point to the importance of terrigenous inputs to coastal systems via groundwater flow (Beck et al., 2007; Chaillou et al., 2016; Couturier et al., 2016; Linkhorst et al., 2017; Seidel et al., 2014; Sirois et al., 2018). In unfrozen coastal sediments, terrigenous organic carbon inputs can undergo microbial mineralization (Chaillou et al., 2024; Liu et al., 2017) and/or sequestration (Linkhorst et al., 2017; Sirois et al., 2018). In some cases, these compounds, along with the metabolites resulting from in-situ transformations, serve as major sources of nutrients and carbon to coastal waters (Anschutz et al., 2009; Moore, 1999, 2010; Robinson et al., 2018) and may be an overlooked control on coastal eutrophication and acidification (Chaillou et al., 2024; Kwon et al., 2017; Liu et al., 2017; Maher et al., 2013; Santos et al., 2011). Accordingly, the biogeochemical role of beaches in regulating carbon discharge from suprapermafrost groundwater and, thus, its impact on the coastal seawater carbonate system remains poorly studied (Demir et al., 2024; Lecher, 2017).

The characterization of the carbonate system helps to quantify and understand the effects of ocean acidification on marine ecosystems. This system is typically assessed using two of the following four analytical parameters: dissolved inorganic carbon (DIC) concentration, total alkalinity (TA), pH, and the fugacity [fCO_2] or partial pressure of CO_2 (pCO_2) of the water (Dickson et al., 2007; Zeebe et al., 2001). The degree of saturation of waters with respect to calcium carbonate ($CaCO_3$) minerals, which can be derived from these parameters provides a measure of the potential deleterious impact of ocean acidification (OA)

on calcifying organisms (Raven et al., 2005; Orr et al., 2005). The fCO_2 or pCO_2 of surface waters determines whether a water mass is a sink or a source of CO_2 to the atmosphere (Takahashi et al., 1997).

As outlined above, coastal permafrost environments are a major source of terrigenous DOM (DOMt or allochthonous DOM). This input can influence the salinity, pH, turbidity, primary production, and respiration rates in coastal seawater (Connelly et al., 2015). DOMt concentrations in coastal waters are modulated by several processes, including microbial activity, photodegradation, and incorporation into sediments (Hansell et al., 2014; Lalonde et al., 2014). A fraction of the DOMt escaping degradation can potentially contribute positively (Song et al., 2020) or negatively (Delaigue et al., 2020) to TA (Egleston et al., 2010; Kerr et al., 2023; Kuliński et al., 2014). DOMt transformation and degradation within the STE can alter its acid-base relevant ions which regulates the pH of coastal seawater and controls the pH buffering capacity of water against CO_2 inputs (Chaillou et al., 2024; Kuliński et al., 2014). Hence, understanding the influence of DOM and DOMt on the acid-base balance is crucial to assess the ability of Arctic coastal environments to buffer atmospheric CO_2 fluctuations. This is especially important at high latitudes since the higher solubility of CO_2 in cold waters makes these ecosystems particularly sensitive to changes in the carbonate chemistry (Cai et al., 2021; Hoppe et al., 2012). Given the ongoing effects of climate change on the global carbon budgets (NOAA, 2024), there is an urgent need to comprehensively characterize and quantify this lateral and non-point source of carbon within Arctic coastal budgets.

This study aims to characterize the role of suprapermafrost groundwater in modulating carbonate chemistry and DOM composition along an Arctic land-to-coastal ocean continuum near Iqaluktuuttiaq (Cambridge Bay, Nunavut, Canada). We provide a comprehensive overview of carbonate system dynamics and DOM molecular composition from terrestrial freshwater to marine coastal waters. Specifically, we 1) characterize spatial variations in carbonate system parameters along the continuum, 2) assess the buffering capacity of suprapermafrost groundwater and identify potential sources and processes

affecting this capacity and, finally 3) characterize DOM composition along the flow path and explore its potential influence on carbonate chemistry.

1.4. METHODS

1.4.1. Site Description – Cambridge Bay

The study area is located about 20 km from Iqaluktuuttiaq, on southern Victoria Island, in the Kitikmeot region of Nunavut, Canada (Figure 5). For the 1991-2020 period, the mean annual air temperature was -13.3 °C and the annual mean precipitation was 150 mm, nearly half of which fell as rain from May to October (Environment Canada, 2025). Summers are short and cold, with a mean air temperature of 9.4°C in July, whereas winter months are long and frigid with a mean air temperature of -32.1°C in February. The area is underlain by Cambrian-Silurian carbonate and siliciclastic bedrock (Kemp et al., 2006). The surficial geology consists of raised marine terraced beach and nearshore sediments, with sandy deposits overlying fine-grained marine sediments (silt to sandy silt and clay) that were deposited in deeper waters (Sharpe, 1993; Gagnon et al. (submitted.)). Permafrost is continuous, with an estimated thickness of at least 100–500 m (Smith & Burgess, 2002). In 2022 and 2023, the active layer reached its maximum depth (~ 100 cm) in late August to early September, as estimated by linearly interpolating the ground temperature profile between two adjacent points above and below the 0°C isotherm (Gagnon et al. (submitted)). The marine terrace has a generally low organic matter content, except in patchy buried peat lenses. Its vertical sediment matrix includes a thin surface organic layer (>5 cm), underlain by medium to coarse sand, with fragments of shells, and a deeper layer of sandy clayey silt (Gagnon et al. (submitted)). The seaward extent of the permafrost and its transition to submarine permafrost in this area are unknown. Nevertheless, the coastal landscape is characterized by ice-rich permafrost, high coastal bluffs and beaches, which are impacted by various degradation processes, including coastal erosion, gullying, and permafrost thaw, likely influencing the geomorphology and sediment budget of the shoreline.

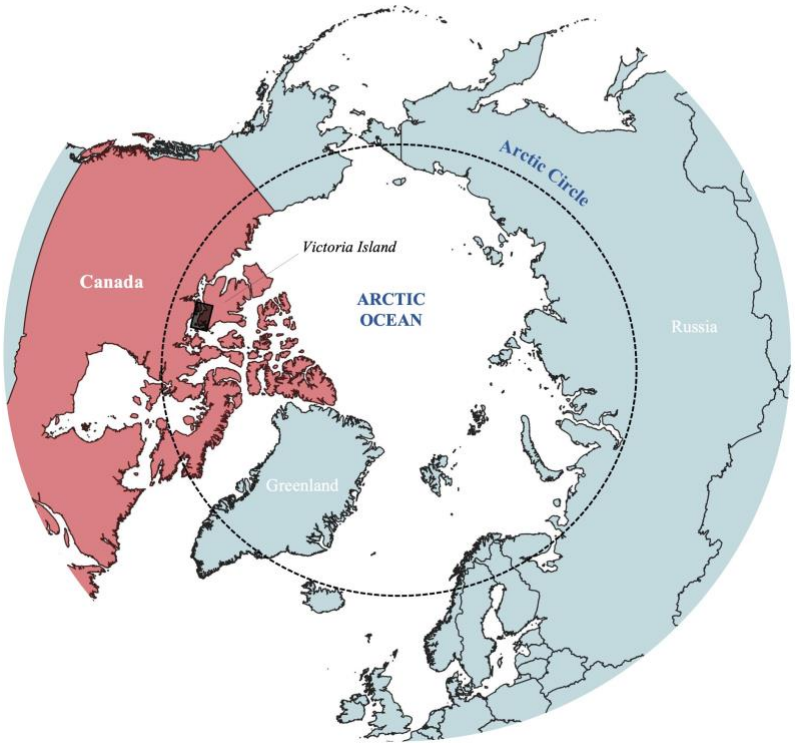

Figure 5. Location of Cambridge Bay (black square) on Victoria Island (Nunavut, Canada) north of the Arctic Circle (black dashed line).

The three sampling sites (Augustus Hill, Longpoint River [a name assigned for this study] and Longpoint) were selected along the coast due to the presence of beaches or eroding bluffs (Figure 6A). Augustus Hill is a key transition zone for members of the Iqaluktuuttiaq community to access traditional fishing and hunting grounds. The Ekaluktutiak Hunters & Trappers Organization has identified this zone as a significant hotspot of coastal erosion. It features a large lake about 2 km inland, delimited from the coastal environment by glaciofluvial sediments. The coastal zone is characterized by permafrost cliffs (~3 to 5 m high). As shown in Figure 6B, the coastline hosts multiple gullies perpendicular to the shoreline that flow onto the beach. The beach is a narrow stretch (~1 to 5 m) of material eroded from the cliffs and rapidly remobilized by waves, tides, alongshore currents, and sea ice. The sedimentary origin of the beach is poorly documented. The Longpoint River mainly drains freshwater from lakes and streams in its upper reaches. All sampling sites were located within 1 km from shore. The area features bluffs composed of thawed permafrost material

(Figure 6C) and a mixing zone influenced by tidal seawater intrusion. The Longpoint site is divided into two areas. The first area consists of a large sand spit with a shallow intertidal zone located approximately 800 meters from shore (Figure 6D). The second area is a flowing stream with a distinct brown color (Figure 6E).

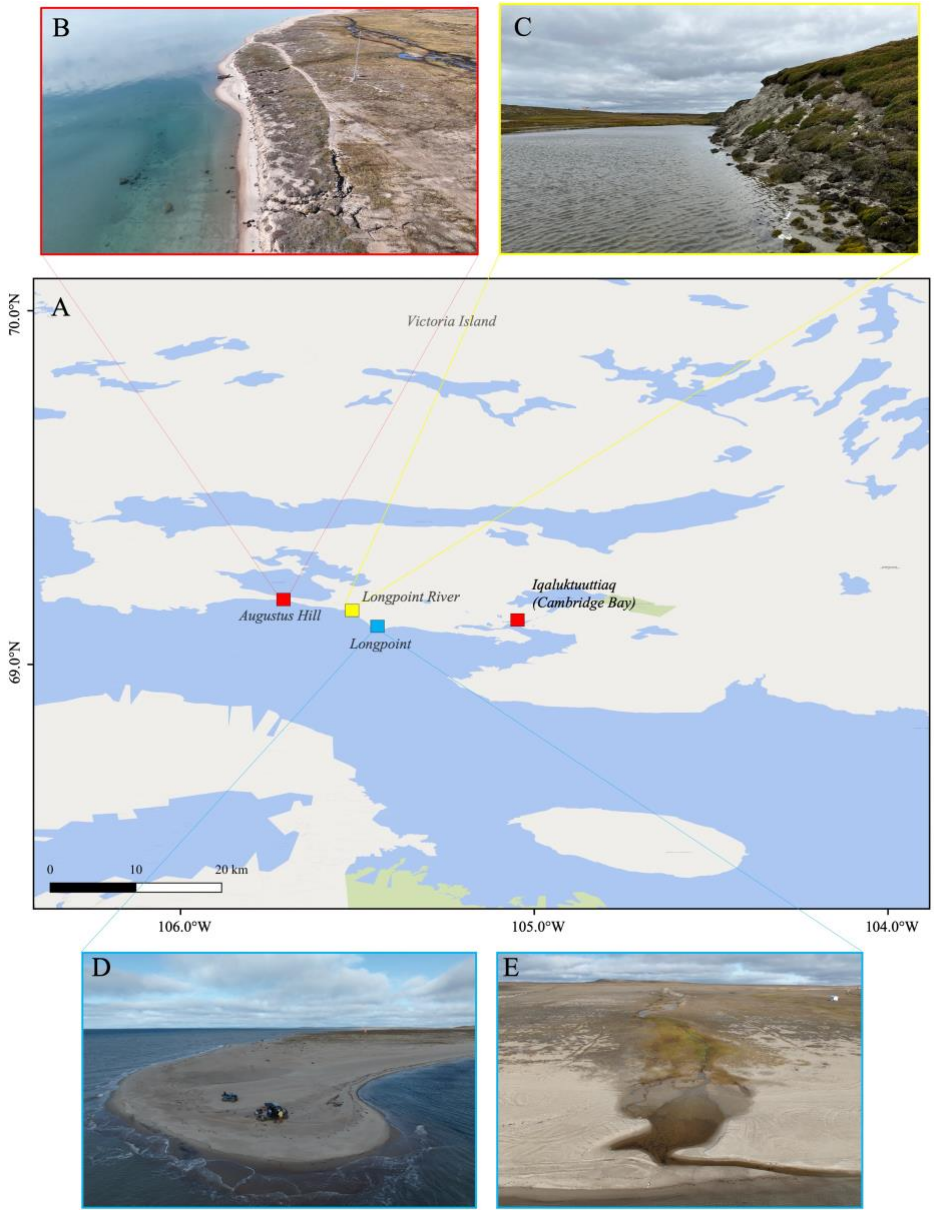

Figure 6. Map of sampling sites in the Cambridge Bay area on Victoria Island (A) in Nunavut, Canada. Sampling sites are marked with squares: B) Augustus Hill, C) Longpoint River, and D-E) Longpoint.

1.4.2. Water and Sediment Core Sampling

A total of 29 discrete samples of supernatant water (SNW), suprapermafrost groundwater in the active layer (hereafter referred to as "active layer groundwater" [ALG]), beach porewater (hereafter referred to as "beach groundwater" [BG]), and surface seawater (SSW) were collected at the three study sites. The distribution of samples at each of the sites and the geochemical characteristics of each sample type are reported in Table 1. At the Augustus Hill site, two frozen sediment cores were retrieved using a portable core drill (Husqvarna DM230) equipped with an 8-cm diameter core barrel. The first core was extracted from a depth interval of 0.31 to 0.41 m [hereafter referred to as the top core], and the second core was extracted from a depth of 0.42 to 0.60 m [hereafter referred to as the bottom core]. Each core was immediately placed in a separate Ziploc® bag and allowed to thaw and decant overnight at room temperature. The following day, SNW was sampled using a Solinst® peristaltic pump. Only samples for parameters that are independent of gas exchange and require a small analytical volume were sampled for: total alkalinity (TA), dissolved organic carbon (DOC), chromophoric dissolved organic matter (CDOM), stable oxygen and hydrogen isotopes ($\delta^{18}O$ and $\delta^{2}H$) of the water. ALG was sampled by digging holes above the frozen surface (~20 to 60 cm below the soil surface) and allowing them to fill with flowing groundwater. The entire volume of water was purged three times through a Teflon tube using a Solinst® peristaltic pump prior to collection to minimize contact of the collected water with the atmosphere. BG was pumped from the beach sediments (~50 cm deep) using a push-point piezometer connected to a peristaltic pump by a Teflon tube. SSW (<1 m below the sea surface) was pumped continuously through a Teflon tube connected to a portable submersible pump that was manually deployed from shore or a small boat. At each site, water samples were pumped into an on-line flow cell where practical salinity (S_P) and temperature (T) were monitored using a daily calibrated multiparametric probe (600QS, YSI Inc.).

Once the S_P and T measurements were stable, water for DIC, pH, and TA analyses was filtered through a 0.45 µm airtight GWV® cartridge and transferred into vials that had been acid-washed and soaked in Milli-Q water overnight to eliminate traces of residual acid. DIC samples were collected in 30 mL borosilicate glass vials after rinsing several times and sealed with a rubber stopper secured by a crimp-seal aluminum cap. Upon returning to the research station laboratory and within 10 hours of sampling, 0.1 mL of a saturated mercuric chloride ($HgCl_2$) solution was injected through the stopper. TA samples were collected in 120 mL narrow-mouth amber glass bottles, tightly sealed with a rubber stopper and a crimp-seal aluminum cap. No preservative was added to the TA samples as the conventional preservation method with mercuric chloride solution can alter the alkalinity of non-marine water samples (Mos et al., 2021). The TA analyses were performed within 24 hours of sampling. Samples for pH analysis were collected in 120 mL narrow-mouth HDPE bottles after multiple rinses and sealed with an HDPE screw cap. Duplicate samples of DOC and TDN were collected using acid-cleaned 60 mL polypropylene syringes and filtered through pre-combusted 0.7 µm glass fiber filters. The filtered samples were acidified to pH < 2 using high-purity HCl (36.5–38.0%) in borosilicate EPA tubes with PTFE caps. Samples for CDOM, DOM, and total dissolved calcium were collected after on-line filtration through a 0.22 µm Millipore Opticap® XL4 cartridge equipped with a Durapore® membrane. CDOM samples were collected in acid-washed 60 mL glass amber bottles, sealed with Parafilm M® and rapidly stored in the dark. DOM samples were collected in 500 mL HDPE narrow-mouth bottles that had been pre-rinsed with pH 2 Milli-Q water and acidified with 1.3 mL of 25% HCl. Total dissolved Ca samples were collected in 50 mL metal-free Falcon® tubes and acidified with 0.1 mL of 70% nitric acid. Nutrient samples were collected using 60 mL acid-cleaned polypropylene syringes and rapidly filtered through a 0.2 µm cellulose acetate filter into duplicate 15 mL Falcon® tubes. Samples for stable oxygen and hydrogen isotope analyses were both collected in 30 mL HDPE scintillation vials with polypropylene caps without filtration and hermetically sealed with Parafilm M®. All samples were placed in a hermetically sealed box with ice packs for transport to the Canadian High Arctic Research

Station (CHARS) (max ~10 hours) and stored at room temperature (DIC, TA, stable isotopes), 4°C (DOC, CDOM, DOM, Ca) or -80°C (nutrients) until analysis.

1.4.3. Carbonate System Parameter Analyses

pH (NBS and total proton concentration scale)

Upon arrival at the CHARS laboratories, pH samples were placed in a temperature-controlled water bath at 25°C for a minimum of 25 minutes. Potentiometric pH determinations were then performed rapidly using a WTW® ProfiLine pH 3310 pocket meter connected to a SenTix® HWS electrode (measurement accuracy: ± 0.05 pH). The electrode was calibrated prior to and after each daily set of measurements (~ 5 samples) using NIST-traceable buffer solutions (4.00, 7.00, and 10.00 at 25ºC) as well as with TRIS buffers of assigned values (Millero, 1986) prepared at various practical salinities (5, 15, or 20). Following this approach, pH values for samples with salinities below 5 were initially reported on the NBS (or NIST, pH_{NBS}, infinite dilution convention) scale and later converted to the total proton scale (pH_T, see *Calculations* section below), whereas samples of higher salinity were directly measured on the total proton scale (constant ionic medium convention). In the latter case, the Nernstian slope was obtained by least-squares fitting of the electrode response to the NBS buffer values and pH_{NBS} was converted to pH_T according to its response to the TRIS buffer solutions of closest practical salinity.

Total Alkalinity (TA) and measured Organic Alkalinity (Org-Alk_m)

The standard definition of TA only considers inorganic alkalinity, including the carbonate alkalinity (Ac, Eq. 12) and the alkalinity of dissolved borates, phosphates, and silicates (Boyd, 2015; Dyrssen & Sillén, 1967). Whereas this standard definition is adequate for the open ocean, it is not suitable for coastal environments where DOMt, a mixture composed of humic acids and organic substances, can act as proton acceptors or donors (Kuliński et al., 2014; Martell-Bonet & Byrne, 2023). This alkalinity, referred to as organic

alkalinity (Org-Alk), can positively (Song et al., 2020) or negatively (Delaigue et al., 2020) contribute to TA (Egleston et al., 2010; Kerr et al., 2023; Kuliński et al., 2014), potentially biasing the interpretation of the buffering capacity of a water body as well as the assessment of other carbonate system parameters (Abril et al., 2015; Dickson, 1981; Kerr et al., 2021; Kim & Lee, 2009; Yang et al., 2015). Therefore, a complete definition of TA includes both organic and inorganic bases, as well as acids, as described in equation 13. Given the significant global stock of organic carbon stored in permafrost (Mishra et al., 2021; Schuur et al., 2015) and its potential release in dissolved form upon thawing, we directly measured both the TA and Org-Alk_m of our filtered samples.

$$Ac = [HCO_3^-] + 2[CO_3^{2-}] + [OH^-] - [H^+] \quad \text{(Eq. 12)}$$

$$TA = [HCO_3^-] + 2\,[CO_3^{2-}] + [OH^-] + [B(OH)_4^-] + [H_3SiO_4^-] + [HS^-] + [HPO_4^{2-}] + 2[PO_4^{3-}] + [NH_3] + [HSO_4^-] - [H^+] - [HF] + [Org\text{-}Alk] \quad \text{(Eq. 13)}$$

TA analyses were conducted in the CHARS laboratories within a few hours of sample collection by open-cell titration with an automated Radiometer Analytical TitraLab® 865 (measurement accuracy: ± 0.001 pH, ± 0.1 mV, ± 0.1°C) potentiometric titrator and a Red Rod® combination pH electrode (pHC2001). A dilute HCl titrant was calibrated before, during, and after each titration session using certified reference materials (CRM – Batch 72) provided by Andrew Dickson (Scripps Institution of Oceanography). The raw data were processed using a proprietary algorithm designed for shallow endpoint detection. Method reproducibility was better than 0.1% based on replicate analyses of samples. After TA analysis, acidified samples were stored at 4°C until organic alkalinity determination (Org-Alk_m, Eq. 14), defined as the sum of non-carbonic alkalinity (NCA) and non-carbonic inorganic bases (N-CIBs, Eq. 15) (Lukawska-Matuszewska, 2016). N-CBIs were calculated as the sum of phosphate, silicate and borate alkalinity contributions, as calculated by the CO_2SYS program (Pierrot et al., 2011) using their total dissolved concentrations and pH as input parameters. NCA analyses were performed using an open-cell back titration procedure with a Metrohm® 848 Tritino plus (measurement accuracy: ± 0.003 pH, ± 0.2 mV, ± 0.2 °C) with a 0.0100N HCl titrant and a Metrohm® 665 Dosimat containing a sodium hydroxide

solution (0.0100N NaOH), as described by Dickson et al. (2003). Purified nitrogen gas was continuously sparged through the samples during the measurements.

$$\text{Org-Alk}_m = \text{NCA} - \text{N-CBIs} \qquad \text{(Eq. 14)}$$

$$\text{N-CBIs} = [HPO_4^{2-}] + 2\,[PO_4^{3-}] + [NH_3] + [HS^-] + [B(OH)_4^-] + [HSO_4^-] - [H_3PO_4] \qquad \text{(Eq. 15)}$$

Dissolved Inorganic Carbon (DIC)

DIC samples were analyzed at the Institut des Sciences de la mer (ISMER) de l'Université du Québec à Rimouski (UQAR) using an Apollo SciTech® DIC Multi-Sample Analyzer (measurement accuracy: ± 2 µM/kg), following the protocol described by Dickson et al. (2007). Briefly, after thermal equilibration at 25°C, 1 mL of a 10% phosphoric acid (H_3PO_4) solution was injected into 3.000 mL of sample that had been introduced into the instrument's reactor. The evolved CO_2 was carried to a LI-COR® LI-7815 infrared analyzer (measurement accuracy: ±0.04 ppm) by a stream of pure nitrogen. Measurements were calibrated with a certified reference material (CRM – Batch 72) provided by Andrew Dickson of the Scripps Institution of Oceanography (San Diego, USA).

1.4.4. Dissolved Organic Matter Analyses

Chromophoric Dissolved Organic Matter (CDOM)

Analyses were performed on a Lambda 850 UV-VIS PerkinElmer spectrophotometer (measurement accuracy: ±0.09 nm) at UQAR one month after collection. Subsamples were transferred into a 1 cm path-length quartz cuvette to measure the absorbance of CDOM (aCDOM) in the UV-visible spectra (220 to 800 nm) at 1 nm intervals, at a scanning speed of 100 $nm \cdot min^{-1}$ and a slit width of 4 nm. The blank was determined using fresh Milli-Q water that was replaced every 5 samples or used for a maximum of 30 minutes. The cuvettes were thoroughly cleaned between measurements with 5% HCl and Milli-Q water. Different CDOM absorbance metrics were calculated using a routine script with the R Studio package starDom (R Studio version 2023.12.1+402 and *starDom* package version 1.1.28 (Pucher et

al., 2019)). In this study, however, we present only the absorption coefficient aCDOM(λ) (m^{-1}), which was calculated from absorbance as 2.303 times the absorbance divided by the cuvette path length (m). The $aCDOM_{350}$ values were used as an estimate of CDOM adsorption and content.

Dissolved Organic Carbon (DOC)

DOC concentration measurements were performed at ISMER-UQAR one month after collection using a Shimadzu TOC-Vcpn analyzer (measurement accuracy: CV ≤ 3%) with a detection limit of 0.07 mg L^{-1}. Instrument stability was monitored by analyzing fresh, acidified, deionized water (blank) and a standard solution (1.02 ± 0.04 mg L^{-1}) every seven samples.

Dissolved Organic Matter (DOM)

Solid phase extraction (SPE) was performed at ISMER-UQAR three months after collection using Agilent 1 g PPL Bond Elut cartridges. Glassware and aluminum foil were pre-combusted at 450°C for four hours, and all materials used were thoroughly rinsed with pH 2 Milli-Q water. The sample volume added to the PPL columns was calculated to achieve a maximum concentration of 200 µmol C on column. DOM was then eluted using 6 mL of methanol. The samples were dried overnight at 45°C under a nitrogen stream. The dried samples were transported to the *Institute for Chemistry and Biology of the Marine Environment* (ICBM) in Oldenburg, Germany, where the extraction efficiency was assessed by measuring the DOC concentration in the PPL extracts using a Shimadzu TOC-Vcpn analyzer. The SPE extraction efficiency was determined as the ratio of the extracted DOC (SPE-DOC) to the bulk DOC in the original sample. Based on the concentration of the SPE-DOC, a predetermined volume of the sample extract was mixed in a 1:1 (v/v) methanol/ultrapure water mixture to a final volume of 1 mL. The molecular composition of the SPE-DOM was then analyzed using a solariX XR FT-ICR-MS system (Bruker Daltonik GmbH, Bremen, Germany) with a 15 Tesla superconducting magnet (Bruker Biospin, Wissembourg, France).

1.4.5. Other Chemical Analyses

Water Isotopes $\delta^{18}O$ and $\delta^{2}H$

The water $\delta^{18}O$ and $\delta^{2}H$ values were determined at the Laboratoire de géochimie des isotopes stables légers (GEOTOP-UQAM, Montréal, QC, Canada) a few months after collection. For oxygen isotopes, samples were equilibrated with purified CO_2 at 40°C for 7 hours, whereas for hydrogen isotopes, equilibration was carried out with purified H2 at 40°C for 4 hours using a hydrophobic platinum catalyst. The isotopic analyses were performed using a Micromass Isoprime isotope ratio mass spectrometer coupled to an AquaPrep system in dual inlet mode. Data were normalized against three internal reference waters, each calibrated against Vienna Standard Mean Ocean Water (V-SMOW) and Vienna Standard Light Arctic Precipitation (V-SLAP). The results are reported using the δ notation in ‰ relative to V-SMOW. Based on replicate analyses of the samples, the average standard deviation of the measurements was better than ± 0.1 ‰ for $\delta^{18}O$ values and ± 2.0 ‰ for $\delta^{2}H$ values.

Total Dissolved Calcium

Samples were analyzed using a Microwave Plasma Atomic Emission Spectroscopy system (MP-AES; measurement accuracy: ±1.45%) at UQAR, a few months after sample collection. Samples were diluted 20-fold in Milli-Q water to adjust the calcium concentration to within the linear operating range of the instrument (0-25 mg L^{-1}). After optimization, dissolved calcium was analyzed at a wavelength of 396.847 nm.

Nutrients

Nutrient analyses (soluble reactive phosphate (SRP), and dissolved silicate (DSi)) were performed with an AA500 Seal Analytical automatic analyzer (measurement accuracy: ± 1%) at ISMER-UQAR a few months after sample collection. The detection limits were 0.12 µmol/L for SRP and 0.027 µmol/L for DSi. The reproducibility of the measurements was estimated at 3.9% and 0.2% for SRP and DSi, respectively, based on replicate analyses of the same samples.

1.4.6. Calculations

NBS pH measurements of low salinity waters ($S_P < 5$) were converted to in-situ pH values on a total proton scale (pH_T) using the "pHinsi" function of the R package "seacarb" (R Studio version 2023.12.1+402 and seacarb version 3.3.3). Using the same package, pCO_2 and the saturation state of waters with respect to calcite (Ω_{cal}) and aragonite (Ω_{arag}) were calculated from DIC and pH values using the "carb" function. The saturation state of these minerals (Ω) is calculated according to equation 16, where [i] refers to the total calcium and carbonate ion concentrations and K^*_{SP} is the stoichiometric solubility constant (defined in terms of the product of the total equilibrium concentrations) of these minerals at a given temperature, salinity and 1 atm total pressure (Mucci, 1983).

$$\Omega_{c,\,a} = [Ca^{2+}]\,[CO_3^{2-}] / K^*_{SP} \qquad \text{(Eq. 16)}$$

SRP and DSi values were used exclusively as inputs to enhance the robustness of the calculations. Abril et al. (2015) demonstrated that using the pH-TA couple to calculate pCO_2 in organic matter-rich waters with a presumably significant Org-Alk contribution can result in an overestimation of pCO_2 of up to 300% compared to in-situ measurements. Therefore, the most robust pair of input parameters, DIC-pH, was recommended and used in this study for pCO_2 calculations (Hunt et al., 2011). The saturation state (Ω) of water with respect to calcite (Ω_{cal}) and aragonite (Ω_{arag}), the dominant marine $CaCO_3$ polymorphs, indicates whether the solution is undersaturated or oversaturated with respect to these minerals,

compounds secreted by several marine organisms to build their skeletons and shells (Doney et al., 2009; Kroeker et al., 2013). Calculated values of Ω_{cal} and Ω_{arag} were corrected using measured total dissolved calcium concentrations for each sample, replacing the default salinity-based estimates assumed in "*seacarb*". In addition, a principal coordinate analysis (PCoA) was conducted to further assess the influence of DOM molecular composition on organic and carbonate system parameters. A Bray-curtis dissimilarity matrix was calculated on DOM molecular data, and the resulting coordinates were correlated with selected biogeochemical parameters (TA, pH, DOC, Org-Alk_m, $aCDOM_{350}$, practical salinity, temperature).

1.5. RESULTS

1.5.1. Physicochemical and water mass properties along the continuum

Within the full dataset (N = 29), the practical salinity (S_P) ranged from ~ 0 to 18 (median of 2.28, IQR: 14.77) (Figure 7), with most ALG and SSW data clustered at the extremes ($3 > S_P > 11$) (Figure 8). S_P was not measured for SNW samples but is assumed to be ~ 0. The lowest or null values were measured in ALG samples (median of 0.19; IQR: 0.20), whereas the highest values were measured in SSW samples (median of 16.10; IQR: 1.22). BG samples exhibited the widest range of S_P, with some showing even higher salinities than adjacent SSW samples, likely due to in-situ evaporation. Temperature ranged from -3.0 to 12.5°C (median of 2.8°C, IQR: 7.5°C) and exhibited an increasing trend along the S_P gradient, with BG samples showing intermediate values (median 2.2°C, IQR: 6.2°C).

Table 1. Geochemical characteristics of the different sample types collected at the 3 study sites: supernatant water (SNW), active layer groundwater (ALG), beach groundwater (BG) and surface seawater (SSW). Median values [and interquartile range] are reported. n.d. no data available for SNW.

	Sample type			
	SNW	*ALG*	*BG*	*SSW*
Augustus Hill	*N=2*	*N=2*	*N=7*	*N=4*
River of Longpoint	-	*N=1*	*N=2*	-
Longpoint	-	*N=4*	*N=6*	*N=1*
Total	*N=2*	*N=7**	*N=15*	*N=5*
pH (total proton scale)	*n.d.***	*7.67 [0.40]*	*7.94 [0.13]*	*7.91 [0.01]*
DIC (µmol kg^{-1})	*784 [0]*	*3738 [1038]*	*2507 [1345]*	*1365 [40]*
TA (µmol kg^{-1})	*3572 [1430]*	*3702 [753]*	*2438 [1271]*	*1378 [70]*
pCO_2 (µatm)	*n.d.*	*2826 [2353]*	*778 [823]*	*424 [15]*
Ω_{cal}	*n.d.*	*0.98 [2.02]*	*1.40 [0.70]*	*1.21 [0.14]*
Ω_{ara}	*n.d.*	*0.59 [1.00]*	*0.81 [0.39]*	*0.71 [0.08]*
Ca^{2+} (mg kg^{-1})	*51*	*48 [14]*	*139 [118]*	*203 [10]*
DOC (µmol kg^{-1})	*956 [18]*	*1139 [254]*	*326 [702]*	*77 [3.75]*
$aCDOM_{350}$ (m^{-1})	*9.14 [0]*	*24.2 [8.72]*	*7.52 [12.4]*	*0.37 [0.13]*
δ^2H (‰)	*-139 [1]*	*-147 [12]*	*-78 [87]*	*-39 [1]*
$\delta^{18}O$ (‰)	*-18 [0]*	*-19 [2]*	*-12 [11]*	*-5 [0]*

** One sample was excluded due to an extreme DIC concentration (10,819 µmol kg^{-1}), most likely related to its collection from a meltwater pond. ** Note that for SNW samples, only parameters that are independent of gas exchange and require a small analytical volume were sampled.*

The δ^2H and $\delta^{18}O$ values follow the S_P and temperature gradients. Cold and fresh ALG samples have highly depleted δ^2H and $\delta^{18}O$ isotopic signatures, reaching -154 ‰ and -20 ‰, respectively (Table 1, Figure 7). The isotopic signature of the supernatant water within the upper frozen core (SNW; Table 1) is also highly depleted, with a δ^2H value of -139 ‰ and a $\delta^{18}O$ value of -18 ‰, and falls within the range of ALG samples (from -150 to -133 ‰ for δ^2H and from -19 to -17 ‰ for $\delta^{18}O$). This implies that the ice content of the suprapermafrost soil and the ALG samples share the same origin, reflecting the hydrogeological connectivity between both and the seasonal freeze-thaw cycle at the top of permafrost soil. In contrast, the warmer seawater samples are less depleted, with a median

δ^2H value of -39 ‰ and a median $\delta^{18}O$ value of -5 ‰ (SSW; Table 1). These two groups of samples align well along the Local Meteoric Water Line (LMWL; IAEA WISER, 2025; Figure 7) for Cambridge Bay, which parallels the Global Meteoric Water Line (GMWL; Craig, 1961; Figure 7). BG samples display isotopic compositions that span the whole range of values between the two endmembers defined by the ALG and SSW samples. BG samples with low salinities fall on the LMWL. Samples with higher salinities, however, sit slightly above the line, suggesting processes that selectively decrease $\delta^{18}O$ while maintaining δ^2H values close to the LMWL. Three BG samples have similar or more depleted $\delta^{18}O$ and δ^2H values than the ALG and SNW samples. These very negative $\delta^{18}O$ and δ^2H values, nonetheless, align well with the LMWL and suggest a common origin from a more depleted source of water, likely deeper permafrost-derived meltwater. The overall isotope values agree well with the water stable isotope signatures measured in deep permafrost cores (>100 cm depth; Bouchard, pers. comm., February 28th, 2025) in the area and, more generally, within hydrological endmembers of western Arctic permafrost (Fritz et al., 2011; Utting et al., 2012).

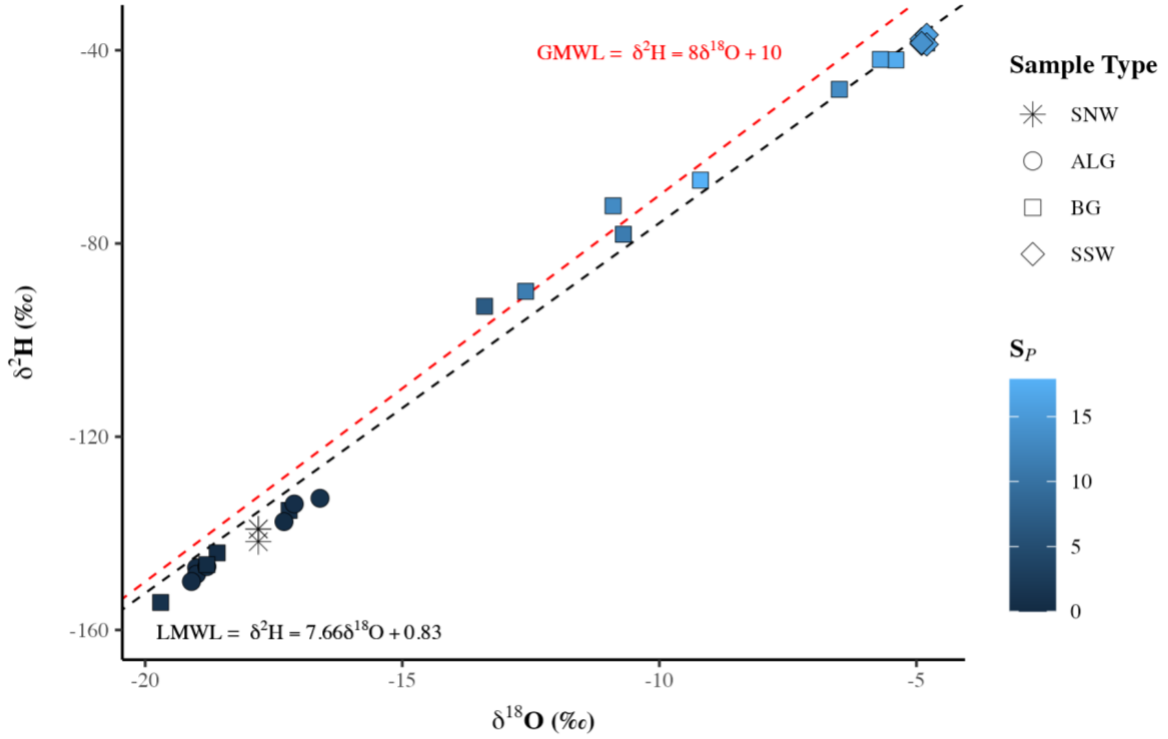

Figure 7. Stable isotope composition ($\delta^{18}O$ and $\delta^{2}H$) of water samples collected along the land-to-coastal ocean continuum of Cambridge Bay, categorized by sample type and practical salinity (S_P). The red dashed line represents the Global Meteoric Water Line (Craig et al., 1961), and the black dashed line represents the Local Meteoric Water Line (IAEA WISER, 2025).

1.5.2. Distribution of carbonate parameters along the continuum

The values of pH_T ranged from 7.37 to 8.25 (Table 1, Figure 8A) along the S_P gradient, with a median value of 7.91 (IQR: 0.15). ALG samples exhibited the lowest median pH_T (7.67; IQR: 0.40), whereas SSW samples had a higher median pH_T (7.91; IQR: 0.01) but a much narrower range, likely reflecting the influence of the marine carbonate buffering capacity of seawater. BG samples had a median pH_T (7.94; IQR: 0.13), higher than ALG samples but similar to SSW samples, with greater variability (Table 1). The DIC and TA concentrations showed a similar decreasing trend along the salinity gradient (Figure 8B andFigure 8C) from SNW to SSW samples. The SNW recovered from the melted top core had a high TA (3572 µmol kg^{-1}), whereas the lowest overall TA (712 µmol kg^{-1}) was

recorded in the melted bottom core. The DIC concentration was only measured in the melted bottom core (784 µmol kg^{-1}) and was similar to the TA. ALG samples exhibited the highest DIC and TA concentrations, with median values of 3738 µmol kg^{-1} and 3702 µmol kg^{-1}, respectively (Table 1). In contrast, SSW samples had the lowest median DIC and TA concentrations (1365 µmol kg^{-1} and 1378 µmol kg^{-1}, respectively), reflecting Arctic coastal seawater concentrations (Beaupré-Laperrière et al., 2020; Burt et al., 2016). The BG samples displayed intermediate DIC and TA concentrations, between the ALG and SSW endmembers. Org-Alk_m ranged from 135 to 803 µmol kg^{-1} and contributed up to ~17% of TA. The highest relative contribution of Org-Alk_m to TA was in SSW samples (~26%), whereas SNW (12%), BG (~13%), and ALG (12%) samples showed lower but still substantial contributions. Hence, Org-Alk has a significant impact on pCO_2 values calculated from the TA-pH pair. For instance, a 12% variation of TA in an ALG sample resulted in a mean calculated pCO_2 variation of 11% at pH ~ 7.7. The variable contributions of Org-Alk to TA among sample types likely reflect the balance between organic alkalinity sources and the buffering influence of carbonate-rich permafrost waters. Whereas SSW samples exhibited the highest relative contribution of Org-Alk to TA, their strong marine carbonate buffering capacity likely mitigates its impact on pH and pCO_2 dynamics. Although ALG samples were expected to be more sensitive to Org-Alk variability due to weaker carbonate buffering (Abril et al., 2015), our data show minimal differences between pCO_2 values computed from the pH-DIC and pH-TA pairings (mean variability: 0.62%; see Annex I).

The pCO_2 concentrations were computed for each sample using the DIC-pH_T pair, avoiding the effect of Org-Alk on TA. The calculated pCO_2 values ranged from 306 to 5155 µatm along the salinity gradient. ALG samples exhibited the highest pCO_2 values (median X µatm; Table 1), significantly exceeding ambient air levels (~420 µatm; NOAA GML, 2025; Figure 8D). In contrast, SSW samples had a median pCO_2 value of 424 µatm (Table 1), only slightly above the atmospheric level. Consistent with the distribution of the other carbonate system parameters, BG had intermediate pCO_2 values (778 µatm; IQR: 823), lower than ALG but still considerably above the atmospheric value.

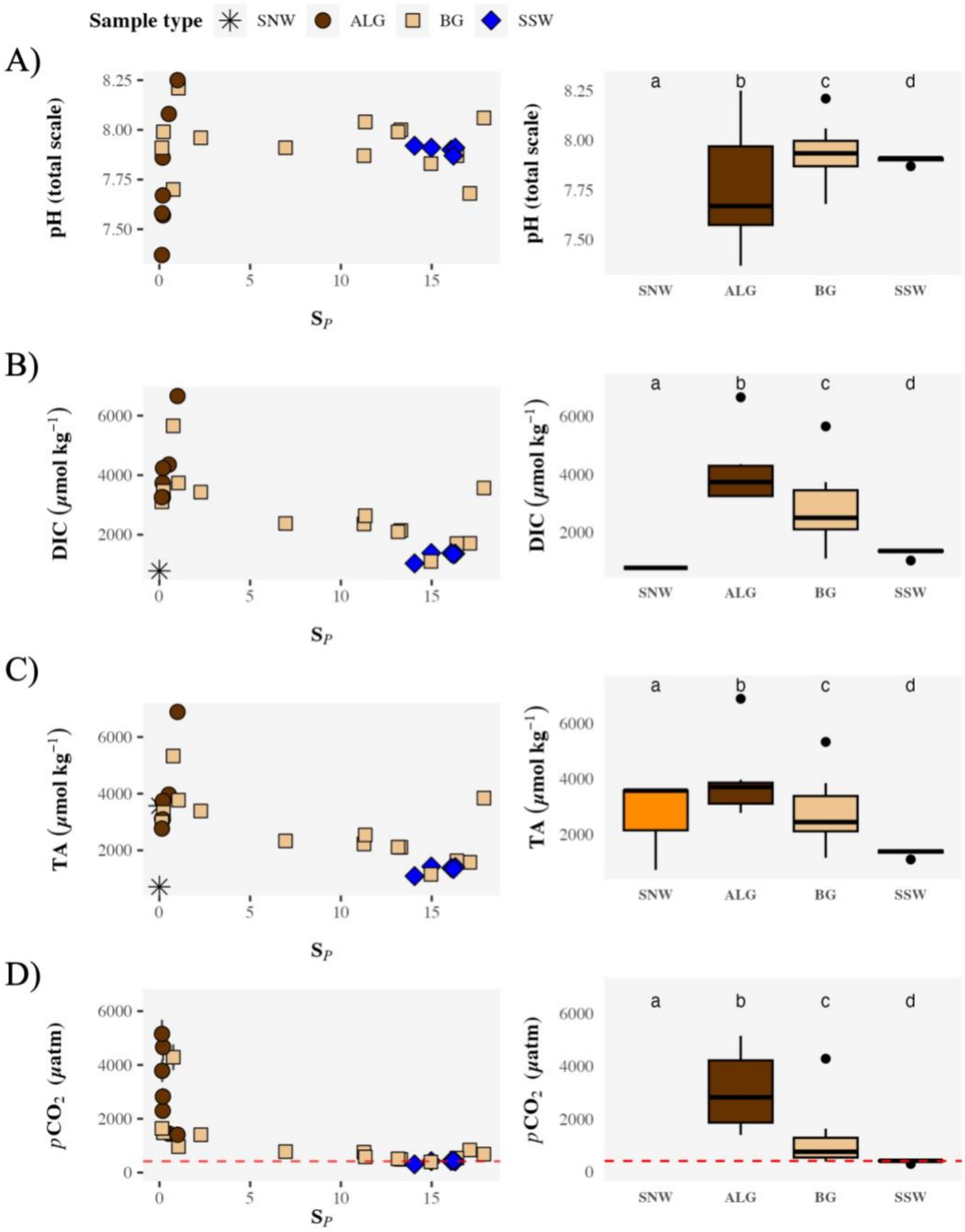

Figure 8. Distribution of carbonate system parameters A) pH (total proton scale), B) dissolved inorganic carbon (DIC), C) total alkalinity (TA), and D) CO_2 partial pressure (pCO_2) along the practical salinity (S_P) gradient for different sample types: a) supernatant water (SNW), b) active layer groundwater (ALG), c) beach groundwater (BG), and d) surface seawater (SSW). The dashed red line represents the atmospheric and, thus, air-sea equilibrium of pCO_2 at 420 µatm.

The Ω_{arag} values did not exhibit a clear trend along the salinity gradient with ALG (0.59; IQR: 1.00), BG (0.81; IQR: 0.39) and SSW (0.71; IQR: 0.08) samples predominantly showing undersaturation (Table 1; Figure 9). Similarly, Ω_{cal} values showed no specific pattern, as all sample types displayed both undersaturated and oversaturated conditions regardless of salinity (Figure 9). The median values were, however, generally close to the equilibrium value with ALG samples at Ω_{cal} = 0.98 (IQR: 2.02), whereas BG (1.40; IQR: 0.70) and SSW (1.21; IQR: 0.14) samples were slightly oversaturated ($\Omega_{cal} > 1$). Overall, BG samples exhibited the highest median Ω values, whereas ALG samples displayed the greatest variability, likely reflecting differential freshwater contributions. Total dissolved calcium concentrations increased along the salinity gradient with SNW and SSW samples positioned at the extremes, and exhibiting little variability along the gradient (Table 1; Figure 9B). Nevertheless, BG samples showed intermediate values, spanning the range between the ALG and SSW endmembers, and displaying greater variability (Table 1). The linear regression revealed a statistically significant positive relationship between Ca^{2+} concentration and practical salinity ($F(1, 26) = 178.6$, $p < 0.01$, $R^2 = 0.87$; Figure 9B), with a non-zero intercept indicating a terrestrial source of calcium at low salinity. This suggests that calcium input is not solely driven by marine mixing, but also influenced by freshwater sources such as mineral weathering within the active layer and the beach.

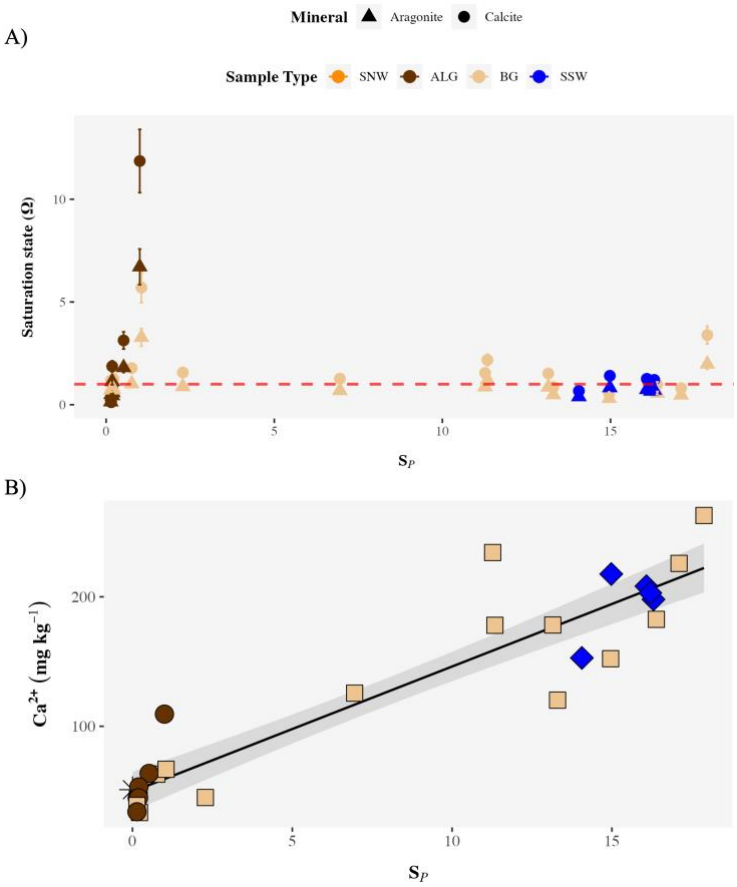

Figure 9. Distribution of A) saturation state of waters with respect to calcite (circles) and aragonite (triangles) minerals and B) total dissolved calcium concentrations along the practical salinity gradient (S_P) for different sample types: supernatant water (SNW), active layer groundwater (ALG), beach groundwater (BG), and surface seawater (SSW). The dashed red line represents the equilibrium state with respect to calcite and aragonite. The black line represents the linear least-squares regression model, and the shadowed area indicates the 95% confidence interval.

1.5.3. Distribution of dissolved organic carbon concentrations and chromophoric dissolved organic matter content along the continuum

The DOC concentrations in all samples ranged from 62 to 1918 µmol kg^{-1}, with a median value of 726 µmol kg^{-1} (IQR: 834 µmol kg^{-1}). The ALG samples exhibited the highest DOC concentrations, with a median value of 1139 µmol kg^{-1}, two orders of magnitude higher than adjacent SSW samples (Figure 11A). Between the ALG and SSW

endmembers, the DOC concentrations in the BG samples ranged from 63 to 973 µmol kg^{-1} (Figure 11A). There is a statistically significant positive correlation between DOC and Org-Alk_m ($F(1, 26) = 6.37$, $p < 0.05$, $R^2 = 0.197$), indicating that higher DOC concentrations are associated with increased organic alkalinity (Figure 10). The relationship, however, explains only a small proportion of the variance (19.7%), suggesting that factors other than the amount of DOC contribute to variations in organic alkalinity.

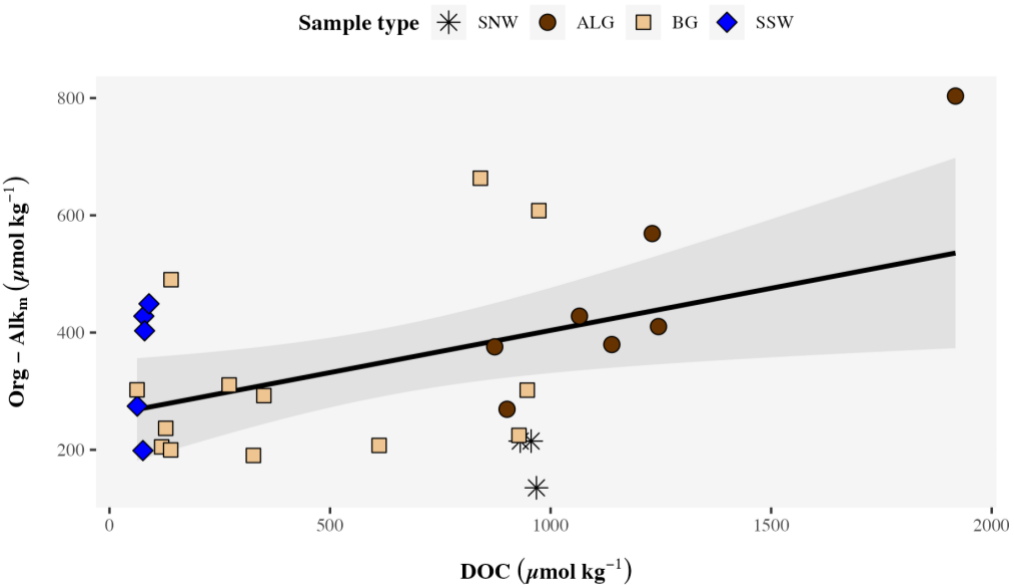

Figure 10. Cross plot of dissolved organic carbon (DOC) concentrations and measured organic alkalinity (Org-Alk_m) across the different sample types: supernatant water (SNW), active layer groundwater (ALG), beach groundwater (BG), and surface seawater (SSW). The black line represents the linear least-squares regression model ($F(1, 26) = 6.37$, $p < 0.05$, $R^2 = 0.197$), and the shadowed area indicates the 95% confidence interval.

The $aCDOM_{350}$ values ranged from 0.15 to 32.74 m^{-1}. Based on $aCDOM_{350}$, the CDOM content decreased progressively from SNW and ALG samples to SSW (Figure 11B). The CDOM content was very high in ALG samples, reaching values above 30 m^{-1} and dropping to 0.4 m^{-1} in SSW. The DOC-aCDOM relationship is often used to identify the DOM source (autochthonous vs. allochthonous) and its optical properties, as well as the biogeochemical processes (e.g., mixing, photo-oxidation, and microbial degradation) that regulate its conservative or non-conservative behavior in aquatic systems (Massicotte et al.,

2017). In our study, a significant coupling was observed between $aCDOM_{350}$ and DOC concentrations ($F(1, 24) = 246.4$, $p < 0.0001$, $R^2 = 0.91$; Figure 11C).

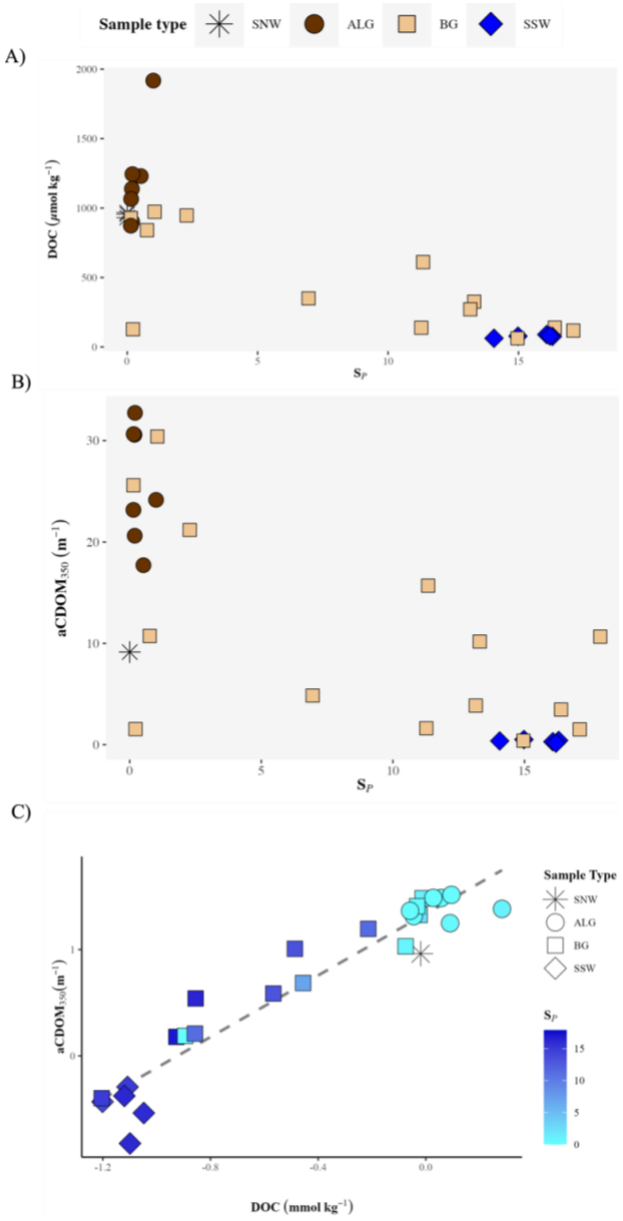

Figure 11. Distribution of A) dissolved organic carbon (DOC) and B) absorbance of chromophoric dissolved organic matter at 350 nm ($aCDOM_{350}$) along the practical salinity gradient (S_P) for different sample types: supernatant water (SNW), active layer groundwater (ALG), beach groundwater (BG), and surface seawater (SSW). The relationship between log-transformed DOC and log-transformed $aCDOM_{350}$ is shown in plot C, where the color scale represents the practical salinity (S_P) of samples, and the shapes represent the different sample types. The dashed black line represents the linear least-squares regression between DOC and $aCDOM_{350}$ ($F(1, 24) = 246.4$, $p < 0.0001$, $R^2 = 0.91$). Note that $aCDOM_{350}$ in supernatant water samples was only measured in the top core.

1.5.4. DOM molecular properties

Based on DOC concentrations, the average DOM extraction efficiency was 42% ± 29%, well within the reported efficiency range for deep-sea DOM using the PPL method (Dittmar et al., 2008). Overall, 16,020 assigned molecular formulas were identified by FT-ICR-MS from a total of 21 samples including ALG (N = 8), BG (N=10) and SSW (N = 3). ALG samples had the lowest number of assigned molecular formulas (3740 ± 559) whereas BG and SSW samples had the highest with 4,433 ± 563 and 4,074 ± 631 formulas, respectively. The mass over charge ratio (m/z) of identified peaks ranged from 101 to 981 Da (Figure 12A). The weighted averages for the hydrogen-to-carbon (H/C) ratios ranged from 1.04 to 1.33 (Figure 12B), and the weighted averages for the oxygen-to-carbon (O/C) ratios ranged from 0.37 to 0.49 (Figure 12C). The aromaticity index (AI_{mod}) was highest in ALG samples (0.328 ± 0.04) and lowest (0.270 ± 0.002) in SSW samples (Figure 12D). The distribution of DOM molecular parameters within the different sample types is detailed in Annex II.

Highly unsaturated compounds were the dominant DOM molecular compound group in all sample types. The proportion was slightly higher in SSW samples (85%), whereas ALG and BG samples showed a similar proportion (82%). All sample types had a very low amount (< 1%) of saturated and unsaturated with nitrogen-containing compounds. Aromatic compounds were slightly more abundant in ALG samples (13%) and their presence decreased in BG (10 %) and SSW (6%) samples. See Annex II for information on the distribution of DOM molecular compound groups across sample types.

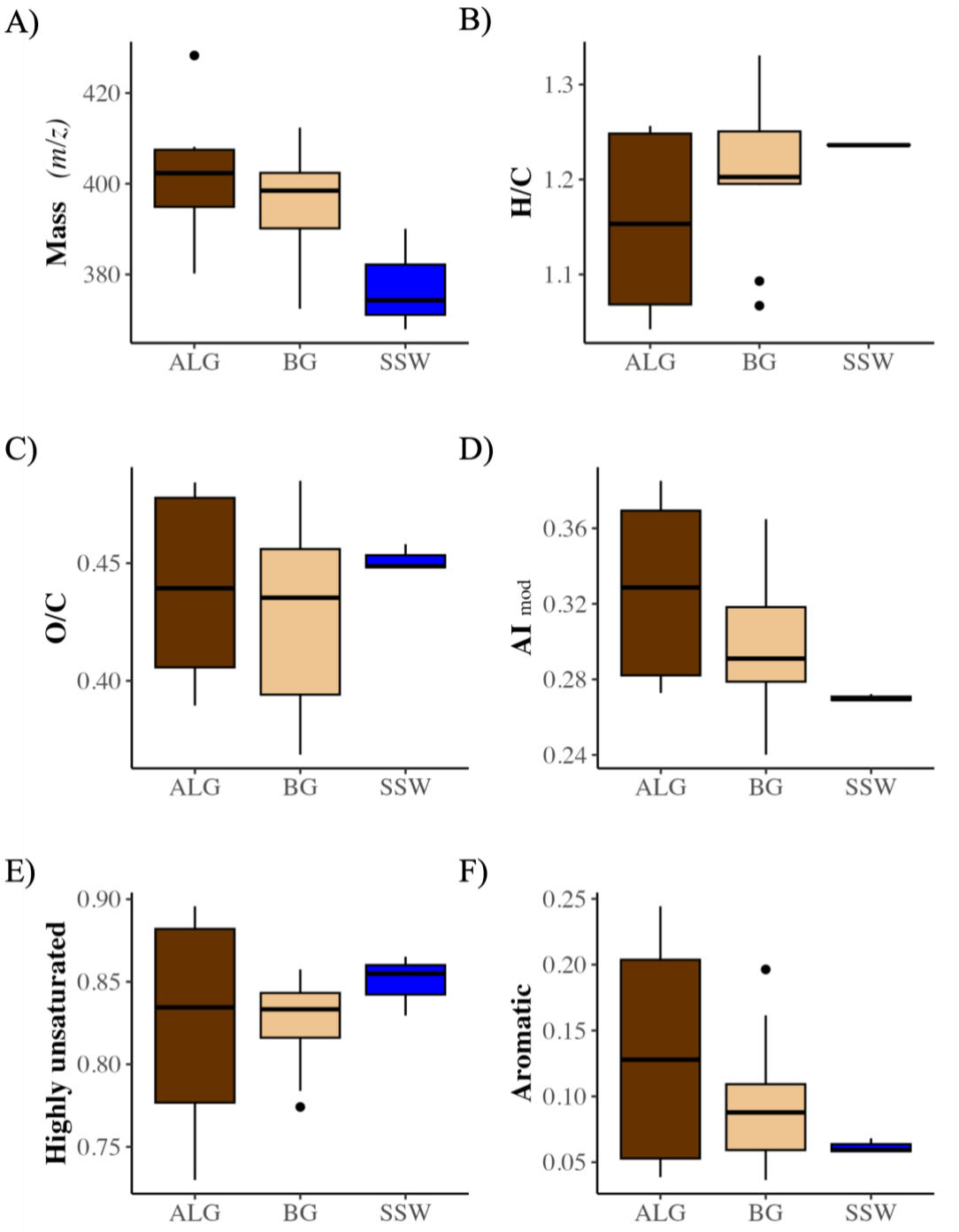

Figure 12. Distribution of DOM molecular parameters of A) mass over charge ratio (m/z), B) hydrogen-to-carbon ratio (H/C), C) oxygen-to-carbon ratio (O/C), D) aromaticity index (AI_{mod}), E) highly unsaturated and F) aromatic for different sample types: active layer groundwater (ALG), beach groundwater (BG), and surface seawater (SSW).

1.6. DISCUSSION

1.6.1. Hydrologic connectivity between the suprapermafrost groundwater and coastal water

Stable water isotope values ($\delta^{18}O$ and $\delta^{2}H$) serve as hydrogeochemical tracers of hydrologic processes and connectivity along the flow path. In Arctic regions, suprapermafrost groundwater originates from surface water infiltration, local precipitation, snowmelt, and active layer thaw within the permafrost watershed (Boike & Hubberten, 1998; Mackay, 1983; Throckmorton et al., 2016). The highly depleted $\delta^{18}O$ and $\delta^{2}H$ signatures of SNW, ALG, and some BG samples are typical of Arctic watersheds (Fritz et al., 2011) and mainly reflect cold and dry meteoric conditions. The $\delta^{18}O$ and $\delta^{2}H$ values become progressively enriched from ALG to SSW along the LMWL, suggesting mixing between inland freshwater and coastal seawater within the beach area, as confirmed by the absence of distinctly different isotopic signatures in BG samples (Figure 7). Whereas low-salinity samples align along the LMWL, mid-salinity samples fall above the line, suggesting that processes other than dilution influence the water isotopic composition. The slight ^{18}O depletion, relative to the expected value derived from the $\delta^{2}H$ value of the LMWL, could result from a variety of processes, such as isotope exchange between recirculated seawater and silicate minerals, oxygen isotope fractionation by DIC-H_2O isotope exchange, CO_2 degassing or absorption (Karolytė et al., 2017; LaBolle et al., 2008; Lécuyer et al., 2009). These exchanges could result in CO_2-water-mineral interactions, including $CaCO_3$ dissolution, during which some ^{18}O is incorporated into dissolved inorganic carbon species (Karolytė et al., 2017; Lécuyer et al., 2009), in agreement with the high DIC and CO_2 levels measured in the BG samples (Figure 8).

The relative contribution of groundwater to each sample can be estimated using a two-endmember mixing model in which the endmembers refer to the most depleted freshwater sample ($\delta^{2}H$ = -154‰ and $\delta^{18}O$ = -20‰, based on deep permafrost cores in the Cambridge Bay area) and the least depleted SSW sample ($\delta^{2}H$ =-39‰ and $\delta^{18}O$ = -5‰). This

was performed using equation 17, where X is the percentage of fresh groundwater in the sample, C_{sample} is the δ^2H or $\delta^{18}O$ value of the sample, $C_{groundwater}$ is the δ^2H or $\delta^{18}O$ value of the freshwater endmember and $C_{surface\ seawater}$ is the δ^2H or $\delta^{18}O$ value of the marine endmember.

$$X = [(C_{sample} - C_{groundwater}) / (C_{surface\ seawater} - C_{groundwater})] \times 100 \qquad \text{(Eq. 17)}$$

Results indicate that groundwater contribution to BG samples covers the whole mixing range, from 100% to 0% (mean of 53% ± 41%), likely reflecting the mixing of freshwater from the active layer and seawater within the beach. In lower-latitude beach systems, the mixing zone is referred to as a STE (Moore, 1999) where terrestrial (e.g., hydraulic gradient, seasonal oscillation of the water table) and marine (e.g., wave and tidal pumping, ripple and bedform migration, bioirrigation) processes interact in complex ways that force flows across the beach (Moore, 2010; Santos et al., 2009). These processes drive mixing between fresh inland groundwater and recirculated saline groundwater and their export to an adjacent embayment. In Arctic systems with continuous permafrost and limited tidal range, wind speed and direction (Bullock et al., 2024; Guimond et al., 2023) as well as the seasonal variation of the active layer depth (Demir et al., 2024; Dimova et al., 2015) mainly control the mixing and export of beach groundwater. Whereas knowledge of Arctic systems is still limited (Lecher, 2017), Demir et al. (2024) proposed a conceptual model of Arctic STE for the Beaufort Sea region (Kaktovik and Simpson Lagoon, Alaska) where fresh, inland groundwater meets recirculated saline groundwater in a nearshore mixing zone, above a deep ice-bounded permafrost table. The isotope signatures of the BG samples are consistent with this model, indicating that, in front of permafrost bluffs, Arctic beaches act as a mixing zone between thawed suprapermafrost groundwater that originates from the active layer or deep permafrost and seawater. Thus, the S_P range of the BG samples is a result of tidal pumping, waves, and seawater recirculation through the permeable beach sediments. Measurements of radon and radium isotopes, used to quantify freshwater export (e.g., Bullock et al., 2024; Kipp et al. (in revision)), would be required to confirm suprapermafrost submarine groundwater discharge in the nearshore area.

1.6.2. Are Arctic beaches biogeochemical reactors?

Processes that affect dissolved organic and inorganic carbon concentrations in suprapermafrost groundwater along the continuum can be inferred from deviations relative to the theoretical conservative mixing curve. This mixing is established using the two-endmember mixing model described by equation 17. The differential behavior of organic and inorganic carbon species, such as DIC, TA and DOM, along the groundwater flow path provides insight into their biogeochemical transformations and ecological impact upon discharge into the Arctic coastal waters and the calculation of chemical fluxes. The high organic carbon concentrations in SNW and BG samples is conducive to the development of both aerobic and anaerobic microbial activity, which leads to the accumulation of metabolites (e.g., CO_2, CH_4, HS^-) (Baker et al., 2000; Fillinger et al., 2023; Madsen & Bollag, 1989). For example, microbial respiration of organic matter produces CO_2, thereby increasing DIC concentrations, whereas sulfate reduction can produce both DIC and TA by generating bicarbonate (HCO_3^-) and carbonate ions (CO_3^{2-}), leading to shifts in acid-base chemistry (Gallagher et al., 2014; Meister, 2013, 2014; Turchyn et al., 2021; Zhang, 2020). Shifts in acid-base dynamics along the flow path can be influenced by both TA and organic alkalinity (Org-Alk). Whereas TA primarily reflects the presence of inorganic acid-base species, Org-Alk includes contributions from weak organic acids and bases, such as humic and fulvic substances, that can also accept or donate protons (Kuliński et al., 2014; Delaigue et al., 2020; Martell-Bonet & Byrne, 2023). Although the quantitative contribution of Org-Alk is generally smaller than that of TA, it can be significant in humic-rich systems and may modulate the pH buffering capacity (Song et al., 2020).

Drivers of carbonate parameters along the flow path

The mixing of carbon-rich groundwater with coastal seawater within the beach can lead to CO_2 emissions from surface waters or their acidification, depending on the balance between DIC input, the buffering capacity of receiving waters, and gas exchange (Cardenas et al., 2020; Liu et al., 2023; Wang et al., 2018). The TA/DIC ratio is a proxy for the water's

capacity to buffer the impact of acid additions (e.g., CO_2) on its pH and CO_2 absorption potential: TA/DIC < 1 characterizes waters more susceptible to acidification, whereas TA/DIC > 1 reflects a greater buffering capacity. In our system, suprapermafrost groundwater from the active layer predominantly exhibits ratios below 1 (Figure 13A and B), suggesting limited buffering capacity of inland groundwater. The carbonate chemistry along the flow path reflects a combination of biological and geochemical influences. The accumulation of DIC and high pCO_2 levels within the active layer groundwater may result from restricted atmospheric exchange and geochemical interactions with mineral substrates in the watershed (Olichwer et al., 2012). Given that the study site is located on raised marine terraces and the presence of shell fragments in sediments, it is likely that soils contain carbonate-bearing material. The dissolution of carbonate minerals could then be promoted by the accumulation of CO_2 produced by aerobic respiration that increases both TA and DIC (Cai et al., 2003), enhancing the buffering capacity and potentially lowering the pCO_2. Therefore, the high pCO_2 in the active layer may indicate that microbial CO_2 production outpaces the rate of carbonate buffering reactions. In contrast, the ALG samples are slightly alkaline (pH > 7) (Figure 8), in equilibrium or slightly oversaturated with respect to calcite (Ω_{ara} and $\Omega_{cal} \geq 1$) and in equilibrium or slightly undersaturated with respect to aragonite ($\Omega_{ara} \leq 1$) (Figure 9A), conditions that could be conducive to calcite precipitation or aragonite dissolution.

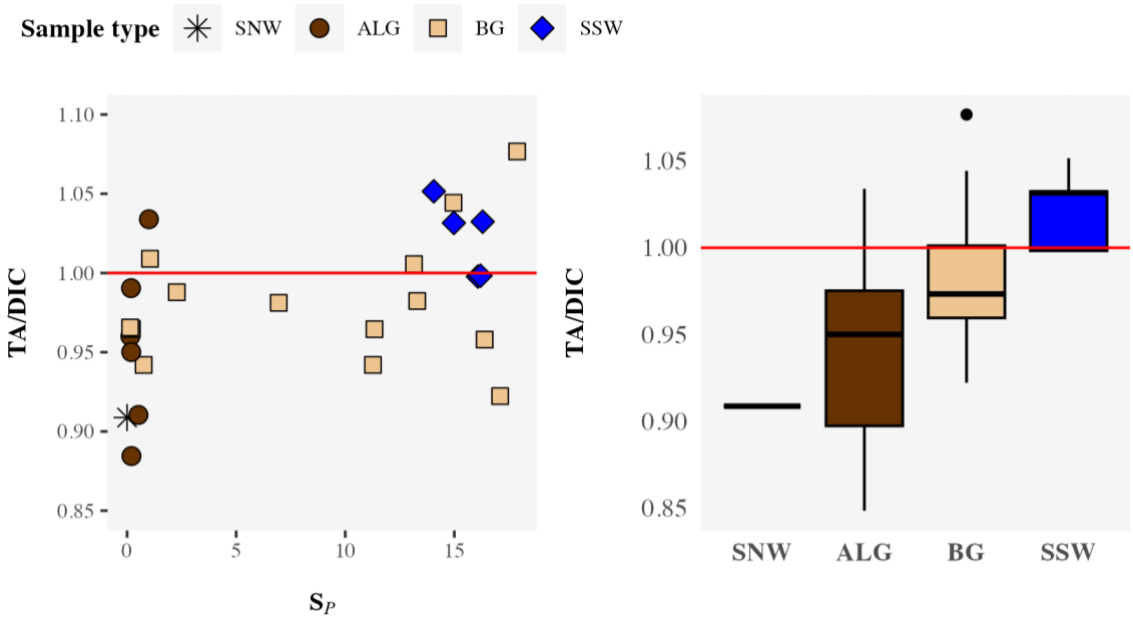

Figure 13. Total alkalinity on dissolved inorganic carbon ratio (TA/DIC) along the practical salinity (S_P) gradient for different sample types: supernatant water (SNW), active layer groundwater (ALG), beach groundwater (BG), and surface seawater (SSW). The solid red line indicates the 1:1 ratio for TA and DIC.

Beach groundwater samples exhibit a sharp decrease in pCO_2 levels, dropping from several thousand µatm in fresh ALG samples to around 500 µatm in the saltiest samples (Figure 8), approaching seawater and atmospheric equilibrium levels. This suggests that CO_2 degassing begins as groundwater interacts with the atmosphere through the beach's permeable sediments (Wang et al., 2018). Along the salinity gradient, CO_2 loss is accompanied by a steady decrease in DIC and TA. The decrease in TA, beyond conservative mixing, suggests that $CaCO_3$ precipitation may occur, as CO_2 degassing raises pH and saturation states (Ω values), favoring carbonate mineral precipitation. The TA/DIC ratio remains slightly below 1 in most BG samples (Figure 13), consistent with insufficient buffering capacity to completely neutralize acid additions. The inorganic and organic carbon-rich and acidic suprapermafrost groundwater appears to primarily affect ALG and BG samples and to be rapidly neutralized upon mixing with surface seawater, likely due to the higher buffering capacity of seawater. This leads to a shift toward marine-like pH values and a stabilization of carbonate system parameters, Ω (Figure 9) and TA/DIC ratios (Figure 13). The buffering effect of seawater is reflected in the saturation state of waters with respect to

calcite, as BG samples exhibit $\Omega_{cal} > 1$ (Figure 9), indicating equilibrium or slight oversaturation and suggesting possible calcite precipitation. On the other hand, Ω_{arag} remains < 1 in most samples, suggesting persistent undersaturation with respect to aragonite. Whereas this might imply insufficient TA input, it could also reflect equilibrium with calcite, particularly if calcite is the dominant phase or if aragonite is converted to calcite. The variability in TA/DIC among BG samples further highlights the dynamic nature of the mixing zone within the beach sediments, where both physical mixing and biogeochemical processes modulate the carbonate chemistry (Chaillou et al., 2024; Charbonnier et al., 2022; Cyronak et al., 2014; Li et al., 2014).

Sources and sinks of inorganic carbon along the flow path

Beyond the mixing zone, broader geochemical controls regulate DIC and TA dynamics in coastal environments. In the infralittoral zone, DIC production is shaped by local lithology (drainage basin geology) and a combination of biotic and abiotic processes within the intertidal zone (Goldsmith et al., 2010; Liu et al., 2021; Meybeck, 1987). Tidal inflow and seasonal hydrogeological variations have been shown to regulate DIC and TA production rates in beach groundwater (Liu et al., 2021). Moreover, diagenetic reactions, including carbonate dissolution and precipitation, as well as aerobic and anaerobic microbial respiration, significantly influence DIC and TA concentrations (Cai et al., 2003). Figure 14 shows the relationship between TA and DIC, expressed as ΔTA and ΔDIC, defined as the deviation of measured concentrations from their conservative mixing behavior between two endmembers: the most depleted freshwater sample (δ^2H = -154‰ and for $\delta^{18}O$ = -20‰) and the least depleted SSW sample (δ^2H =-39‰ and $\delta^{18}O$ = -5‰). The slope of their relationship (ΔTA/ΔDIC) is then compared with the ΔTA/ΔDIC of selected key reactions, including the dissolution and precipitation of carbonate minerals (ΔTA/ΔDIC = 2/1 and -2/1, respectively), CO_2 uptake/degassing (ΔTA/ΔDIC = 0/1 ∞), nitrate reduction (ΔTA/ΔDIC = 84.8/106), iron reduction (ΔTA/ΔDIC = 848/106) and sulfate reduction (ΔTA/ΔDIC = (53x2)/106) (Figure 14; Cai et al., 2003; Chen & Wang, 1999; Rassmann et al., 2020). Methanogenesis, not illustrated in Figure 14, has a ΔTA/ΔDIC ratio of 0/53 (Chen & Wang, 1999). When seawater

mixes with fresh groundwater influenced by anaerobic microbial respiration and $CaCO_3$ dissolution, TA/DIC should then increase to a ratio between 1 and 2 (Cai et al., 2003). In this study, the ΔTA/ΔDIC across all samples is around 1 ($R^2 = 0.964$, with a *p*-value < 0.001), suggesting that anaerobic processes, potentially sulfate reduction, control DIC and TA production in a 1:1 ratio.

In our system, the evolution of the carbonate chemistry along the continuum reflects the combined influence of these processes, particularly microbial respiration and carbonate mineral reactions. The acidifying effect of microbial CO_2 production is buffered primarily through carbonate mineral dissolution in the permafrost watershed, which increases both TA and DIC. The distribution of total dissolved calcium along the flow path (Figure 9B) further supports this interpretation, as the non-zero intercept suggests an input of calcium from terrestrial sources, consistent with carbonate weathering in the active layer and beach sediments. In addition, the degassing of excess CO_2 and the 1:1 co-production of TA and DIC by anaerobic processes, such as sulfate reduction, contribute to the observed ΔTA:ΔDIC ratio of ~1 and help maintain the buffering capacity of carbonate-rich suprapermafrost groundwater. Our lack of δ^{13}C-DIC and/or Δ^{14}C-DIC data limits our ability to identify the primary sources of DIC. We can, however, further assess carbon processing along the flow path by examining the relationship between DIC and DOC to infer potential sources of DIC, including carbonate weathering, organic carbon mineralization, and silicate weathering mediated by CO_2 or carbonic acid (H_2CO_3; Campeau et al., 2017, 2018), or the extent of organic carbon remineralization.

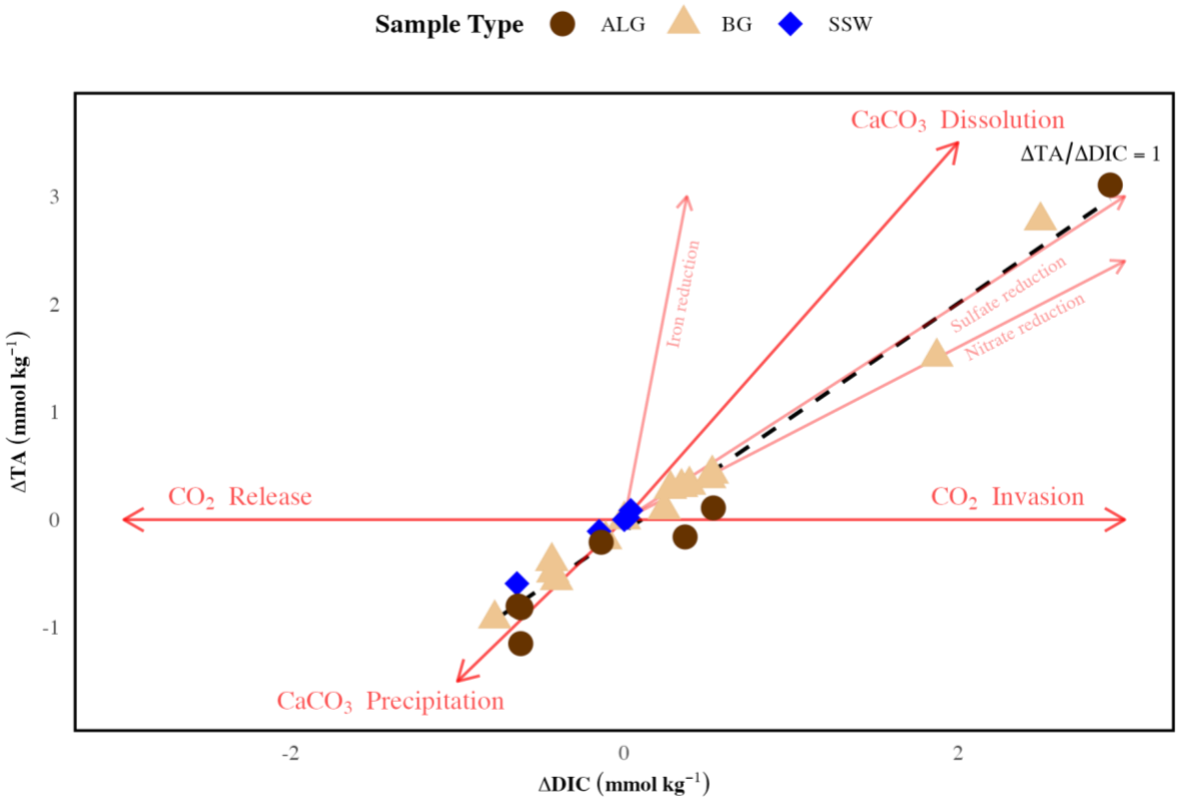

Figure 14. Relationship between total alkalinity (TA) and dissolved inorganic carbon (DIC) along the land-to-coastal ocean continuum for different sample types: active layer groundwater (ALG), beach groundwater (BG), and surface seawater (SSW). TA and DIC are expressed as ΔTA and ΔDIC, the differences between the measured concentrations and their conservative mixing values between the most depleted (freshwater BG sample) and least depleted (SSW sample) $\delta^{18}O$ and $\delta^{2}H$ signatures. The stoichiometric ratios of selected individual diagenetic reactions are reported as red arrows. CO_2 uptake from the atmosphere increases DIC with no change in TA, whereas CO_2 degassing to the atmosphere decreases DIC with no change in TA. The stoichiometric ratio of ΔTA/ ΔDIC across all samples is shown as the dashed black line.

Organic carbon pool dynamics: interactions with inorganic chemistry

The DIC:DOC ratios across all sample types are consistently higher than the 1:1 ratio (3.0-27.1), except for the SNW in the bottom core (DIC:DOC = 0.8). This threshold marks the theoretical balance point for heterotrophic remineralization, particularly anaerobic processes like sulfate reduction, which generate one mole of DIC for each mole of DOC consumed (Soetaert et al., 2007). Ratios higher than one suggest a stronger influence of

geogenic processes and highlight significant interactions between minerals and DIC dynamics, in agreement with the observed variations in carbonate system parameters. While OM mineralization can contribute to metabolic DIC and TA production, the net effect on TA depends on the dominant prevailing redox pathways. In the active layer, most organic matter is likely remineralized via oxic respiration and, under more reducing conditions, through denitrification and iron/manganese reduction which are pathways that contribute less or even negatively to TA. Sulfate reduction may further contribute to TA generation. As suprapermafrost groundwater travels toward the coast, its composition is shaped by meteoric inputs and chemical interactions with soils and mineral substrates (Olichwer et al., 2012) which, in turn, can influence OM remineralization in Arctic sandy beaches by modifying redox conditions, pH and mineral surface reactivity (Kaiser & Guggenberger, 2003). These interconnected processes ultimately regulate the fate of terrestrial DOM before it reaches the ocean, with organic alkalinity (Org-Alk) playing a key role, as it is influenced by DOM remineralization and microbial activity. In the Beaufort Sea, Flamand et al. (in revision) showed that DOM transported by suprapermafrost groundwater rapidly lost its terrigenous signature, likely due to selective trapping and/or mineralization in the beach discharge zone before reaching the ocean. Whereas, Connolly et al. (2020) reported a sustained export of DOMt from suprapermafrost groundwater to coastal waters, Waska et al. (2021) observed molecular shifts within the STE, supporting the role of this zone as a biogeochemical filter controlled by DOM removal and microbial transformation.

DOC concentrations and $aCDOM_{350}$ values are commonly used as proxies for the amount of terrestrial DOM (Li et al., 2014; Müller et al., 2011). Whereas their conservative mixing behavior may suggest physical dilution as a dominant process, their strong correlation may also reflect concurrent biogeochemical transformations. Microbial mineralization may alter DOC and $aCDOM_{350}$ concentrations at similar rates, thus, retaining stable DOC and $aCDOM_{350}$ ratios while contributing to DIC production, which highlights the role of beach discharge zones in shaping DOM composition (Seidel et al., 2014; Waska et al., 2021). Additionally, the weak yet significant correlation between DOC and $Org\text{-}Alk_m$ (Figure 10) suggests that whereas organic carbon contributes to the buffering capacity of suprapermafrost

groundwater, additional factors such as DOM composition, microbial processing, and mineral interactions likely influence its variability. These processes may modulate the contribution of organic alkalinity to TA along the groundwater flow path. To better understand the cumulative effects of these transformations to Org-Alk and DOC dynamics along the flow path, further investigation of the DOM composition was conducted.

1.6.3. Fate of permafrost-derived DOM along flow path

Molecular composition of DOM

Allochthonous inputs to coastal oceans include organic matter derived from vegetation and soil from the surrounding watershed (Aitkenhead-Peterson et al., 2003). These OM sources are rich in aromatic compounds that are typically resistant to microbial degradation and persist in the environment, supporting their use as a marker of terrestrial DOM (Koch & Dittmar, 2006). In our samples, aromatic compound abundances and, consequently, the aromaticity index (AI_{mod}) were highest in ALG samples and progressively decreased along the flow path to surface seawaters (Figure 12), indicating decreasing contributions of terrestrially derived and recalcitrant DOM from inland groundwater to the coastal waters. The reduction in both aromatic compounds and AI_{mod} in BG and SSW samples may be attributed to DOM mineralization or removal through processes such as heterotrophic consumption, molecular aggregation and flocculation (Von Wachenfeldt et al., 2008, 2009), and organo-mineral interactions (Linkhorst et al., 2017; Sirois et al., 2018; Waska et al., 2021; Flamand et al., (in revision)). Although the absence of light in the subsurface excludes photodegradation, microbial transformation and abiotic processes likely contribute to DOM alteration along the flow path. DOM in BG and SSW samples also exhibited lower molecular masses compared to ALG samples (Figure 12), a trend consistent with microbial degradation/biotransformation (and/or photooxidation for the SSW samples) which fragment high-molecular-weight compounds into smaller, more bioavailable forms (Burdige & Gardner, 1998; Kim et al., 2006). This shift is accompanied by an increase in the H/C ratios,

suggesting the addition of more saturated and aliphatic compounds which are indicative of more labile DOM that can result from both the breakdown of macromolecular DOM or the incorporation of marine DOM. In contrast, the O/C ratios remain relatively constant among sample types, suggesting stable DOM oxidation state despite changes in aromaticity. This shift, reflected in increasing H/C ratios and a decrease in highly unsaturated and aromatic molecular formulas from ALG to SSW samples (Figure 12), supports the concept of ongoing DOM processing and compositional transformation along the flow path.

Figure 15 further illustrates the compositional diversity of DOM along the flow path. Almost half of the detected molecular formulas were present in all 3 sample types (n= 4379), thus representing either a set of relatively persistent compounds that survive transformations during transport from land to the coastal ocean or a set of compounds with ubiquitous sources on land and in the coastal ocean. These common formulas are mostly highly unsaturated and both oxygen-poor and oxygen-rich, consistent with condensed hydrocarbons, lignin, molecules resistant to degradation and transformation (Koch & Dittmar, 2006), as well as peptides. In contrast, unique molecular formulas offer insights into distinct DOM sources or processing environments. Unique formulas in ALG samples (n= 444) are also mostly oxygen-rich and highly unsaturated compounds with H/C and O/C fingerprints of condensed hydrocarbons (e.g., polycyclic aromatic hydrocarbons) and lignin, supporting the terrestrial signature of permafrost-derived and active layer DOM (MacDonald et al., 2021). BG samples exhibited the widest range in molecular composition (Figure 15), with many unique molecular formulas (n= 1995). These unique beach groundwater formulas are diverse, spanning a wide range of H/C and O/C ratios, including both highly unsaturated oxygen-poor and more saturated, oxygen-rich compounds, indicating a larger amount of more bioavailable compounds such as amino sugars, peptides, and lipids. This observation reinforces the concept of the beach being a dynamic zone of DOM transformation.

Unique formulas in SSW samples (n= 155) are more saturated and more oxygenated, likely reflecting autochthonous production or selective preservation of marine compounds (Broek et al., 2020). Whereas a large number of molecular formulas (n = 4379) are shared

between sample types, mostly highly unsaturated and oxygen-rich compounds commonly attributed to terrigenous sources such as lignin and PAHs (Koch & Dittmar, 2006), the low overlap of common formulas between ALG and SSW samples suggests a selective loss or transformation of terrestrially derived DOM in the beach zone. This points to the beach acting as a dynamic interface where terrestrial DOM may undergo significant remineralization or alteration before reaching coastal waters. These findings support the idea that the beach functions as a biogeochemical reactor for terrigenous DOM, mediating its transformation through microbial and abiotic processes and thereby modulating the composition and reactivity of carbon exported to Arctic coastal waters, as proposed by Flamand et al. (in revision) and Waska et al. (2021).

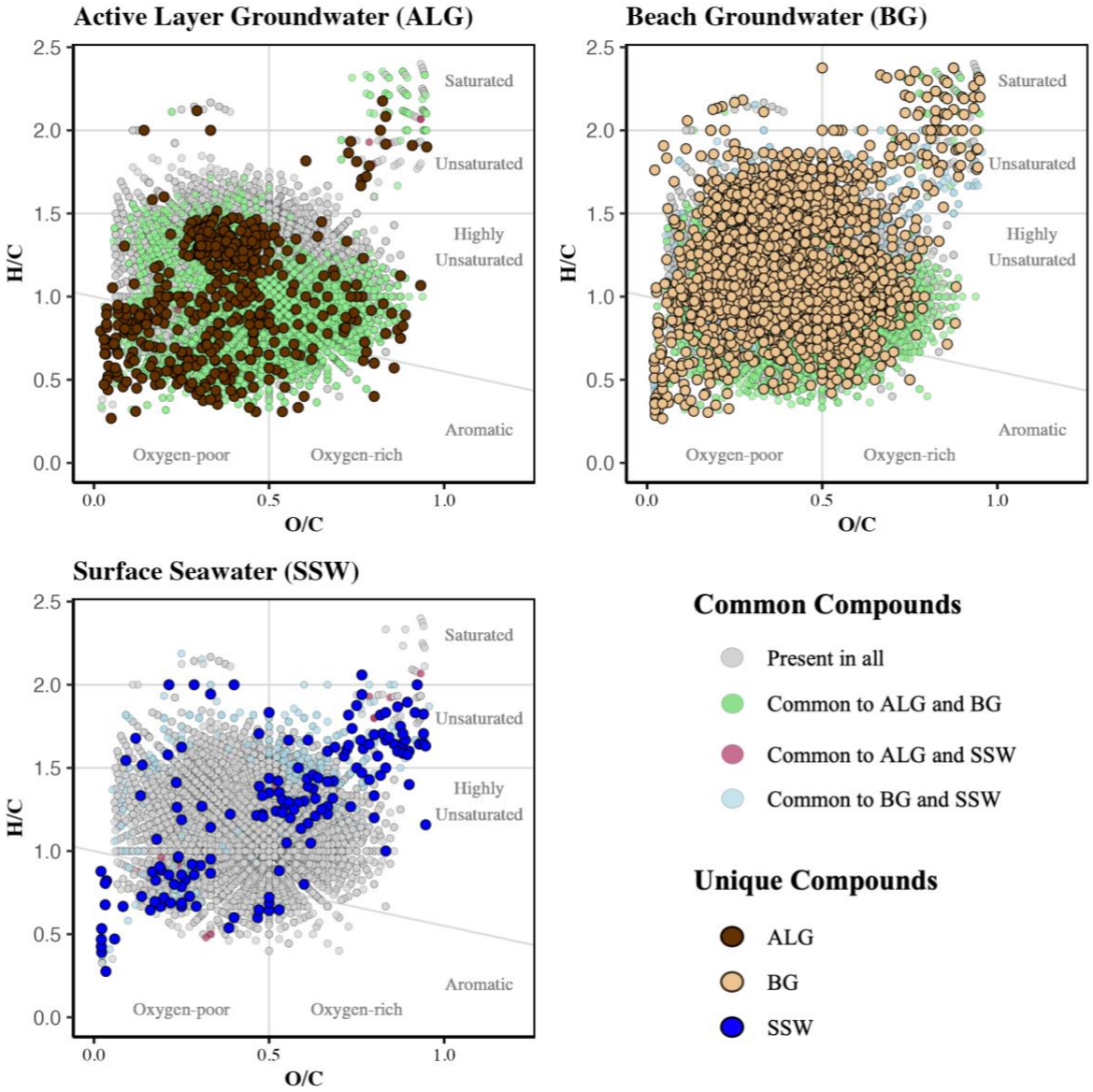

Figure 15. Van Krevelen plots illustrating the hydrogen-to-carbon (H/C) ratio vs. the oxygen-to-carbon (O/C) ratio for compounds detected by FT-ICR-MS (n=9864). Compounds detected across all sample types are highlighted in light grey (n=4379), while those shared between two sample types are shown in light green, for active layer groundwater (ALG) and beach groundwater (BG) (n=2288), in light pink, for active layer groundwater and surface seawater (SSW) (n=28), and in light blue, for beach groundwater and surface seawater (n=575). Unique compounds were exclusively detected in a single sample type for active layer groundwater (n=444), beach groundwater (n=1995), and surface seawater (n=155).

Contribution of DOM to biogeochemistry along the flow path

The PCoA revealed that the first two principal coordinate (PC) axes (Figure 16) together explained ~81% of the variance in DOM molecular composition. BG samples were widely distributed across both PC axes, reinforcing the role of the beach as a zone of active DOM processing and high molecular diversity. This variability is likely driven by the transformation of plant-derived material within intertidal sediments. PC1 (56.1%) and PC2 (24.7%) represent compositional variance associated with both oxidation state and aromaticity, as reflected by the contributions of O/C and AI_{mod} to both axes. Although active layer groundwater samples tended to exhibit higher AI_{mod} and O/C values, the observed overlap among sample types suggests that DOM compositional changes do not follow a strict spatial pattern. PC2 (24.7%) was positively associated with DOC, TA, and to a lesser extent with aCDOM350, and negatively associated with salinity and temperature. This pattern suggests that colder freshwater hosts more organic carbon and has a greater buffering capacity. However, the large structural diversity of DOM observed, particularly in ALG and BG samples, appears largely independent of environmental factors. This suggests that DOM composition ("quality") has limited influence on carbonate parameters like TA or $Org\text{-}Alk_m$, whereas DOM concentration ("quantity"), as reflected by DOC, plays a more dominant role. These findings highlight the need to further quantify DOM's acid-base properties along the continuum to better understand its buffering role in Arctic coastal waters.

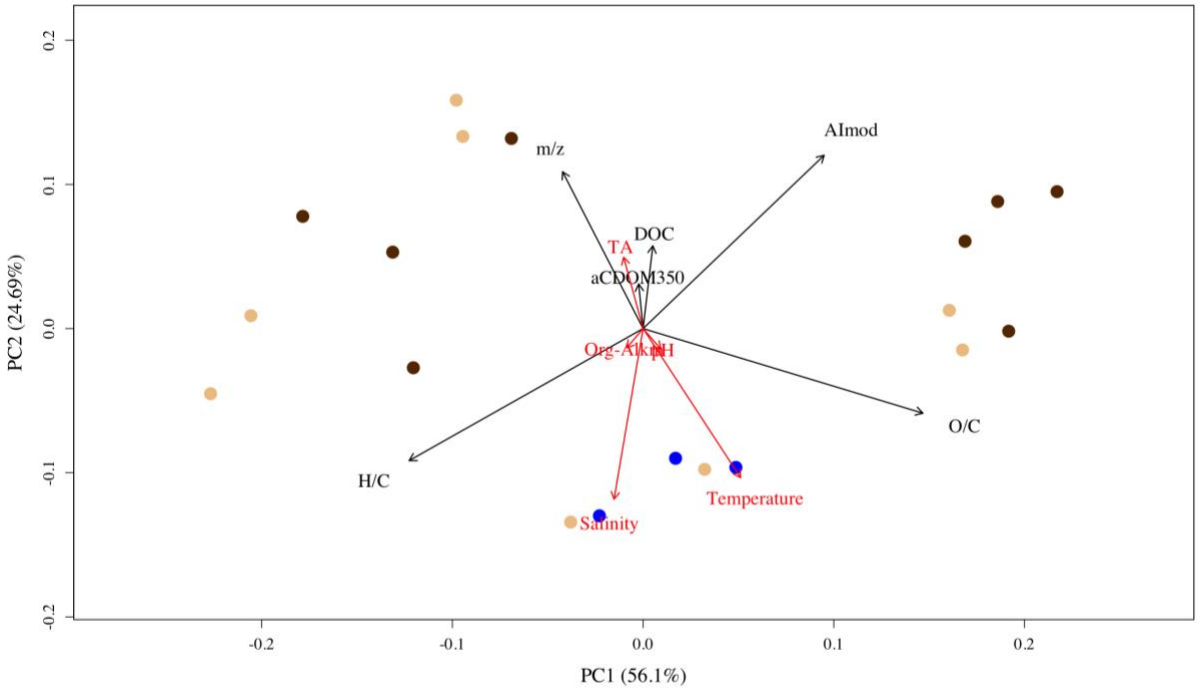

Figure 16. Principal coordinate analysis (PCoA) of carbonate parameters (DIC, pH and Org-Alk_m), temperature, practical salinity, organic parameters (DOC and $aCDOM_{350}$), and FT-ICR-MS derived molecular characteristics (H/C, O/C and AI_{mod}). Percentages on the axis represent the proportion of variation in DOM molecular composition explained by PC1 and PC2. The red arrows indicate explanatory variables, while black arrows represent response variables related to DOM quantity and quality. Point colors indicate sample types.

1.7. CONCLUSION

Our study highlights the dynamic interplay and complexity of hydrological and biogeochemical processes in shaping groundwater composition and carbonate chemistry along an Arctic land-to-coastal ocean continuum. Along the flow path, isotopic signatures reveal that water composition is influenced not only by dilution but also by additional processes such as seawater recirculation, silicate weathering, DIC-H_2O isotope exchange, and CO_2 degassing or absorption. These processes seem confined to the beach, where freshwater from the active layer and surface seawater mix due to tidal pumping and wave-driven exchange through permeable sediments. Beaches, situated in front of permafrost bluffs, emerge as chemical reactors where permafrost-derived inorganic and organic carbon

are actively transformed. The active layer provides acidic, organic carbon-rich groundwater enriched in DIC and pCO_2, the result of soil alteration, restricted atmospheric exchange, carbonate buffering, and microbial CO_2 production. These inputs are rapidly neutralized upon mixing with seawater in the beach zone, stabilizing pH, Ω, and TA/DIC ratios and thereby mitigating potential acidification of receiving waters. Heterotrophic mineralization processes, likely including sulfate reduction, drive DIC and TA production while decreasing DOC and DOM content along the flow path. This transformation results in the production of fewer aromatic molecules, evidenced by increasing H/C ratios and a shift in DOM composition. The sharp drop in pCO_2 between active layer and beach groundwater samples suggests CO_2 degassing once groundwater interacts with the atmosphere through the beach permeable sediments. This degassing likely limits the amount of permafrost derived DIC entering coastal waters, buffering against acidification and reducing the impact of terrestrial carbon on marine carbonate chemistry. Whereas a core set of molecular formulas was shared across all sample types, the limited overlap in unique formulas between active layer groundwater and surface seawater indicates that most DOMt is either retained or substantially transformed within the beach zone. Despite the high variability in DOM molecular composition, its influence on carbonate system parameters appears limited compared to that of DOM concentration. These findings collectively reinforce the concept that Arctic beaches act not only as a physical mixing zone**,** but also as biogeochemical filters and sinks**,** modulating the transfer of both inorganic and organic carbon from terrestrial thawing permafrost to the coastal ocean.

CONCLUSION GÉNÉRALE

La contribution du pergélisol côtier arctique au cycle global du carbone est nettement moins abordée que celle du pergélisol continental. Pourtant, il représente environ un tiers des côtes mondiales et se trouve aux premières loges des pressions thermiques et mécaniques induites par le réchauffement climatique. Ces pressions entrainent la remobilisation de « vieux » composés, notamment du carbone organique et inorganique ainsi que de la matière organique dissoute, via les écoulements suprapergélisol. Ces apports peuvent perturber l'équilibre acide-base de l'eau de mer et contribuer à son acidification, un phénomène d'autant plus préoccupant dans les eaux froides arctiques, où la capacité tampon est plus faible. Par conséquent, cette étude visait à caractériser les apports de carbone et de DOM issus du pergélisol côtier arctique, et à documenter leur transformation le long du continuum hydrologique allant des eaux souterraines de la couche active jusqu'aux eaux marines côtières.

Cette étude a permis d'illustrer le rôle clé que joue la plage en tant que zone de transition et de transformation, agissant comme filtre biogéochimique influençant à la fois la quantité de carbone et la qualité de la DOM transportés vers les eaux côtières de surface (Figure 17). Les processus hydrologiques et microbiens dans les sédiments de plage modulent à la fois la distribution du carbone inorganique (TA, DIC, pCO_2), ainsi que la composition moléculaire et la concentration de DOM transportée. Une forte diminution de la pCO_2 entre les eaux souterraines de la couche active et de la plage indique un dégazage important, limitant alors le transfert de CO_2 à l'océan côtier. Parallèlement, la perte progressive des composés aromatiques et hautement insaturés, combinée à une augmentation des rapports H/C, suggère une transformation active de la DOM. Cette transformation résulte probablement de processus tels que la minéralisation microbienne, la floculation ou encore les interactions organo-minérales. La variabilité observée dans les ratios TA/DIC et les états de saturation (Ω) le long du gradient de salinité renforce l'idée que la plage n'est pas une simple zone de mélange physique entre eau douce et eau salée, mais bien une zone réactive, capable de moduler les apports de carbone issus du bassin versant. Ainsi, les plages arctiques

agissent comme des zones tampons où la matière organique et inorganique dérivée du pergélisol est partiellement transformée, retenue ou reminéralisée avant d'atteindre l'océan côtier.

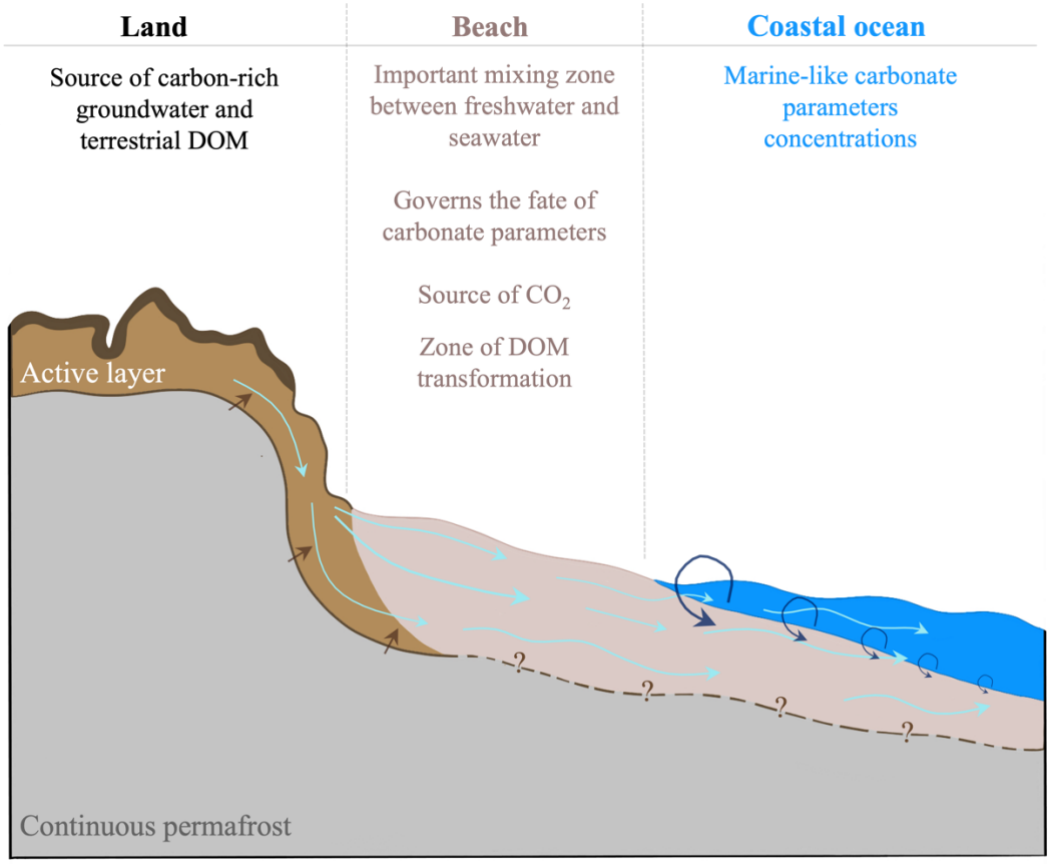

Figure 17. Représentation schématique d'une coupe transversale d'un milieu de pergélisol côtier illustrant le continuum hydrologique et biogéochimique reliant la couche active terrestre aux eaux côtières marines. La matière organique dissoute (DOM) et le carbone inorganique dissous (DIC), d'origine terrestre, sont remobilisés à partir de la couche active et transportés via les eaux souterraines suprapergélisol jusqu'à la plage. Dans cette dernière, une zone de mélange entre eau douce et eau salée agit comme un réacteur biogéochimique, où la DOM est transformée (perte de composés aromatiques, augmentation de composés aliphatiques) et une partie du CO_2 est dégazée. Ces processus modulent la quantité de carbone et de DOM exportée à l'océan côtier. Dans l'eau de mer, les paramètres du système des carbonates deviennent progressivement d'allure marine en raison du pouvoir tampon de l'eau de mer. L'extension vers le large du pergélisol continu demeure incertaine (indiquée par « ? »).

LIMITES DU PROJET

Bien que cette étude ait permis de répondre aux principaux objectifs et d'offrir d'uniques interprétations quant au rôle des plages arctiques dans la modulation des apports biogéochimiques issus de la couche active terrestre, certaines analyses complémentaires pourraient être effectuées afin de confirmer ou complémenter nos interprétations. Tout d'abord, l'analyse isotopique du carbone inorganique dissout (δ^{13}C-DIC) permettrait d'identifier les principales sources de DIC des eaux souterraines du suprapergélisol, en distinguant notamment la contribution des processus de respiration hétérotrophique et d'altération de carbonates. De plus, l'absence d'analyses sédimentaires et minéralogiques afin de déterminer la présence de minéraux carbonatées (ex. calcite ou l'aragonite), combinée à l'absence de données de carbone particulaire total et organique représentent des limitations à nos interprétations. En effet, ces données permettraient de confirmer la présence de réactions affectant l'alcalinité totale, telle que la dissolution ou la précipitation de carbonates, et d'évaluer leur contribution à la production de TA et de DIC. Il serait également intéressant d'intégrer des analyses de sulfures dissous (HS^-) afin de cibler les processus diagenétiques et les voies de respiration anaérobique qui gouverne la transformation du carbone dans les eaux souterraines.

PERSPECTIVE

Cette étude a permis d'apporter de premières connaissances sur la transformation du carbone organique et inorganique des eaux suprapergélisol en milieux côtier arctique. En perspective de ce projet, certains questionnements peuvent être soulevés. En effet, il serait bénéfique de récolter des données en continu puisque les données discrètes récoltées lors de cette étude ne permettent pas de caractériser les variations temporelles des processus biogéochimiques. Une instrumentation adaptée permettrait d'estimer les flux de carbone, autant inorganique (DIC, CO_2) qu'organique (DOM), et d'identifier de potentiels « hot spot » de transformation ou de dégazage. Certaines périodes saisonnières, telles que la fonte printanière et l'été, nécessiteraient une attention particulière en raison des conditions hydrologiques changeantes et de l'épaisseur de la couche active.

ANNEXE I

COMPARISON OF pCO_2 COMPUTATION FROM pH-DIC AND pH-TA PAIRINGS

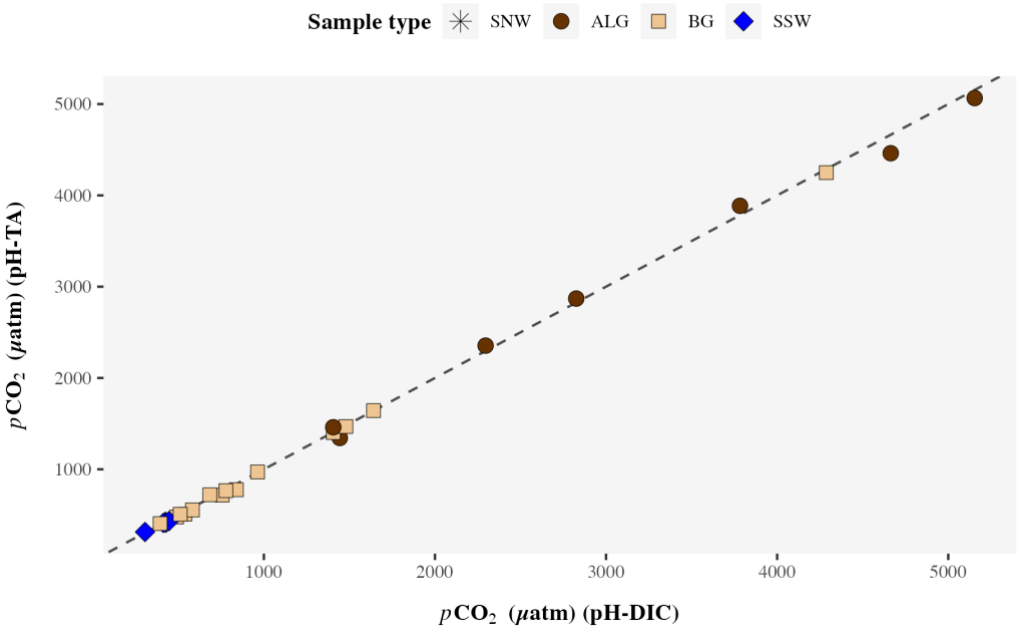

Figure 18. Comparison of pCO_2 (µatm) computed from the pH-DIC and pH-TA parings for the different sample types: active layer groundwater (ALG), beach groundwater (BG), and surface seawater (SSW). The black dashed line represents the 1:1 ratio.

Table 2. Mean (± standard deviation), mean difference and relative variability (%) of pCO_2 computed using the pH–DIC and pH–TA pairings for each sample type.

	Sample type			
	pCO_2 (µatm) (pH-DIC)	*pCO_2 (µatm) (pH-TA)*	*Mean Difference (µatm)*	*Variability* (%)*
ALG	*3082 ± 1498*	*3063 ± 1455*	*-19*	*0.62*
BG	*1096 ± 999*	*1083 ± 993*	*-13*	*1.19*
SSW	*403 ± 56*	*399 ± 48*	*-4*	*1*

**Variability is calculated from |Mean difference|.*

ANNEXE II

DOM MOLECULAR CHARACTERISTICS AND COMPOUNDS

Table 3. Distribution of DOM molecular parameters across sample types. Maximum values are in bold.

	ALG (8)	*BG (10)*	*SSW (3)*
Mass (m/z)	***401* ± 15**	*396* ± 12	*377* ± 11
AI mod	***0.328* ± 0.047**	*0.299* ± 0.039	*0.270* ± 0.002
H/C	*1.15* ± 0.091	*1.20* ± 0.078	***1.24* ± 0.001**
O/C	*0.440* ± 0.041	*0.428* ± 0.042	***0.452* ± 0.006**
Highly unsaturated	*0.824* ± 0.065	*0.824* ± 0.027	***0.850* ± 0.018**
Aromatic	*0.134* ± 0.084	*0.097* ± 0.050	*0.062* ± *0.006*

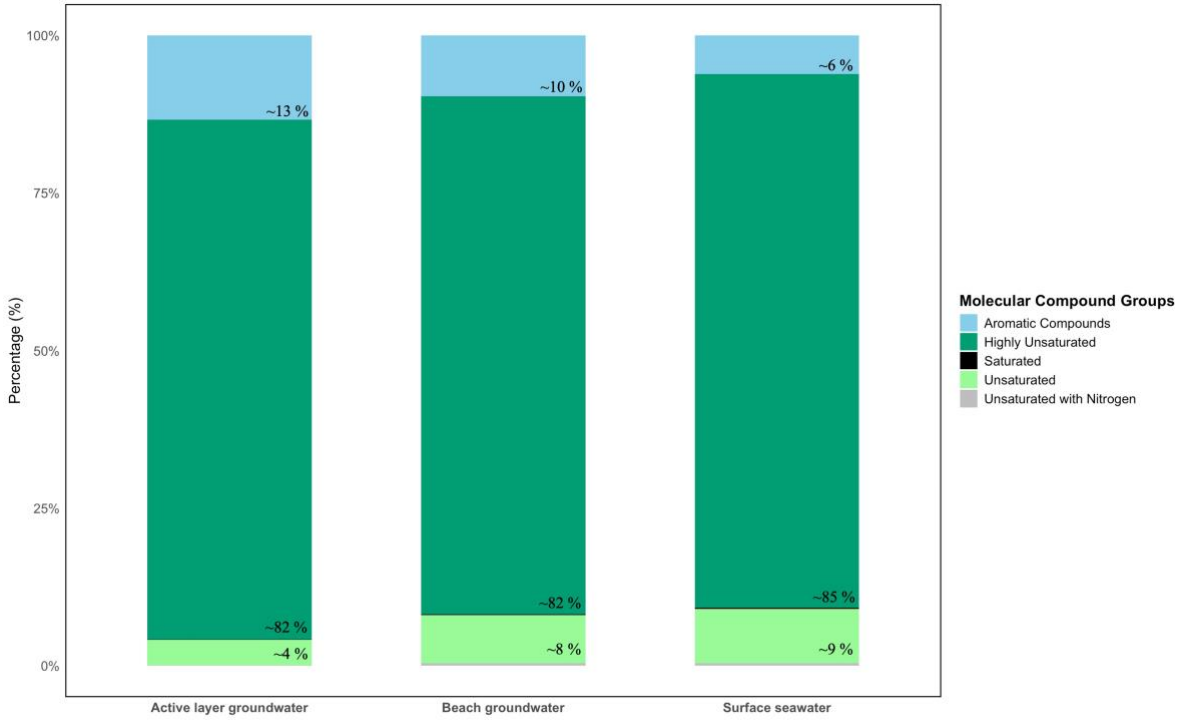

Figure 19. Distribution of molecular compounds groups across sample types.

RÉFÉRENCES BIBLIOGRAPHIQUES

Abril, G., Bouillon, S., Darchambeau, F., Teodoru, C. R., Marwick, T. R., Tamooh, F., Ochieng Omengo, F., Geeraert, N., Deirmendjian, L., Polsenaere, P., & Borges, A. V. (2015). Technical note: Large overestimation of pCO_2 calculated from pH and alkalinity in acidic, organic-rich freshwaters. *Biogeosciences*, *12*(1), 67–78. https://doi.org/10.5194/bg-12-67-2015

Aitkenhead-Peterson, J. A., McDowell, W. H., & Neff, J. C. (2003). Sources, production, and regulation of allochthonous dissolved organic matter inputs to surface waters. *Aquatic Ecosystems*, 25–70. https://doi.org/10.1016/B978-012256371-3/50003-2

Anschutz, P., Smith, T., Mouret, A., Deborde, J., Bujan, S., Poirier, D., & Lecroart, P. (2009). Tidal sands as biogeochemical reactors. *Estuarine, Coastal and Shelf Science*, *84*(1), 84–90. https://doi.org/10.1016/j.ecss.2009.06.015

Azam, F. (1987). Bacterial utilization of organic matter in the sea. *41th Symposium of the Society for General Microbiology*, 261–281. https://cir.nii.ac.jp/crid/1573105974497678464

Baines, S. B., & Pace, M. L. (1991). The production of dissolved organic matter by phytoplankton and its importance to bacteria: Patterns across marine and freshwater systems. *Limnology and Oceanography*, *36*(6), 1078–1090. https://doi.org/10.4319/lo.1991.36.6.1078

Baker, M. A., Dahm, C. N., & Valett, H. M. (2000). Anoxia, anaerobic metabolism, and biogeochemistry of the stream-water-ground-water interface. In *Streams and ground waters* (pp. 259–283). Academic Press San Diego. https://books.google.com/books?hl=fr&lr=&id=iFj5pZWSTjMC&oi=fnd&pg=PA259&dq=Anoxia,+anaerobic+metabolism,+and+biogeochemistry+of+the+stream-water-ground-water+interface&ots=uV6e22UUSt&sig=AlqEtD-GFsmDZwUf9EBkjd9fWuI

Beaupré-Laperrière, A., Mucci, A., & Thomas, H. (2020). The recent state and variability of the carbonate system of the Canadian Arctic Archipelago and adjacent basins in the context of ocean acidification. *Biogeosciences*, *17*(14), 3923–3942. https://doi.org/10.5194/bg-17-3923-2020

Beck, A. J., Tsukamoto, Y., Tovar-Sanchez, A., Huerta-Diaz, M., Bokuniewicz, H. J., & Sañudo-Wilhelmy, S. A. (2007). Importance of geochemical transformations in determining submarine groundwater discharge-derived trace metal and nutrient fluxes. *Applied Geochemistry*, *22*(2), 477–490. https://doi.org/10.1016/j.apgeochem.2006.10.005

Belshe, E. F., Schuur, E. A. G., Bolker, B. M., & Bracho, R. (2012). Incorporating spatial heterogeneity created by permafrost thaw into a landscape carbon estimate. *Journal of Geophysical Research: Biogeosciences*, *117*(G1), 2011JG001836. https://doi.org/10.1029/2011JG001836

Benner, R. (2003). Molecular indicators of the bioavailability of dissolved organic matter. In *Aquatic ecosystems* (pp. 121–137). Elsevier. https://www.sciencedirect.com/science/article/pii/B9780122563713500068

Bianchi, T. S., & Bauer, J. E. (2011). 5.03—Particulate organic carbon cycling and transformation. In E. Wolanski & D. McLusky (Eds.), *Treatise on Estuarine and Coastal Science* (pp. 69–117). Academic Press. https://doi.org/10.1016/B978-0-12-374711-2.00503-9

Blough, N. V. (2002). Chromophoric DOM in the coastal environment. *Biogeochemistry of Marine Dissolved Organic Matter*. https://cir.nii.ac.jp/crid/1573950400289510016

Boike, J., & Hubberten, H.-W. (1998). Climatological and hydrological influences on stable hydrogen and oxygen isotopes of active layer waters, Levinson-Lessing Lake area, Taymyr Peninsula. *Permafrost, Proceedings of the Seventh International Conference on Permafrost*, 23–27. http://www.arlis.org/docs/vol1/ICOP/40770716/CD-ROM/Proceedings/PDF001189/011430.pdf

Borges, A., & Abril, G. (2011). 5.04-Carbon dioxide and methane dynamics in estuaries. *9780080878850*. https://doi.org/10.1016/B978-0-12-374711-2.00504-0

Boudreau, B. P., Huettel, M., Forster, S., Jahnke, R. A., McLachlan, A., Middelburg, J. J., Nielsen, P., Sansone, F., Taghon, G., Van Raaphorst, W., Webster, I., Weslawski, J. M., Wiberg, P., & Sundby, B. (2001). Permeable marine sediments: Overturning an old paradigm. *Eos, Transactions American Geophysical Union*, *82*(11), 133–136. https://doi.org/10.1029/EO082i011p00133-01

Boyd, C. E. (2015). pH, carbon dioxide, and alkalinity. In C. E. Boyd, *Water Quality* (pp. 153–178). Springer International Publishing. https://doi.org/10.1007/978-3-319-17446-4_8

Broek, T. A. B., Walker, B. D., Guilderson, T. P., Vaughn, J. S., Mason, H. E., & McCarthy, M. D. (2020). Low molecular weight dissolved organic carbon: aging, compositional changes, and selective utilization during global ocean circulation. *Global Biogeochemical Cycles*, *34*(6), e2020GB006547. https://doi.org/10.1029/2020GB006547

Brown, J., Sidlauskas, F. J., & Delinski, G. F. (1997). *Circum-Arctic map of permafrost and ground ice conditions*. US Geological Survey Reston, VA. https://scholar.archive.org/work/l5nagtjnkbhcpfbivxsen2abua/access/wayback/https://pubs.usgs.gov/cp/45/report.pdf

Bullock, E. J., Schaal, I. V., Cardenas, M. B., McClelland, J. W., Henderson, P. B., & Charette, M. A. (2024). Seasonality of submarine groundwater discharge to an Arctic coastal lagoon. *Limnology and Oceanography*, *69*(6), 1429–1438. https://doi.org/10.1002/lno.12585

Burdige, D. J., & Gardner, K. G. (1998). Molecular weight distribution of dissolved organic carbon in marine sediment pore waters. *Marine Chemistry*, *62*(1–2), 45–64. https://doi.org/10.1016/S0304-4203(98)00035-8

Burke, E. J., Hartley, I. P., & Jones, C. D. (2012). Uncertainties in the global temperature change caused by carbon release from permafrost thawing. *The Cryosphere*, *6*(5), 1063–1076. https://doi.org/10.5194/tc-6-1063-2012

Burn, C. R. (1998). The active layer: Two contrasting definitions. *Permafrost and Periglacial Processes*, *9*(4), 411–416. https://doi.org/10.1002/(SICI)1099-1530(199810/12)9:4<411::AID-PPP292>3.0.CO;2-6

Burt, W. J., Thomas, H., Miller, L. A., Granskog, M. A., Papakyriakou, T. N., & Pengelly, L. (2016). Inorganic carbon cycling and biogeochemical processes in an Arctic inland sea (Hudson Bay). *Biogeosciences*, *13*(16), 4659–4671. https://doi.org/10.5194/bg-13-4659-2016

Butler, J. N. (1982). *Carbon dioxide equilibria and their applications*. Addison-Wesley.

Cai, W.-J., Feely, R. A., Testa, J. M., Li, M., Evans, W., Alin, S. R., Xu, Y.-Y., Pelletier, G., Ahmed, A., Greeley, D. J., Newton, J. A., & Bednaršek, N. (2021). Natural and anthropogenic drivers of acidification in large estuaries. *Annual Review of Marine Science*, *13*(1), 23–55. https://doi.org/10.1146/annurev-marine-010419-011004

Cai, W.-J., Wang, Y., Krest, J., & Moore, W. S. (2003). The geochemistry of dissolved inorganic carbon in a surficial groundwater aquifer in North Inlet, South Carolina, and the carbon fluxes to the coastal ocean. *Geochimica et Cosmochimica Acta*, *67*(4), 631–639. https://doi.org/10.1016/S0016-7037(02)01167-5

Caldeira, K., & Wickett, M. E. (2003). Anthropogenic carbon and ocean pH. *Nature*, *425*(6956), 365–365. https://doi.org/10.1038/425365a

Caldeira, K., & Wickett, M. E. (2005). Ocean model predictions of chemistry changes from carbon dioxide emissions to the atmosphere and ocean. *Journal of Geophysical Research: Oceans*, *110*(C9), 2004JC002671. https://doi.org/10.1029/2004JC002671

Campeau, A., Bishop, K., Nilsson, M. B., Klemedtsson, L., Laudon, H., Leith, F. I., Öquist, M., & Wallin, M. B. (2018). Stable carbon isotopes reveal soil-stream dic linkages in contrasting headwater catchments. *Journal of Geophysical Research: Biogeosciences*, *123*(1), 149–167. https://doi.org/10.1002/2017JG004083

Campeau, A., Wallin, M. B., Giesler, R., Löfgren, S., Mörth, C.-M., Schiff, S., Venkiteswaran, J. J., & Bishop, K. (2017). Multiple sources and sinks of dissolved inorganic carbon across Swedish streams, refocusing the lens of stable C isotopes. *Scientific Reports*, *7*(1), 9158.

Cardenas, M. B., Rodolfo, R. S., Lapus, M. R., Cabria, H. B., Fullon, J., Gojunco, G. R., Breecker, D. O., Cantarero, D. M., Evaristo, J., Siringan, F. P., & Zhang, T. (2020). Submarine groundwater and vent discharge in a volcanic area associated with coastal acidification. *Geophysical Research Letters*, *47*(1), e2019GL085730. https://doi.org/10.1029/2019GL085730

Carlson, C. A., Del Giorgio, P. A., & Herndl, G. J. (2007). Microbes and the dissipation of energy and respiration: From cells to ecosystems. *Oceanography*, *20*(2), 89–100.

Carlson, C. A., & Hansell, D. A. (2015). DOM sources, sinks, reactivity, and budgets. *Biogeochemistry of Marine Dissolved Organic Matter*, 65–126. https://doi.org/10.1016/B978-0-12-405940-5.00003-0

Catalán, N., Pastor, A., Borrego, C. M., Casas-Ruiz, J. P., Hawkes, J. A., Gutiérrez, C., von Schiller, D., & Marcé, R. (2021). The relevance of environment vs. Composition on dissolved organic matter degradation in freshwaters. *Limnology and Oceanography*, *66*(2), 306–320. https://doi.org/10.1002/lno.11606

Chaillou, G., Lemay-Borduas, F., & Couturier, M. (2016). Transport and transformations of groundwater-borne carbon discharging through a sandy beach to a coastal ocean. *Canadian Water Resources Journal / Revue Canadienne Des Ressources Hydriques*, *41*(4), 455–468. https://doi.org/https://doi.org/10.1080/07011784.2015.1111775

Chaillou, G., Tommi-Morin, G., & Mucci, A. (2024). Production and fluxes of inorganic carbon and alkalinity in a subarctic subterranean estuary. *Frontiers in Marine Science*, *11*. https://doi.org/10.3389/fmars.2024.1323463

Charbonnier, C., Anschutz, P., Abril, G., Mucci, A., Deirmendjian, L., Poirier, D., Bujan, S., & Lecroart, P. (2022). Carbon dynamics driven by seawater recirculation and groundwater discharge along a forest-dune-beach continuum of a high-energy meso-macro-tidal sandy coast. *Geochimica et Cosmochimica Acta*, *317*, 18–38. https://doi.org/10.1016/j.gca.2021.10.021

Chen, C. A., & Wang, S. (1999). Carbon, alkalinity and nutrient budgets on the East China Sea continental shelf. *Journal of Geophysical Research: Oceans*, *104*(C9), 20675–20686. https://doi.org/10.1029/1999JC900055

Coble, P., Hu, C., Richard W. Gould, J., Chang, G., & Wood, A. M. (2015). Colored dissolved organic matter in the coastal ocean: an optical tool for coastal zone environmental assessment and management | *Oceanography*. https://doi.org/10.5670/oceanog.2004.47

Connelly, T. L., McClelland, J. W., Crump, B. C., Kellogg, C. T., & Dunton, K. H. (2015). Seasonal changes in quantity and composition of suspended particulate organic matter in lagoons of the Alaskan Beaufort Sea. *Marine Ecology Progress Series*, *527*, 31–45. https://doi.org/10.3354/meps11207

Connolly, C. T., Cardenas, M. B., Burkart, G. A., Spencer, R. G. M., & McClelland, J. W. (2020). Groundwater as a major source of dissolved organic matter to Arctic coastal waters. *Nature Communications*, *11*(1), 1479. https://doi.org/10.1038/s41467-020-15250-8

Couturier, M., Nozais, C., & Chaillou, G. (2016). Microtidal subterranean estuaries as a source of fresh terrestrial dissolved organic matter to the coastal ocean. *Marine Chemistry*, *186*, 46–57. https://doi.org/10.1016/j.marchem.2016.08.001

Craig, H. (1961). Isotopic variations in meteoric waters. *Science*, *133*(3465), 1702–1703. https://doi.org/10.1126/science.133.3465.1702

Cyronak, T., Santos, I. R., Erler, D. V., Maher, D. T., & Eyre, B. D. (2014). Drivers of pCO_2 variability in two contrasting coral reef lagoons: The influence of submarine groundwater discharge. *Global Biogeochemical Cycles*, *28*(4), 398–414. https://doi.org/10.1002/2013GB004598

DeGrandpre, M. D., Hammar, T. R., Smith, S. P., & Sayles, F. L. (1996). In situ measurements of seawater pCO_2. *Oceanographic Literature Review*, *4*(43), 353. https://doi.org/10.4319/lo.1995.40.5.0969

Delaigue, L., Thomas, H., & Mucci, A. (2020). Spatial variations in CO_2 fluxes in the Saguenay Fjord (Quebec, Canada) and results of a water mixing model. *Biogeosciences*, *17*(2), 547–566. https://doi.org/10.5194/bg-17-547-2020

Demir, C., McClelland, J. W., Bristol, E., Charette, M. A., & Cardenas, M. B. (2024). Coastal supra-permafrost aquifers of the Arctic and their significant groundwater, carbon, and nitrogen fluxes. *Geophysical Research Letters*, *51*(22), e2024GL109142. https://doi.org/10.1029/2024GL109142

Dickson, A. G. (1981). An exact definition of total alkalinity and a procedure for the estimation of alkalinity and total inorganic carbon from titration data. *Deep Sea Research Part A. Oceanographic Research Papers*, *28*(6), 609–623. https://doi.org/10.1016/0198-0149(81)90121-7

Dickson, A. G., Afghan, J. D., & Anderson, G. C. (2003). Reference materials for oceanic CO_2 analysis: A method for the certification of total alkalinity. *Marine Chemistry*, *80*(2–3), 185–197. https://doi.org/10.1016/S0304-4203(02)00133-0

Dickson, A. G. (Andrew G., Sabine, C. L., Christian, J. R., & North Pacific Marine Science Organization. (2007). *Guide to best practices for ocean CO_2 measurements*. North Pacific Marine Science Organization.

Dimova, N. T., Paytan, A., Kessler, J. D., Sparrow, K. J., Garcia-Tigreros Kodovska, F., Lecher, A. L., Murray, J., & Tulaczyk, S. M. (2015). Current magnitude and mechanisms of groundwater discharge in the Arctic: case study from Alaska. *Environmental Science & Technology*, *49*(20), 12036–12043. https://doi.org/10.1021/acs.est.5b02215

Dittmar, T., Koch, B., Hertkorn, N., & Kattner, G. (2008). A simple and efficient method for the solid-phase extraction of dissolved organic matter (SPE-DOM) from seawater. *Limnology and Oceanography: Methods*, *6*(6), 230–235. https://doi.org/10.4319/lom.2008.6.230

Dittmar, T., & Stubbins, A. (2014). Dissolved organic matter in aquatic systems. https://doi.org/10.1016/B978-0-08-095975-7.01010-X

Dobiński, W. (2020). Permafrost active layer. *Earth-Science Reviews*, *208*, 103301. https://doi.org/10.1016/j.earscirev.2020.103301

Doney, S. C., Fabry, V. J., Feely, R. A., & Kleypas, J. A. (2009). Ocean acidification: the other CO_2 problem. *Annual Review of Marine Science*, *1*(1), 169–192. https://doi.org/10.1146/annurev.marine.010908.163834

Duarte, C. M., Hendriks, I. E., Moore, T. S., Olsen, Y. S., Steckbauer, A., Ramajo, L., Carstensen, J., Trotter, J. A., & McCulloch, M. (2013). Is ocean acidification an open-ocean syndrome? Understanding anthropogenic impacts on seawater pH. *ESTUARIES AND COASTS*, *36*(2), 221–236. https://doi.org/10.1007/s12237-013-9594-3

Dutta, K., Schuur, E. A. G., Neff, J. C., & Zimov, S. A. (2006). Potential carbon release from permafrost soils of Northeastern Siberia. *Global Change Biology*, *12*(12), 2336–2351. https://doi.org/10.1111/j.1365-2486.2006.01259.x

Dyrssen, D., & Sillén, L. G. (1967). Alkalinity and total carbonate in sea water. A plea for *p-T* - independent data. *Tellus*, *19*(1), 113–121. https://doi.org/10.1111/j.2153-3490.1967.tb01464.x

Egleston, E. S., Sabine, C. L., & Morel, F. M. M. (2010). Revelle revisited: Buffer factors that quantify the response of ocean chemistry to changes in DIC and alkalinity. *Global Biogeochemical Cycles*, *24*(1), 2008GB003407. https://doi.org/10.1029/2008GB003407

Environment Canada. (2025). Données des normales climatiques canadiennes pour 1991-2020—Climat—Environnement et Changement climatique Canada. https://climat.meteo.gc.ca/climate_normals/results_1991_2020_f.html?searchType=stnProv&lstProvince=&txtCentralLatMin=0&txtCentralLatSec=0&txtCentralLongMin=0&txtCentralLongSec=0&stnID=371000000&dispBack=0

Everdingen, van R. (2005). Multi-language glossary of permafrost and related ground-ice terms. *International Permafrost Association*. https://cir.nii.ac.jp/crid/1370017279830020359

Fillinger, L., Griebler, C., Hellal, J., Joulian, C., & Weaver, L. (2023). Chapter 9 – Microbial diversity and processes in groundwater. In F. Malard, C. Griebler, & S. Rétaux (Eds.), *Groundwater Ecology and Evolution (Second Edition)* (pp. 211–240). Academic Press. https://doi.org/10.1016/B978-0-12-819119-4.00009-3

Flamand, A., Lapierre, J. F., & Chaillou, G. (2024). Fate of dissolved organic matter across the permafrost–nearshore water continuum: role of the intertidal sediments. EGUsphere, 2024, 1-38.

French, H. M. (2017). The periglacial environment. John Wiley & Sons. https://books.google.com/books?hl=fr&lr=&id=JFw6DwAAQBAJ&oi=fnd&pg=PR15&dq=French,+2010+(Periglacial+Environment)&ots=iXI1pivUZW&sig=d1X-fvJgJER55aGz9WpaSEZ0Kno

Friedlingstein, P., Jones, M. W., O'Sullivan, M., Andrew, R. M., Bakker, D. C., Hauck, J., Le Quéré, C., Peters, G. P., Peters, W., & Pongratz, J. (2022). Global carbon budget 2021. *Earth System Science Data*, *14*(4), 1917–2005. https://doi.org/10.5194/essd-14-1917-2022

Fritz, M., Opel, T., Tanski, G., Herzschuh, U., Meyer, H., Eulenburg, A., & Lantuit, H. (2015). Dissolved organic carbon (DOC) in Arctic ground ice. *The Cryosphere Discussions*, *9*(1), 77–114.

Fritz, M., Vonk, J. E., & Lantuit, H. (2017). Collapsing Arctic coastlines. *Nature Climate Change*, *7*(1), 6–7. https://doi.org/10.1038/nclimate3188

Fritz, M., Wetterich, S., Meyer, H., Schirrmeister, L., Lantuit, H., & Pollard, W. H. (2011). Origin and characteristics of massive ground ice on Herschel Island (western Canadian Arctic) as revealed by stable water isotope and Hydrochemical signatures. *Permafrost and Periglacial Processes*, *22*(1), 26–38. https://doi.org/10.1002/ppp.714

Gagnon, S., Coulombe, S., Didier, D., Binette, S., Chaillou, G., Kurylyk, B., Maksagak, I., Evetalegak, J., (In review). Coastal gullies formed by piping on a permafrost marine terrace near Iqaluktuuttiaq (Cambridge Bay), Nunavut, Canada.

Gallagher, K. L., Dupraz, C., & Visscher, P. T. (2014). Two opposing effects of sulfate reduction on carbonate precipitation in normal marine, hypersaline, and alkaline environments: COMMENT. *Geology*, *42*(1), e313–e314. https://doi.org/10.1130/G34639C.1

Gattuso, J.-P., & Hansson, L. (2011). Ocean acidification. Oxford University Press, USA. https://books.google.com/books?hl=fr&lr=&id=8yjNFxkALjIC&oi=fnd&pg=PP1&dq=Gattuso,+J.+P.+and+Hansson,+L.:+Ocean+acidification,+Oxford+University+Press,+Oxford,+2011.&ots=NjqVIVcqU2&sig=_4pOAfABXE541cdholgUvpcJgI4

Goldsmith, S. T., Carey, A. E., Johnson, B. M., Welch, S. A., Lyons, W. B., McDowell, W. H., & Pigott, J. S. (2010). Stream geochemistry, chemical weathering and CO_2 consumption potential of andesitic terrains, Dominica, Lesser Antilles. *Geochimica et Cosmochimica Acta*, *74*(1), 85–103. https://doi.org/10.1016/j.gca.2009.10.009

Goodrich, L. E. (1982). The influence of snow cover on the ground thermal regime. *Canadian Geotechnical Journal*, *19*(4), 421–432. https://doi.org/10.1139/t82-047

Gorham, E. (1991). Northern Peatlands: Role in the Carbon Cycle and Probable Responses to Climatic Warming. *Ecological Applications*, *1*(2), 182–195. https://doi.org/10.2307/1941811

Gruber, N., Bakker, D. C., DeVries, T., Gregor, L., Hauck, J., Landschützer, P., McKinley, G. A., & Müller, J. D. (2023). Trends and variability in the ocean carbon sink. *Nature Reviews Earth & Environment*, *4*(2), 119–134. https://doi.org/10.1038/s43017-022-00381-x

Guillemot, A. (2020). *Surveillance sismologique des glaciers rocheux: Pour mieux contraindre un risque émergent* [PhD Thesis, Université Grenoble Alpes [2020-....]]. https://inria.hal.science/tel-03094893/

Guimond, J. A., Demir, C., Kurylyk, B. L., Walvoord, M. A., McClelland, J. W., & Cardenas, M. B. (2023). Wind-modulated groundwater discharge along a microtidal Arctic coastline. *Environmental Research Letters*, *18*(9), 094042. https://doi.org/10.1088/1748-9326/acf0d8

Günther, F., Overduin, P. P., Yakshina, I. A., Opel, T., Baranskaya, A. V., & Grigoriev, M. N. (2015). Observing Muostakh disappear: Permafrost thaw subsidence and erosion of a ground-ice-rich island in response to arctic summer warming and sea ice reduction. *The Cryosphere*, *9*(1), 151–178. https://doi.org/10.5194/tc-9-151-2015

Hayase, K., & Shinozuka, N. (1995). Vertical distribution of fluorescent organic matter along with AOU and nutrients in the equatorial Central Pacific. *Marine Chemistry*, *48*(3–4), 283–290. https://doi.org/10.1016/0304-4203(94)00051-E

He, W., Chen, M., Schlautman, M. A., & Hur, J. (2016). Dynamic exchanges between DOM and POM pools in coastal and inland aquatic ecosystems: A review. *Science of the Total Environment*, *551*, 415–428. https://doi.org/10.1016/j.scitotenv.2016.02.031

Heginbottom, J. A., Dubreuil, M. A., & Harker, P. T. (1995a). Canada, permafrost (4177; 5th ed., p. 4177). https://doi.org/10.4095/294672

Heginbottom, J. A., Dubreuil, M.-A., & Harker, P. (1995b). Canada, permafrost. In the National Atlas of Canada (5 ed.). *Ressources naturelles Canada, Géomatique Canada, Collection MCR*, 4177. https://doi.org/10.4095/294672

Helms, J. R., Stubbins, A., Ritchie, J. D., Minor, E. C., Kieber, D. J., & Mopper, K. (2008). Absorption spectral slopes and slope ratios as indicators of molecular weight, source, and photobleaching of chromophoric dissolved organic matter. *Limnology and Oceanography*, *53*(3), 955–969. https://doi.org/10.4319/lo.2008.53.3.0955

Hinzman, L. D., Kane, D. L., Gieck, R. E., & Everett, K. R. (1991). Hydrologic and thermal properties of the active layer in the Alaskan Arctic. *Cold Regions Science and Technology*, *19*(2), 95–110. https://doi.org/10.1016/0165-232X(91)90001-W

Hofmann, M., & Schellnhuber, H. J. (2010). Ocean acidification: A millennial challenge. *Energy & Environmental Science*, *3*(12), 1883–1896.

Hoppe, C. J. M., Langer, G., Rokitta, S. D., Wolf-Gladrow, D. A., & Rost, B. (2012). Implications of observed inconsistencies in carbonate chemistry measurements for ocean acidification studies. *Biogeosciences*, *9*(7), 2401–2405. https://doi.org/10.5194/bg-9-2401-2012

Huettel, M., Ziebis, W., & Forster, S. (1996). Flow-induced uptake of particulate matter in permeable sediments. *Limnology and Oceanography*, *41*(2), 309–322. https://doi.org/10.4319/lo.1996.41.2.0309

Hugelius, G., Strauss, J., Zubrzycki, S., Harden, J. W., Schuur, E. A. G., Ping, C. L., Schirrmeister, L., Grosse, G., Michaelson, G. J., Koven, C. D., O'Donnell, J. A., Elberling, B., Mishra, U., Camill, P., Yu, Z., Palmtag, J., & Kuhry, P. (2014). Estimated stocks of circumpolar permafrost carbon with quantified uncertainty ranges and identified data gaps. *Biogeosciences*, *11*(23), 6573–6593. https://doi.org/10.5194/bg-11-6573-2014

Hunt, C. W., Salisbury, J. E., & Vandemark, D. (2011). Contribution of non-carbonate anions to total alkalinity and overestimation of pCO_2 in New England and New Brunswick rivers. *Biogeosciences*, *8*(10), 3069–3076. https://doi.org/10.5194/bg-8-3069-2011

IAEA WISER. (2025). Global network of isotopes in precipitation. https://www.iaea.org/services/networks/gnip

Jickells, T. D., & Rae, J. E. (2005). Biogeochemistry of intertidal sediments. https://ui.adsabs.harvard.edu/abs/2005bis..book.....J/abstract

Jones, B. M., Arp, C. D., Jorgenson, M. T., Hinkel, K. M., Schmutz, J. A., & Flint, P. L. (2009). Increase in the rate and uniformity of coastline erosion in Arctic Alaska. *Geophysical Research Letters*, *36*(3), 2008GL036205. https://doi.org/10.1029/2008GL036205

Joos, F., Sarmiento, J. L., & Siegenthaler, U. (1991). Estimates of the effect of Southern Ocean iron fertilization on atmospheric CO_2 concentrations. *Nature*, *349*(6312), 772–775. https://doi.org/10.1038/349772a0

Judge, A. (1973). The prediction of permafrost thicknesses. *Canadian Geotechnical Journal*, *10*(1), 1–11. https://doi.org/10.1139/t73-001

Kaiser, K., & Guggenberger, G. (2003). Mineral surfaces and soil organic matter. *European Journal of Soil Science*, *54*(2), 219–236. https://doi.org/10.1046/j.1365-2389.2003.00544.x

Kaplan, L. A., & Newbold, J. D. (2003). The role of monomers in stream ecosystem metabolism. In *Aquatic ecosystems* (pp. 97–119). Elsevier. https://www.sciencedirect.com/science/article/pii/B9780122563713500056

Karolytė, R., Serno, S., Johnson, G., & Gilfillan, S. M. (2017). The influence of oxygen isotope exchange between CO_2 and H_2O in natural CO_2-rich spring waters: Implications for geothermometry. *Applied Geochemistry*, *84*, 173–186. https://doi.org/10.1016/j.apgeochem.2017.06.012

Kemp, E. A., Gilbert, C., & James, D. T. (2006). *Geological survey of Canada, Map D1860A*.

Kerr, D. E., Brown, P. J., Grey, A., & Kelleher, B. P. (2021). The influence of organic alkalinity on the carbonate system in coastal waters. *Marine Chemistry*, *237*. https://doi.org/10.1016/J.MARCHEM.2021.104050

Kerr, D. E., Turner, C., Grey, A., Keogh, J., Brown, P. J., & Kelleher, B. P. (2023). $OrgAlk_{Calc}$: Estimation of organic alkalinity quantities and acid-base properties with proof of concept in Dublin Bay. *Marine Chemistry*, *251*, 104234. https://doi.org/10.1016/j.marchem.2023.104234

Kim, H. C., & Lee, K. (2009). Significant contribution of dissolved organic matter to seawater alkalinity. *Geophysical Research Letters*, *36*(20). https://doi.org/10.1029/2009GL040271

Kim, S., Kaplan, L. A., & Hatcher, P. G. (2006). Biodegradable dissolved organic matter in a temperate and a tropical stream determined from ultra-high resolution mass spectrometry. *Limnology and Oceanography*, *51*(2), 1054–1063. https://doi.org/10.4319/lo.2006.51.2.1054

Kim, T.-H., Waska, H., Kwon, E., Suryaputra, I. G. N., & Kim, G. (2012). Production, degradation, and flux of dissolved organic matter in the subterranean estuary of a large tidal flat. *Marine Chemistry*, *142*, 1–10. https://doi.org/10.1016/j.marchem.2012.08.002

Kipp, L., Chaillou, G., Kienast, M., Tamborski, J., & Whalen, D. (in revision). Utility of radium isotopes as tracers of massive ice-derived solutes in a changing Arctic.

Knoblauch, C., Beer, C., Liebner, S., Grigoriev, M. N., & Pfeiffer, E.-M. (2018). Methane production as key to the greenhouse gas budget of thawing permafrost. *Nature Climate Change*, *8*(4), 309–312. https://doi.org/10.1038/s41558-018-0095-z

Koch, B. P., & Dittmar, T. (2006). From mass to structure: An aromaticity index for high-resolution mass data of natural organic matter. *Rapid Communications in Mass Spectrometry*, *20*(5), 926–932. https://doi.org/10.1002/rcm.2386

Koven, C. D., Ringeval, B., Friedlingstein, P., Ciais, P., Cadule, P., Khvorostyanov, D., Krinner, G., & Tarnocai, C. (2011). Permafrost carbon-climate feedbacks accelerate global warming. *Proceedings of the National Academy of Sciences*, *108*(36), 14769–14774. https://doi.org/10.1073/pnas.1103910108

Kroeker, K. J., Kordas, R. L., Crim, R., Hendriks, I. E., Ramajo, L., Singh, G. S., Duarte, C. M., & Gattuso, J.-P. (2013). Impacts of ocean acidification on marine organisms: Quantifying sensitivities and interaction with warming. *Global Change Biology*, *19*(6), 1884–1896. https://doi.org/10.1111/gcb.12179

Kuliński, K., Schneider, B., Hammer, K., Machulik, U., & Schulz-Bull, D. (2014). The influence of dissolved organic matter on the acid-base system of the Baltic Sea. *Journal of Marine Systems*, *132*, 106–115. https://doi.org/10.1016/J.JMARSYS.2014.01.011

Kwon, H. K., Kang, H., Oh, Y. H., Park, S. R., & Kim, G. (2017). Green tide development associated with submarine groundwater discharge in a coastal harbor, Jeju, Korea. *Scientific Reports*, *7*(1), 6325. https://doi.org/10.1038/s41598-017-06711-0

Laane, R., & Koole, L. (1982). The relation between fluorescence and dissolved organic carbon in the Ems-Dollart estuary and the western Wadden Sea. *Netherlands Journal of Sea Research*, *15*(2), 217–227. https://doi.org/10.1016/0077-7579(82)90005-9

LaBolle, E. M., Fogg, G. E., Eweis, J. B., Gravner, J., & Leaist, D. G. (2008). Isotopic fractionation by diffusion in groundwater. *Water Resources Research*, *44*(7), 2006WR005264. https://doi.org/10.1029/2006WR005264

Lantuit, H., Overduin, P. P., Couture, N., Wetterich, S., Aré, F., Atkinson, D., Brown, J., Cherkashov, G., Drozdov, D., & Forbes, D. L. (2012). The Arctic coastal dynamics database: A new classification scheme and statistics on Arctic permafrost coastlines. *Estuaries and Coasts*, *35*, 383–400. https://doi.org/10.1007/s12237-010-9362-6

Lantuit, H., Overduin, P. P., & Wetterich, S. (2013). Recent Progress Regarding Permafrost Coasts. *Permafrost and Periglacial Processes*, *24*(2), 120–130. https://doi.org/10.1002/ppp.1777

Lecher, A. L. (2017). Groundwater discharge in the Arctic: A review of studies and implications for biogeochemistry. *Hydrology*, *4*(3), 41. https://doi.org/10.3390/hydrology4030041

Lechtenfeld, O. J., Kaesler, J., Jennings, E. K., & Koch, B. P. (2024). Direct analysis of marine dissolved organic matter using LC-FT-ICR MS. *Environmental Science & Technology*, *58*(10), 4637–4647. https://doi.org/10.1021/acs.est.3c07219

Lécuyer, C., Gardien, V., Rigaudier, T., Fourel, F., Martineau, F., & Cros, A. (2009). Oxygen isotope fractionation and equilibration kinetics between CO_2 and H_2O as a function of salinity of aqueous solutions. *Chemical Geology*, *264*(1–4), 122–126. https://doi.org/10.1016/j.chemgeo.2009.02.017

Lee, H., Calvin, K., Dasgupta, D., Krinner, G., Mukherji, A., Thorne, P., Trisos, C., Romero, J., Aldunce, P., & Barrett, K. (2023). Climate change 2023: Synthesis report. Contribution of working groups I, II and III to the sixth assessment report of the intergovernmental panel on climate change. The Australian National University.

Lee, J.-Y., Marotzke, J., Bala, G., Cao, L., Corti, S., Dunne, J. P., Engelbrecht, F., Fischer, E., Fyfe, J. C., & Jones, C. (2021). Future global climate: Scenario-based projections and near-term information. In Climate change 2021: The physical science basis. Contribution of working group I to the sixth assessment report of the intergovernmental panel on climate change (pp. 553–672). Cambridge University Press. https://www.cambridge.org/core/services/aop-cambridge-core/content/view/309359EDDCFABB031C078AE20CEE04FD/stamped-9781009157889c4_553-672.pdf/future_global_climate_scenariobased_projections_and_nearterm_information.pdf

Leung, J. Y. S., Zhang, S., & Connell, S. D. (2022). Is ocean acidification really a threat to marine calcifiers? A systematic review and meta-analysis of 980+ studies spanning two decades. *Small*, *18*(35), 2107407. https://doi.org/10.1002/smll.202107407

Li, C., Wei, Y., Liu, Y., Li, L., Peng, L., Chen, J., Liu, L., Dou, T., & Wu, X. (2022). Active layer thickness in the northern hemisphere: Changes from 2000 to 2018 and future simulations. *Journal of Geophysical Research: Atmospheres*, *127*(12), e2022JD036785. https://doi.org/10.1029/2022JD036785

Li, G., Liu, J., Ma, Y., Zhao, R., Hu, S., Li, Y., Wei, H., & Xie, H. (2014). Distribution and spectral characteristics of chromophoric dissolved organic matter in a coastal bay in northern China. *Journal of Environmental Sciences*, *26*(8), 1585–1595.

Linkhorst, A., Dittmar, T., & Waska, H. (2017). Molecular fractionation of dissolved organic matter in a shallow subterranean estuary: the role of the iron curtain. *Environmental Science & Technology*, *51*(3), 1312–1320. https://doi.org/10.1021/acs.est.6b03608

Liu, Q., Charette, M. A., Breier, C. F., Henderson, P. B., McCorkle, D. C., Martin, W., & Dai, M. (2017). Carbonate system biogeochemistry in a subterranean estuary–Waquoit Bay, USA. *Geochimica et Cosmochimica Acta*, *203*, 422–439. https://doi.org/10.1016/j.gca.2017.01.041

Liu, Y., Jiao, J. J., Liang, W., Santos, I. R., Kuang, X., & Robinson, C. E. (2021). Inorganic carbon and alkalinity biogeochemistry and fluxes in an intertidal beach aquifer: Implications for ocean acidification. *Journal of Hydrology*, *595*, 126036. https://doi.org/10.1016/j.jhydrol.2021.126036

Liu, Y., Song, Y., & Jiao, J. J. (2023). Submarine groundwater discharge strengthens acidification in the coastal semi-closed bays. *Geophysical Research Letters*, *50*(17), e2023GL103788. https://doi.org/10.1029/2023GL103788

Lizotte, M., Juhls, B., Matsuoka, A., Massicotte, P., Mével, G., Obie, D., Anikina, J., Antonova, S., Bécu, G., Béguin, M., Bélanger, S., Bossé-Demers, T., Bröder, L., Bruyant, F., Chaillou, G., Comte, J., Couture, R.-M., Devred, E., Deslongchamps, G., … Babin, M. (2022). Nunataryuk field campaigns: Understanding the origin and fate of terrestrial organic matter in the coastal waters of the Mackenzie Delta region. *Earth System Science Data, 15(4),* 1617-1653. https://doi.org/10.5194/essd-2022-163

Lukawska-Matuszewska, K. (2016). Contribution of non-carbonate inorganic and organic alkalinity to total measured alkalinity in pore waters in marine sediments (Gulf of Gdansk, SE Baltic Sea). *Marine Chemistry*, *186*, 211–220. https://doi.org/10.1016/j.marchem.2016.10.002

Luo, D., Wu, Q., Jin, H., Marchenko, S. S., Lü, L., & Gao, S. (2016). Recent changes in the active layer thickness across the northern hemisphere. *Environmental Earth Sciences*, *75*(7), 555. https://doi.org/10.1007/s12665-015-5229-2

MacDonald, E. N., Tank, S. E., Kokelj, S. V., Froese, D. G., & Hutchins, R. H. S. (2021). Permafrost-derived dissolved organic matter composition varies across permafrost end-members in the western Canadian Arctic. *Environmental Research Letters*, *16*(2). https://doi.org/10.1088/1748-9326/abd971

Mackay, J. R. (1983). *Oxygen isotope variations in permafrost, Tuktoyaktuk Peninsula area, Northwest Territories*. https://inis.iaea.org/search/search.aspx?orig_q=RN:16029753

Madsen, E. L., & and Bollag, J. (1989). Aerobic and anaerobic microbial activity in deep subsurface sediments from the savannah river plant. *Geomicrobiology Journal*, *7*(1–2), 93–101. https://doi.org/10.1080/01490458909377852

Maher, D. T., Santos, I. R., Golsby-Smith, L., Gleeson, J., & Eyre, B. D. (2013). Groundwater-derived dissolved inorganic and organic carbon exports from a mangrove tidal creek: The missing mangrove carbon sink? *Limnology and Oceanography*, *58*(2), 475–488. https://doi.org/10.4319/lo.2013.58.2.0475

Martell-Bonet, L., & Byrne, R. H. (2023). A differential titration method for determining the dissociation characteristics of natural organic acids in the coastal zone. *Chemical Geology*, *636*, 121634. https://doi.org/10.1016/j.chemgeo.2023.121634

Massicotte, P., Asmala, E., Stedmon, C., & Markager, S. (2017). Global distribution of dissolved organic matter along the aquatic continuum: Across rivers, lakes and oceans. *ScienceDirect*. *Volume 609*, 180–191. https://doi.org/10.1016/j.scitotenv.2017.07.076

McDonough, L. K., Rutlidge, H., O'Carroll, D. M., Andersen, M. S., Meredith, K., Behnke, M. I., Spencer, R. G., McKenna, A. M., Marjo, C. E., & Oudone, P. (2020). Characterisation of shallow groundwater dissolved organic matter in aeolian, alluvial and fractured rock aquifers. *Geochimica et Cosmochimica Acta*, *273*, 163–176. https://doi.org/10.1016/j.gca.2020.01.022

McLachlan, A., & Brown, A. C. (2006). The ecology of sandy shores. *Burlington, MA*.

Meister, P. (2013). Two opposing effects of sulfate reduction on carbonate precipitation in normal marine, hypersaline, and alkaline environments. *Geology*, *41*(4), 499–502. https://doi.org/10.1130/G34185.1

Meister, P. (2014). Two opposing effects of sulfate reduction on carbonate precipitation in normal marine, hypersaline, and alkaline environments: REPLY. *42*(1). https://doi.org/10.1130/G35240Y.1

Meybeck, M. (1987). Global chemical weathering of surficial rocks estimated from river dissolved loads. *American Journal of Science*, *287*(5), 401–428.

Middelburg, J. J. (2019). Biogeochemical processes and inorganic carbon dynamics. In J. J. Middelburg, *Marine Carbon Biogeochemistry* (pp. 77–105). Springer International Publishing. https://doi.org/10.1007/978-3-030-10822-9_5

Millero, F. J. (1986). The pH of estuarine waters: pH of estuarine waters. *Limnology and Oceanography*, *31*(4), 839–847. https://doi.org/10.4319/lo.1986.31.4.0839

Millero, F. J., Pierrot, D., Lee, K., Wanninkhof, R., Feely, R., Sabine, C. L., Key, R. M., & Takahashi, T. (2002). Dissociation constants for carbonic acid determined from field measurements. *Deep Sea Research Part I: Oceanographic Research Papers*, *49*(10), 1705–1723. https://doi.org/10.1016/S0967-0637(02)00093-6

Mishra, U., Hugelius, G., Shelef, E., Yang, Y., Strauss, J., Lupachev, A., Harden, J. W., Jastrow, J. D., Ping, C.-L., Riley, W. J., Schuur, E. A. G., Matamala, R., Siewert, M., Nave, L. E., Koven, C. D., Fuchs, M., Palmtag, J., Kuhry, P., Treat, C. C., … Orr, A. (2021). Spatial heterogeneity and environmental predictors of permafrost region soil organic carbon stocks. *Science Advances*, *7*(9), eaaz5236. https://doi.org/10.1126/sciadv.aaz5236

Moore, W. S. (1999). The subterranean estuary: A reaction zone of ground water and sea water. *Marine Chemistry*, *65*(1–2), 111–125. https://doi.org/10.1016/S0304-4203(99)00014-6

Moore, W. S. (2010). The effect of submarine groundwater discharge on the ocean. *Annual Review of Marine Science*, *2*(1), 59–88. https://doi.org/10.1146/annurev-marine-120308-081019

Mos, B., Holloway, C., Kelaher, B. P., Santos, I. R., & Dworjanyn, S. A. (2021). Alkalinity of diverse water samples can be altered by mercury preservation and borosilicate vial storage. *Scientific Reports*, *11*(1). https://doi.org/10.1038/s41598-021-89110-w

Mucci, A. (1983). The solubility of calcite and aragonite in seawater at various salinities, temperatures, and one atmosphere total pressure. *American Journal of Science*, *283*(7), 780–799.

Müller, S., Vähätalo, A. V., Granskog, M. A., Autio, R., & Kaartokallio, H. (2011). Behaviour of dissolved organic matter during formation of natural and artificially grown Baltic Sea ice. *Annals of Glaciology*, *52*(57), 233–241. https://doi.org/10.3189/172756411795931886

Münster, U. (1993). Concentrations and fluxes of organic carbon substrates in the aquatic environment. *Antonie van Leeuwenhoek*, *63*, 243–274. https://doi.org/10.1007/BF00871222

Nielsen, D. M., Pieper, P., Barkhordarian, A., Overduin, P., Ilyina, T., Brovkin, V., Baehr, J., & Dobrynin, M. (2022). Increase in Arctic coastal erosion and its sensitivity to warming in the twenty-first century. *Nature Climate Change*, *12*(3), 263–270. https://doi.org/10.1038/s41558-022-01281-0

NOAA. (2024). Climate change: atmospheric carbon dioxide | *NOAA Climate.gov*. https://www.climate.gov/news-features/understanding-climate/climate-change-atmospheric-carbon-dioxide

Noetzli, J., & Gruber, S. (2009). Transient thermal effects in Alpine permafrost. *The Cryosphere*, *3*(1), 85–99. https://doi.org/10.5194/tc-3-85-2009

Obu, J., Westermann, S., Bartsch, A., Berdnikov, N., Christiansen, H. H., Dashtseren, A., Delaloye, R., Elberling, B., Etzelmüller, B., & Kholodov, A. (2019). Northern Hemisphere permafrost map based on TTOP modelling for 2000–2016 at 1 km2 scale. *Earth-Science Reviews*, *193*, 299–316. https://doi.org/10.1016/j.earscirev.2019.04.023

Olichwer, T., Tarka, R., & Modelska, M. (2012). Chemical composition of groundwaters in the Hornsund region, southern Spitsbergen. *Hydrology Research*, *44*(1), 117–130. https://doi.org/10.2166/nh.2012.075

Oliver, B. G., Thurman, E. M., & Malcolm, R. L. (1983). The contribution of humic substances to the acidity of colored natural waters. *Geochimica et Cosmochimica Acta*, *47*(11), 2031–2035. https://doi.org/10.1016/0016-7037(83)90218-1

Orr, J. C., Epitalon, J.-M., Dickson, A. G., & Gattuso, J.-P. (2018). Routine uncertainty propagation for the marine carbon dioxide system. *Marine Chemistry*, *207*, 84–107. https://doi.org/10.1016/j.marchem.2018.10.006

Orr, J. C., Fabry, V. J., Aumont, O., Bopp, L., Doney, S. C., Feely, R. A., Gnanadesikan, A., Gruber, N., Ishida, A., & Joos, F. (2005). Anthropogenic ocean acidification over the twenty-first century and its impact on calcifying organisms. *Nature*, *437*(7059), 681–686. https://doi.org/10.1038/nature04095

Pachauri, R. K., & Reisinger, A. (2007). Climate change 2007: Synthesis report. Contribution of working groups I, II and III to the fourth assessment report of the Intergovernmental Panel on Climate Change. IPCC. https://research.usq.edu.au/item/q6wy0/climate-change-2007-synthesis-report-contribution-of-working-groups-i-ii-and-iii-to-the-fourth-assessment-report-of-the-intergovernmental-panel-on-climate-change

Peng, T.-H., & Broecker, W. S. (1991). Dynamical limitations on the Antarctic iron fertilization strategy. *Nature*, *349*(6306), 227–229. https://doi.org/10.1038/349227a0

Philipp, M., Dietz, A., Ullmann, T., & Kuenzer, C. (2023). A circum-Arctic monitoring framework for quantifying annual erosion rates of permafrost coasts. *Remote Sensing*, *15*(3), 818. https://doi.org/10.3390/rs15030818

Pierrot, D. E., Wallace, D. W. R., & Lewis, E. (2011). MS Excel program developed for CO_2 system calculations. *Carbon Dioxide Information Analysis Center*. https://doi.org/10.3334/cdiac/otg.co2sys_xls_cdiac105a

Ping, C. L., Jastrow, J. D., Jorgenson, M. T., Michaelson, G. J., & Shur, Y. L. (2015). Permafrost soils and carbon cycling. *SOIL*, *1*(1), 147–171. https://doi.org/10.5194/soil-1-147-2015

Pomeroy, L. R. (1974). The ocean's food web, a changing paradigm. *Bioscience*, *24*(9), 499–504. https://doi.org/10.2307/1296885

Pucher, M., Wünsch, U., Weigelhofer, G., Murphy, K., Hein, T., & Graeber, D. (2019). staRdom: Versatile software for analyzing spectroscopic data of dissolved organic matter in R. *Water*, *11*(11), 2366. https://doi.org/10.3390/w11112366

Rassmann, J., Eitel, E. M., Lansard, B., Cathalot, C., Brandily, C., Taillefert, M., & Rabouille, C. (2020). Benthic alkalinity and dissolved inorganic carbon fluxes in the Rhône River prodelta generated by decoupled aerobic and anaerobic processes. *Biogeosciences*, *17*(1), 13–33. https://doi.org/10.5194/bg-17-13-2020

Raven, J., Caldeira, K., Elderfield, H., Hoegh-Guldberg, O., Liss, P., Riebesell, U., Shepherd, J., Turley, C., & Watson, A. (2005). Ocean acidification due to increasing atmospheric carbon dioxide. The Royal Society. https://oceanrep.geomar.de/id/eprint/7878/1/965_Raven_2005_OceanAcidification DueToIncreasing_Monogr_pubid13120.pdf

Rawlins, M. A., & Karmalkar, A. V. (2023). Regime shifts in Arctic terrestrial hydrology manifested from impacts of climate warming. *The Cryosphere Discussions*, *2023*, 1–38. https://doi.org/10.5194/tc-18-1033-2024

Repeta, D., & Aluwihare, L. (2024). Chemical characterization and cycling of dissolved organic matter. In *Biogeochemistry of marine dissolved organic matter* (pp. 13–67). Elsevier. https://www.sciencedirect.com/science/article/pii/B9780443138584000113

Rhein, M., Rintoul, S. R., Aoki, S., Campos, E., Chambers, D., Feely, R. A., Gulev, S., Johnson, G. C., Josey, S. A., & Kostianoy, A. (2013). Observations: Ocean in climate change 2013: the physical science basis. Contribution of working group I to the fifth assessment report of the intergovernmental panel on climate change. *Fifth Assessment Report of the Intergovernmental Panel on Climate Change*, 255–316.

Riedl, R. J., & Machan, R. (1972). Hydrodynamic patterns in lotic intertidal sands and their bioclimatological implications. *Marine Biology*, *13*, 179–209. https://doi.org/10.1007/BF00391378

Riser, S. C., Freeland, H. J., Roemmich, D., Wijffels, S., Troisi, A., Belbéoch, M., Gilbert, D., Xu, J., Pouliquen, S., & Thresher, A. (2016). Fifteen years of ocean observations with the global Argo array. *Nature Climate Change*, *6*(2), 145–153. https://doi.org/10.1038/nclimate2872

Robinson, C., Wallace, D., Hyun, J.-H., Polimene, L., Benner, R., Zhang, Y., Cai, R., Zhang, R., & Jiao, N. (2018). An implementation strategy to quantify the marine microbial carbon pump and its sensitivity to global change. *National Science Review*, *5*(4), 474–480. https://doi.org/10.1093/nsr/nwy070

Rodenhizer, H., Ledman, J., Mauritz, M., Natali, S. M., Pegoraro, E., Plaza, C., Romano, E., Schädel, C., Taylor, M., & Schuur, E. (2020). Carbon thaw rate doubles when accounting for subsidence in a permafrost warming experiment. *Journal of Geophysical Research: Biogeosciences*, *125*(6), e2019JG005528. https://doi.org/10.1029/2019JG005528

Roemmich, D., Alford, M. H., Claustre, H., Johnson, K., King, B., Moum, J., Oke, P., Owens, W. B., Pouliquen, S., & Purkey, S. (2019). On the future of Argo: A global, full-depth, multi-disciplinary array. *Frontiers in Marine Science*, *6*, 439. https://doi.org/10.3389/fmars.2019.00439Sabine

Romanovsky, V. E., & Osterkamp, T. E. (2000). Effects of unfrozen water on heat and mass transport processes in the active layer and permafrost. *Permafrost and Periglacial Processes*, *11*(3), 219–239. https://doi.org/10.1002/1099-1530(200007/09)11:3<219::AID-PPP352>3.0.CO;2-7

Sabine, C. L., Feely, R. A., Gruber, N., Key, R. M., Lee, K., Bullister, J. L., Wanninkhof, R., Wong, C. S., Wallace, D. W. R., Tilbrook, B., Millero, F. J., Peng, T.-H., Kozyr, A., Ono, T., & Rios, A. F. (2004). The oceanic sink for anthropogenic CO_2. *Science*, *305*(5682), 367–371. https://doi.org/10.1126/science.1097403

Santos, I. R., Burnett, W. C., Dittmar, T., Suryaputra, I. G., & Chanton, J. (2009). Tidal pumping drives nutrient and dissolved organic matter dynamics in a Gulf of Mexico subterranean estuary. *Geochimica et Cosmochimica Acta*, *73*(5), 1325–1339. https://doi.org/10.1016/j.gca.2008.11.029

Santos, I. R., Glud, R. N., Maher, D., Erler, D., & Eyre, B. D. (2011). Diel coral reef acidification driven by porewater advection in permeable carbonate sands, Heron Island, Great Barrier Reef: DIEL CORAL REEF ACIDIFICATION. *Geophysical Research Letters*, *38*(3), n/a-n/a. https://doi.org/10.1029/2010GL046053

Sawyer, A. H., Michael, H. A., & Schroth, A. W. (2016). From soil to sea: The role of groundwater in coastal critical zone processes. *WIREs Water*, *3*(5), 706–726. https://doi.org/10.1002/wat2.1157

Schädel, C., Bader, M. K.-F., Schuur, E. A., Biasi, C., Bracho, R., Čapek, P., De Baets, S., Diáková, K., Ernakovich, J., & Estop-Aragones, C. (2016). Potential carbon emissions dominated by carbon dioxide from thawed permafrost soils. *Nature Climate Change*, *6*(10), 950–953. https://doi.org/10.1038/nclimate3054

Schuur, E. A., & Abbott, B. (2011). High risk of permafrost thaw. *Nature*, *480*(7375), 32–33. https://doi.org/10.1038/480032a

Schuur, E. A. G., & Mack, M. C. (2018). Ecological response to permafrost thaw and consequences for local and global ecosystem services. *Annual Review of Ecology, Evolution, and Systematics*, *49*(1), 279–301. https://doi.org/10.1146/annurev-ecolsys-121415-032349

Schuur, E. A. G., McGuire, A. D., Schädel, C., Grosse, G., Harden, J. W., Hayes, D. J., Hugelius, G., Koven, C. D., Kuhry, P., Lawrence, D. M., Natali, S. M., Olefeldt, D., Romanovsky, V. E., Schaefer, K., Turetsky, M. R., Treat, C. C., & Vonk, J. E. (2015). Climate change and the permafrost carbon feedback. *Nature*, *520*(7546), 171–179. https://doi.org/10.1038/nature14338

Seidel, M., Beck, M., Greskowiak, J., Riedel, T., Waska, H., Suryaputra, I. N., Schnetger, B., Niggemann, J., Simon, M., & Dittmar, T. (2015). Benthic-pelagic coupling of nutrients and dissolved organic matter composition in an intertidal sandy beach. *Marine Chemistry*, *176*, 150–163. https://doi.org/10.1016/j.marchem.2015.08.011

Seidel, M., Beck, M., Riedel, T., Waska, H., Suryaputra, I. G. N. A., Schnetger, B., Niggemann, J., Simon, M., & Dittmar, T. (2014). Biogeochemistry of dissolved organic matter in an anoxic intertidal creek bank. *Geochimica et Cosmochimica Acta*, *140*, 418–434. https://doi.org/10.1016/j.gca.2014.05.038

Seidel, M., Vemulapalli, S. P. B., Mathieu, D., & Dittmar, T. (2022). Marine dissolved organic matter shares thousands of molecular formulae yet differs structurally across major water masses. *Environmental Science & Technology*, *56*(6), 3758–3769. https://doi.org/10.1021/acs.est.1c04566

Sharp, J. H. (2002). Analytical methods for total DOM pools. *Biogeochemistry of Marine Dissolved Organic Matter*, 35–58. https://doi.org/10.1016/B978-012323841-2/50004-X

Sharpe, D. R. (1993). Surficial geology, Cambridge Bay, District of Franklin, Northwest Territories. *(No Title)*. https://cir.nii.ac.jp/crid/1130282270391444992

Shaver, G. R., Canadell, J., Chapin, F. S., Gurevitch, J., Harte, J., Henry, G., Ineson, P., Jonasson, S., Melillo, J., & Pitelka, L. (2000). Global Warming and Terrestrial Ecosystems: A Conceptual Framework for Analysis: Ecosystem responses to global warming will be complex and varied. Ecosystem warming experiments hold great potential for providing insights on ways terrestrial ecosystems will respond to upcoming decades of climate change. Documentation of initial conditions provides the context for understanding and predicting ecosystem responses. *Bioscience*, *50*(10), 871–882. https://doi.org/10.1641/0006-3568(2000)050[0871:GWATEA]2.0.CO;2

Shen, C., Testa, J. M., Li, M., Cai, W.-J., Waldbusser, G. G., Ni, W., Kemp, W. M., Cornwell, J., Chen, B., Brodeur, J., & Su, J. (2019). Controls on carbonate system dynamics in a coastal plain estuary: a modeling study. *Journal of Geophysical Research: Biogeosciences*, *124*(1), 61–78. https://doi.org/10.1029/2018JG004802

Sirois, M., Couturier, M., Barber, A., Gelinas, Y., & Chaillou, G. (2018). Interactions between iron and organic carbon in a sandy beach subterranean estuary. *Marine Chemistry*, *202*, 86–96. https://doi.org/10.1016/j.marchem.2018.02.004

Smith, S., & Burgess, M. (2002). A digital database of permafrost thickness in Canada. Geological Survey of Canada.

Soetaert, K., Hofmann, A. F., Middelburg, J. J., Meysman, F. J., & Greenwood, J. (2007). Reprint of "The effect of biogeochemical processes on pH." *Marine Chemistry*, *106*(1–2), 380–401. https://doi.org/10.1016/j.marchem.2007.06.008

Song, S., Wang, Z. A., Gonneea, M. E., Kroeger, K. D., Chu, S. N., Li, D., & Liang, H. (2020). An important biogeochemical link between organic and inorganic carbon cycling: Effects of organic alkalinity on carbonate chemistry in coastal waters influenced by intertidal salt marshes. *Geochimica et Cosmochimica Acta*, *275*, 123–139. https://doi.org/10.1016/j.gca.2020.02.013

Spencer, R. G. M., Mann, P. J., Dittmar, T., Eglinton, T. I., McIntyre, C., Holmes, R. M., Zimov, N., & Stubbins, A. (2015). Detecting the signature of permafrost thaw in Arctic rivers. *Geophysical Research Letters*, *42*(8), 2830–2835. https://doi.org/10.1002/2015GL063498

Stenson, A. C., Marshall, A. G., & Cooper, W. T. (2003). Exact masses and chemical formulas of individual suwannee river fulvic acids from ultrahigh resolution electrospray ionization fourier transform ion cyclotron resonance mass spectra. *Analytical Chemistry*, *75*(6), 1275–1284. https://doi.org/10.1021/ac026106p

Stevenson, F. J., & Cole, M. A. (1999). Cycles of soils: Carbon, nitrogen, phosphorus, sulfur, micronutrients. John Wiley & Sons. https://books.google.com/books?hl=fr&lr=&id=KdnWIzM-OHIC&oi=fnd&pg=PR17&dq=Cycles+of+Soils:+Carbon,+Nitrogen,+Phosphorus,+Sulfur,+Micronutrients&ots=98pUCmrCu7&sig=ZJRM1WPGUczoHi93p13BED0fTHA

Stubbins, A., Niggemann, J., & Dittmar, T. (2012). Photo-lability of deep ocean dissolved black carbon. *Biogeosciences*, *9*(5), 1661–1670. https://doi.org/10.5194/bg-9-1661-2012

Stubbins, A., Spencer, R. G. M., Chen, H., Hatcher, P. G., Mopper, K., Hernes, P. J., Mwamba, V. L., Mangangu, A. M., Wabakanghanzi, J. N., & Six, J. (2010). Illuminated darkness: Molecular signatures of Congo River dissolved organic matter and its photochemical alteration as revealed by ultrahigh precision mass spectrometry. *Limnology and Oceanography*, *55*(4), 1467–1477. https://doi.org/10.4319/lo.2010.55.4.1467

Subcommittee, P. (1988). Glossary of permafrost and related ground-ice terms. *Associate Committee on Geotechnical Research, National Research Council of Canada, Ottawa*, *156*, 63–64.

Tarnocai, C., Canadell, J. G., Schuur, E. A. G., Kuhry, P., Mazhitova, G., & Zimov, S. (2009). Soil organic carbon pools in the northern circumpolar permafrost region. *Global Biogeochemical Cycles*, *23*(2), 2008GB003327. https://doi.org/10.1029/2008GB003327

Throckmorton, H. M., Newman, B. D., Heikoop, J. M., Perkins, G. B., Feng, X., Graham, D. E., O'Malley, D., Vesselinov, V. V., Young, J., Wullschleger, S. D., & Wilson, C. J. (2016). Active layer hydrology in an arctic tundra ecosystem: Quantifying water sources and cycling using water stable isotopes. *Hydrological Processes*, *30*(26), 4972–4986. https://doi.org/10.1002/hyp.10883

Turchyn, A. V., Bradbury, H. J., Walker, K., & Sun, X. (2021). Controls on the precipitation of carbonate minerals within marine sediments. *Frontiers in Earth Science*, *9*. https://doi.org/10.3389/feart.2021.618311

Urtizberea, A., Dupont, N., Rosland, R., & Aksnes, D. L. (2013). Sensitivity of euphotic zone properties to CDOM variations in marine ecosystem models. *Ecological Modelling*, *256*, 16–22. https://doi.org/10.1016/j.ecolmodel.2013.02.010

Utting, N., Clark, I., Lauriol, B., Wieser, M., & Aeschbach-Hertig, W. (2012). Origin and flow dynamics of perennial groundwater in continuous permafrost terrain using isotopes and noble gases: case study of the fishing Branch River, Northern Yukon, Canada. *Permafrost and Periglacial Processes*, *23*(2), 91–106. https://doi.org/10.1002/ppp.1732

von Wachenfeldt, E., Sobek, S., Bastviken, D., & Tranvik, L. J. (2008). Linking allochthonous dissolved organic matter and boreal lake sediment carbon sequestration: The role of light-mediated flocculation. *Limnology and Oceanography*, *53*(6), 2416–2426. https://doi.org/10.4319/lo.2008.53.6.2416

Vonk, J. E., & Gustafsson, Ö. (2013). Permafrost-carbon complexities. *6*, 675–676. https://doi.org/10.1038/ngeo1937

Wachenfeldt, E. von, Bastviken, D., & Tranvika, L. J. (2009). Microbially induced flocculation of allochthonous dissolved organic carbon in lakes. *Limnology and Oceanography*, *54*(5), 1811–1818. https://doi.org/10.4319/lo.2009.54.5.1811

Walvoord, M. A., & Striegl, R. G. (2007). Increased groundwater to stream discharge from permafrost thawing in the Yukon River basin: Potential impacts on lateral export of carbon and nitrogen. *Geophysical Research Letters*, *34*(12), 2007GL030216. https://doi.org/10.1029/2007GL030216

Wang, J., Li, D., Cao, W., Lou, X., Shi, A., & Zhang, H. (2022). Remote sensing analysis of erosion in Arctic coastal areas of Alaska and eastern Siberia. *Remote Sensing*, *14*(3), 589. https://doi.org/10.3390/rs14030589

Wang, S.-L., Chen, C.-T. A., Huang, T.-H., Tseng, H.-C., Lui, H.-K., Peng, T.-R., Kandasamy, S., Zhang, J., Yang, L., Gao, X., Lou, J.-Y., Kuo, F.-W., Chen, X.-G., Ye, Y., & Lin, Y.-J. (2018). Submarine Groundwater Discharge helps making nearshore waters heterotrophic. *Scientific Reports*, *8*(1), 11650. https://doi.org/10.1038/s41598-018-30056-x

Waska, H., Simon, H., Ahmerkamp, S., Greskowiak, J., Ahrens, J., Seibert, S. L., Schwalfenberg, K., Zielinski, O., & Dittmar, T. (2021). Molecular traits of dissolved organic matter in the subterranean estuary of a high-energy beach: indications of sources and sinks. *Frontiers in Marine Science*, *8*. https://doi.org/10.3389/fmars.2021.607083

Way, R. G. (2024). *Pergélisol*. https://atlasdespeuplesautochtonesducanada.ca/article/pergelisol/

Wegner, C., Bennett, K. E., De Vernal, A., Forwick, M., Fritz, M., Heikkilä, M., Łącka, M., Lantuit, H., Laska, M., Moskalik, M., O'Regan, M., Pawłowska, J., Promińska, A., Rachold, V., Vonk, J. E., & Werner, K. (2015). Variability in transport of terrigenous material on the shelves and the deep Arctic Ocean during the Holocene. *Polar Research*, *34*(1), 24964. https://doi.org/10.3402/polar.v34.24964

Wetzel, R. G. (1992). Gradient-dominated ecosystems: Sources and regulatory functions of dissolved organic matter in freshwater ecosystems. *Hydrobiologia*, *229*, 181–198. https://doi.org/10.1007/BF00007000

Wolf-Gladrow, D. A., Zeebe, R. E., Klaas, C., Körtzinger, A., & Dickson, A. G. (2007). Total alkalinity: The explicit conservative expression and its application to biogeochemical processes. *Marine Chemistry*, *106*(1–2), 287–300. https://doi.org/10.1016/j.marchem.2007.01.006

Wright, L. D., & Nichols, C. R. (Eds.). (2019). Tomorrow's Coasts: Complex and Impermanent (Vol. 27). Springer International Publishing. https://doi.org/10.1007/978-3-319-75453-6

Yang, B., Byrne, R. H., & Lindemuth, M. (2015). Contributions of organic alkalinity to total alkalinity in coastal waters: A spectrophotometric approach. *Marine Chemistry*, *176*, 199–207. https://doi.org/10.1016/j.marchem.2015.09.008

Zeebe, R. E., & Wolf-Gladrow, D. (2001). CO_2 in seawater: equilibrium, kinetics, isotopes (Vol. 65). Gulf Professional Publishing. https://books.google.com/books?hl=fr&lr=&id=g3j3Zn4kEscC&oi=fnd&pg=PA1&dq=R.E.+Zeebe,+D.+Wolf-Gladrow+CO2+in+seawater:+equilibrium,+kinetics,+isotopes+Elsevier+Oceanographic+Series,+vol.+65,+Elsevier,+New+York+(2001)&ots=ldStIZslrJ&sig=luEgRGRytBuI0Epfu1POLG17MF8

Zhang, S. (2020). The relationship between organoclastic sulfate reduction and carbonate precipitation/dissolution in marine sediments. *Marine Geology*, *428*, 106284. https://doi.org/10.1016/j.margeo.2020.106284

Zhao, W., Bao, H., Huang, D., Niggemann, J., Dittmar, T., & Kao, S.-J. (2023). Evidence from molecular marker and FT-ICR-MS analyses for the source and transport of dissolved black carbon under variable water discharge of a subtropical Estuary. *Biogeochemistry*, *162*(1), 43–55. https://doi.org/10.1007/s10533-022-00987-9

Zimov, S. A., Schuur, E. A. G., & Chapin, F. S. (2006). Permafrost and the global carbon budget. *Science*, *312*(5780), 1612–1613. https://doi.org/10.1126/science.1128908